nature geoscience

REVIEW ARTICLE

PUBLISHED ONLINE: 22 SEPTEMBER 2013 | DOI: 10.1038/NGEO1955

Three decades of global methane sources and sinks

Stefanie Kirschke *et al.**

Methane is an important greenhouse gas, responsible for about 20% of the warming induced by long-lived greenhouse gases since pre-industrial times. By reacting with hydroxyl radicals, methane reduces the oxidizing capacity of the atmosphere and generates ozone in the troposphere. Although most sources and sinks of methane have been identified, their relative contributions to atmospheric methane levels are highly uncertain. As such, the factors responsible for the observed stabilization of atmospheric methane levels in the early 2000s, and the renewed rise after 2006, remain unclear. Here, we construct decadal budgets for methane sources and sinks between 1980 and 2010, using a combination of atmospheric measurements and results from chemical transport models, ecosystem models, climate chemistry models and inventories of anthropogenic emissions. The resultant budgets suggest that data-driven approaches and ecosystem models overestimate total natural emissions. We build three contrasting emission scenarios — which differ in fossil fuel and microbial emissions — to explain the decadal variability in atmospheric methane levels detected, here and in previous studies, since 1985. Although uncertainties in emission trends do not allow definitive conclusions to be drawn, we show that the observed stabilization of methane levels between 1999 and 2006 can potentially be explained by decreasing-to-stable fossil fuel emissions, combined with stable-to-increasing microbial emissions. We show that a rise in natural wetland emissions and fossil fuel emissions probably accounts for the renewed increase in global methane levels after 2006, although the relative contribution of these two sources remains uncertain.

Reconstructions of atmospheric methane (CH_4) concentrations between 1850 and the 1970s have been made using air trapped in polar ice cores and compacted snow. The data reveal an exponential increase in CH_4 levels in the atmosphere from 830 ppb to 1500 ppb in the late 1970s[1]. Direct measurements of CH_4 in the atmosphere began in 1978[2], and reached global coverage after 1983. Today, CH_4 concentrations can be assessed using discrete air samples collected regularly at the surface, continuous measurements made at the surface[2–6] or in the troposphere[7–9], and remotely sensed measurements of atmospheric CH_4 columns retrieved from the surface or from space[10–12] (see Supplementary Section ST1). Surface-based observations from four networks (National Oceanic and Atmospheric Administration, NOAA[13]; Advanced Global Atmospheric Gases Experiment, AGAGE[14]; Commonwealth Scientific and Industrial Research Organization, CSIRO[5]; and University of California Irvine, UCI[15]) show consistent changes in the global growth rate of annual CH_4 concentrations since 1980 (Fig. 1 and Supplementary Section ST1). The agreement between these networks has improved with increasing coverage. The standard deviation for the global annual growth rate decreased from ±3.3 ppb yr^{-1} in the 1980s to ±1.3 ppb yr^{-1} in the 2000s. These data reveal a sustained increase in atmospheric CH_4 levels in the 1980s (by an average of 12 ± 6 ppb yr^{-1}), a slowdown in growth in the 1990s (6 ± 8 ppb yr^{-1}), and a general stabilisation from 1999 to 2006 to 1773 ± 3 ppb. Since 2007, CH_4 levels have been rising again[14], and reached 1799 ± 2 ppb in 2010. This increase reflects a recent imbalance between CH_4 sources and sinks that is not yet fully understood[13].

Previous reviews of the global CH_4 budget have focused on results from a few studies only[13,16–19]. These studies covered different time windows and employed different assumptions, making it difficult to interpret the decadal changes presented. Only very few studies addressed multi-decadal changes in CH_4 levels[20,21]. Here we construct a global CH_4 budget for the past three decades by combining bottom-up and top-down estimates of CH_4 sources and the chemical CH_4 sink (Box 1). We use chemical transport models — constrained by atmospheric CH_4 measurements — to estimate CH_4 fluxes using top-down atmospheric inversions. We compare these fluxes with those simulated by ecosystem models of wetland and biomass burning emissions and by data-driven approaches for other natural sources (Methods and Supplementary Section II). We also gather recent data from fossil fuel CH_4 emission inventories based on energy use statistics, and from agricultural and waste inventories based on livestock and rice paddy statistical data.

Sources and sinks

The global atmospheric CH_4 budget is determined by many terrestrial and aquatic surface sources, balanced primarily by one sink in the atmosphere. CH_4 emissions can be broadly grouped into three categories: biogenic, thermogenic and pyrogenic. Biogenic sources contain CH_4-generating microbes (methanogens)[17], and comprise anaerobic environments such as natural wetlands and rice paddies, oxygen-poor freshwater reservoirs (such as dams), digestive systems of ruminants and termites, and organic waste deposits (such as manure, sewage and landfills). Thermogenic CH_4, formed over millions of years through geological processes, is a fossil fuel. It is vented from the subsurface into the atmosphere through natural features (such as terrestrial seeps, marine seeps and mud volcanoes), and through the exploitation of fossil fuels, that is, through the exploitation of coal, oil and natural gas. Pyrogenic CH_4 is produced by the incomplete combustion of biomass and soil carbon during wildfires, and of biofuels and fossil fuels. These three types of emissions have different isotopic $\delta^{13}C$ signatures ($\delta^{13}C = [(^{13}C/^{12}C)_{sample}/(^{13}C/^{12}C)_{standard}] - 1) \times 1000$): −55 to −70‰ for biogenic emissions, −25 to −55‰ for thermogenic emissions, and −13 to −25‰ for pyrogenic emissions[20,22,23]. The isotopic composition of atmospheric CH_4 — measured at a subset of surface stations — has therefore been used to constrain its source[20–24]. CH_4 emissions by living plants under aerobic conditions do not seem to play a significant role in the global CH_4 budget (Supplementary Section ST8); some very large[25] estimates of this source published in 2006 have not been confirmed[26].

The primary sink for atmospheric CH_4 is oxidation by hydroxyl radicals (OH), mostly in the troposphere, which accounts for around 90% of the global CH_4 sink. Additional oxidation sinks include methanotrophic bacteria in aerated soils[27,28] (~4%), reactions with

*A full list of authors and their affiliations appears at the end of the paper.

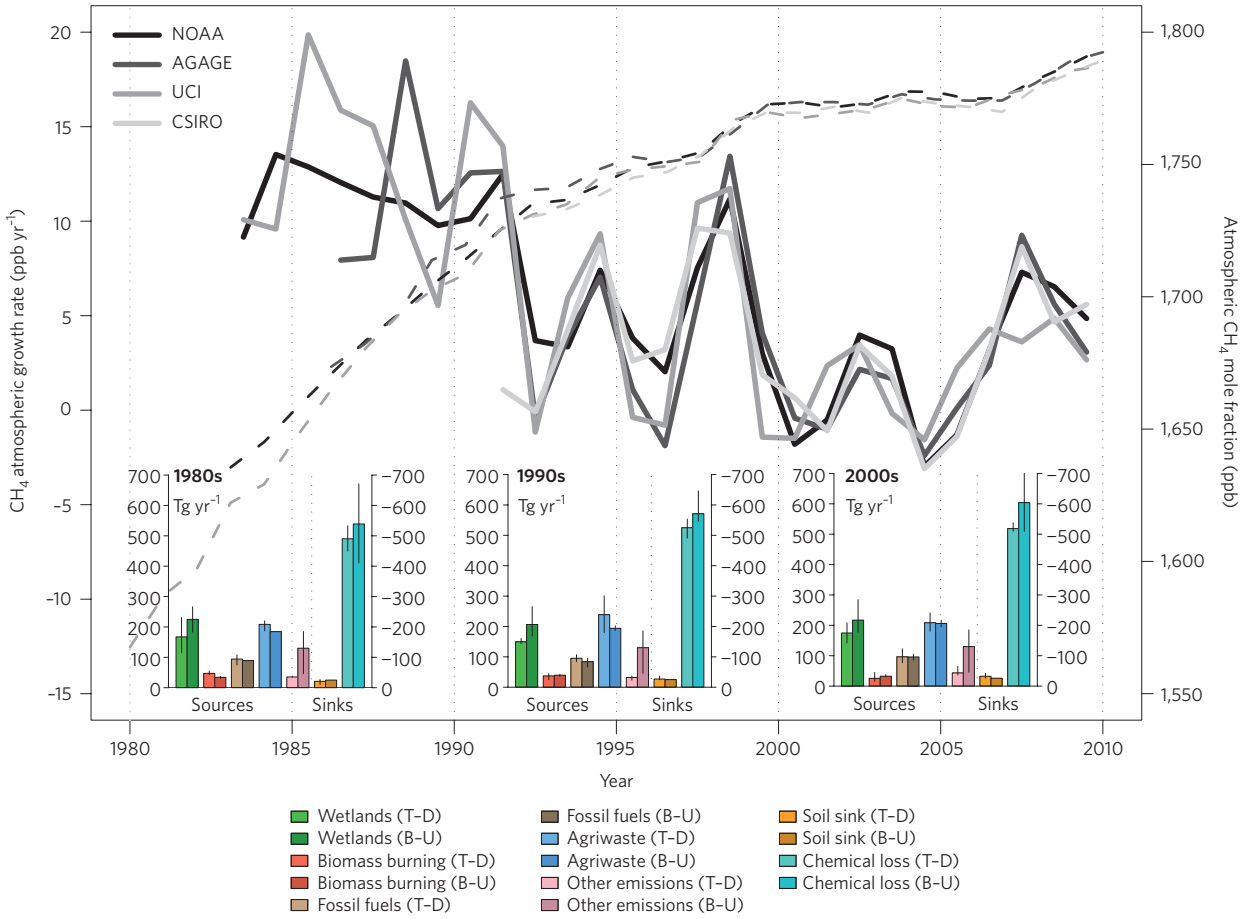

Figure 1 | Evolution of the atmospheric global mole fraction, growth rate and budget of methane for the past three decades. The mole fraction (dashed lines) and growth rate (solid lines) from NOAA, AGAGE, UCI and CSIRO networks are shown in varying shades of black/grey. Bar charts show global decadal surface emissions and sinks calculated from top-down (T-D, light-coloured bars) and bottom-up (B-U, dark-coloured bars) approaches. Categories are split into: natural wetlands, biomass burning, fossil fuels, agriculture and waste, other sources (see Table 1), soil uptake and chemical loss by OH oxidation. Error bars spread between minimum and maximum values.

chlorine radicals and atomic oxygen radicals in the stratosphere[17] (~3%), and reactions with chlorine radicals from sea salt in the marine boundary layer[29] (~3%).

Global decadal budget

We combine state-of-the-art top-down and bottom-up approaches (Box 1) using a consistent methodology (see Methods) to assess global CH_4 sources and sinks over the past three decades. At the global scale for the 2000s, top-down inversions yield total global emissions of 548 Tg of CH_4 per year with a minimum–maximum range of 526–569 (six models in Table 1) and a global sink of 540 [514–560] Tg CH_4 yr^{-1}. The source–sink mismatch reflects the observed average imbalance of 6 Tg CH_4 yr^{-1} of the CH_4 growth rate in the 2000s, which is smaller than that of the 1980s and 1990s (34 Tg CH_4 yr^{-1} and 17 Tg CH_4 yr^{-1}, respectively; Fig. 1). In fact, stabilization of atmospheric CH_4 prevailed in the early 2000s, and the atmospheric increase resumed after 2006.

Summing up all bottom-up emission estimates, a different picture emerges for the global source for the 2000s. We obtain a value of 678 Tg CH_4 yr^{-1}, which is 20% larger than the inversion-based estimate (P<0.01; Table 1). The higher global source in bottom-up estimates is explained by a larger sum of natural emissions (from wetlands, freshwater, and geological sources) than in the inversions (Table 1). For the 2000s, the bottom-up estimate of the total sink is 632 Tg CH_4 yr^{-1}, with a large range (592–785). Most of this sink — 604 Tg CH_4 yr^{-1} — is due to the hydroxyl radical CH_4 sink, as estimated by the nine bottom-up chemistry climate models (CCMs)[30]. The OH sink simulated by the seven models that run time slices from the 1980s to the 2000s is found to increase with time, which contrasts with the stability of the OH sink inferred from top-down inversions for the 1990s and the 2000s (Table 1). The positive trend in the OH sink in the CCMs can be explained by the fact that the chemical consumption of OH, for instance through reactions with CH_4 and carbon monoxide, is offset by the production of OH through photochemical reactions, involving water vapour, nitrogen oxides and stratospheric ozone. The stable OH sink inferred from top-down inversions relates to the observed atmospheric record of methyl chloroform, which is used to infer OH changes on decadal scales[30].

We group decadal estimates of emissions (top-down and bottom-up) into five categories: natural wetlands; other natural emissions (termites, geological, fresh water systems, permafrost and hydrates); agriculture and waste; fossil fuels; and biomass and biofuel burning (Table 1). Freshwater systems include lakes, reservoirs, streams and rivers. In the 2000s, natural wetland emissions (top-down, 142–208 Tg CH_4 yr^{-1}; and bottom-up, 177–284 Tg CH_4 yr^{-1}) and agriculture and waste emissions (top-down, 180–241 Tg CH_4 yr^{-1}; and bottom-up, 187–224 Tg CH_4 yr^{-1}) dominate CH_4 emissions, followed by anthropogenic fossil fuel emissions, other natural emissions and emissions from biomass and biofuel burning (Table 1). Together with natural CH_4 emissions from lake and freshwater sources[31,32], we find an imbalance of almost 50 Tg CH_4 yr^{-1} (in the 2000s) between the mean global emission and the mean global sink in the

bottom-up approach, which is larger than the observed growth rate of around 6 Tg CH_4 yr^{-1}.

This discrepancy, combined with the fact that the global mean emission is 130 Tg CH_4 yr^{-1} greater in the bottom-up approach than in the top-down approach (Table 1), suggests that CH_4 emissions are overestimated in the bottom-up approach. Indeed, the bottom-up global emission estimate is obtained by adding up independently estimated flux components, and thus lacks a constraint on its global magnitude. In contrast, the global CH_4 emission derived from the top-down approach is constrained at the global scale by the atmospheric CH_4 growth rate, using atmospheric CH_4 measurements, and by the magnitude of the chemical sink, using proxy atmospheric observations, such as the concentration of methyl chloroform, to estimate OH concentrations. Such proxy methods have proven to be reliable indicators of mean OH levels in the troposphere, although their ability to capture OH changes has been widely discussed[33,34]. These proxy methods suggest that the mean global chemical sink for CH_4 derived from bottom-up estimates may also be overestimated, especially in the 2000s (Table 1).

When summing up anthropogenic fossil emissions, natural fossil CH_4 from onshore and offshore seeps[35,36] (part of geological emissions in Table 1) and hydrates, bottom-up total fossil emissions account for 28% (~156 Tg CH_4 yr^{-1}) of the global CH_4 source between 1985 and 2000. This is consistent with an analysis of ^{14}C-CH_4 atmospheric measurements[37] in both hemispheres inferring a 30 ± 2% fossil fraction in the global CH_4 source. However, fossil emissions of this magnitude are not confirmed by a recent analysis of the global atmospheric record of ethane[15], which is co-emitted with geological CH_4. Top-down inversions cannot provide useful information to settle this debate, as they generally do not separate this source from other natural emissions (Table 1). Consideration of the natural fossil CH_4 source, neglected in previous Intergovernmental Panel on Climate Change (IPCC) assessments, thus represents a significant update to the global CH_4 budget, although it is still debated.

Global budget uncertainty

Uncertainties associated with decadal CH_4 budgets are expressed by the minimum–maximum range between different decadal estimates, due to the small number of studies available for calculating reliable standard deviations (Table 1). For the 2000s, the uncertainty range for bottom-up estimates — defined as (max–min)/mean — is 50% for natural wetlands and typically 100% for other natural sources, though the other individual natural sources have smaller fluxes than wetlands. Anthropogenic sources seem to be known more precisely, with an uncertainty range of 30% for agriculture/waste- and fossil-fuel-related emissions, and 20% for biomass burning. The uncertainty range of the global sink is 40%, but drops to 20% when removing one outlier with very high total OH loss in a recent comparison of climate chemistry models[30,38]. Note that the uncertainties reported in Table 1 are correlated to some extent. Because of more recent and robust estimates for each decade, each term in the budget has a smaller error range than in the IPCC AR4 report: 50% smaller for wetlands, 60% smaller for biomass burning, and 40% smaller for agriculture and waste emissions (Table 1).

Natural wetlands have the largest absolute uncertainty of any of the emission categories, with a min–max range of 107 Tg CH_4 yr^{-1} in the bottom-up approach (177–284 Tg CH_4 yr^{-1}). This large range is confirmed by a recent multi-model analysis[39] showing a ±40% range of wetland emissions around an average of 190 Tg CH_4 yr^{-1}. In the three wetland emission models used here[40–42], emissions were calculated for each grid point as the product of a flux rate and a wetland area, both having uncertainties. Uncertainties in wetland extent seem to be the dominant source of discrepancy in modelled CH_4 emissions[39,43].

The OH sink seems to have a smaller error range using proxy methods in the top-down approach (max–min range of 30 Tg CH_4) than in bottom-up CCMs (max–min range of 250 Tg CH_4, dropping to 110 Tg CH_4 when removing one outlier model from the Atmospheric Chemistry and Climate Model Intercomparison Project (ACCMIP)[30,38]), in which different humidity and temperature fields cause a large spread of the OH sink[38].

Following IPCC AR5 guidelines for the treatment of uncertainties[44], we defined a level of confidence for both top-down estimates and bottom-up estimates, based on robustness (number of published studies) and agreement (difference between maximum and minimum estimates, relative to the mean). Many studies have focused on constraining the CH_4 budget during the 1990s and 2000s, but fewer estimates are available for the 1980s. As a result,

Box 1 | New data to assess the CH_4 budget

The top-down approach is based on atmospheric inversion models, which determine 'optimal' surface fluxes[92,93] that best fit atmospheric CH_4 observations given an atmospheric transport model including chemistry, prior estimates of fluxes, and their uncertainties. Global atmospheric inversions provide a time-varying distribution of CH_4 fluxes, albeit with limited insight into the underlying processes when different sources overlap in the same region. This is, for example, often the case for agricultural, waste and fossil emissions in densely populated areas of east Asia, Europe and North America. We collected results from nine inversion systems (Supplementary Table S1).

The bottom-up approach includes process-based models estimating CH_4 emissions, and CCMs estimating the OH sink. Eight bottom-up models for wetland and fire CH_4 emissions are parameterized with empirical knowledge of local processes and driven by global data sets of climate, or satellite-observed burned area, to simulate CH_4 fluxes on spatial and temporal scales relevant for regional and global budgets (Supplementary Section II). Bottom-up emission inventories[56,81,82] based on energy use, agricultural activity, and emission factors from different sectors provide yearly or decadal mean estimates of anthropogenic waste-related, rice, livestock, biofuel, and fossil fuel emissions, usually at national scales. Three inventories for anthropogenic emissions are used, updated to 2008 (Supplementary Information).

The photochemical sink of CH_4 is large and difficult to quantify, given the very short lifetime of OH (~1 sec) and its control by a myriad of precursor species. Direct measurements of atmospheric OH radicals do not have the required accuracy and coverage to derive global OH concentrations and consequently the magnitude of the CH_4 sink. We estimated CH_4 loss due to OH from the output of nine numerical CCMs[65], which are categorized here as an atmospheric bottom-up approach. The OH concentration as calculated by CCMs can be further adjusted, at a large scale, by inversions based on measurements of tracers with known emissions and whose dominant sink is oxidation by OH, such as methyl chloroform[34,49,85,94] or chloromethanes[33,34].

Combining top-down and bottom-up approaches allows us to investigate the consistency of each term of the CH_4 budget[21]. In this comparison, it should be noted that bottom-up models and inventories are not independent from inversions, because they are usually used in inversions to prescribe a prior spatial, and sometimes temporal, distribution of the emissions and sinks. However, inversions use independent atmospheric observations to partially correct the prior values.

Table 1 | CH_4 budget for the past three decades.

	Tg CH_4 yr^{-1}					
	1980–1989		1990–1999		2000–2009	
	Top-down	Bottom-up	Top-down	Bottom-up	Top-down	Bottom-up
Natural sources	203 [150–267]	355 [244–466]	182 [167–197]	336 [230–465]	218 [179–273]	347 [238–484]
Natural wetlands	167 [115–231][19,21,76]	225 [183–266][40,41]	150 [144–160][21,74,77]	206 [169–265][40–42]	175 [142–208][46,53,73,75,77,86]	217 [177–284][40–42]
Other sources	36 [35–36][19,21,76]	130 [61–200]	32 [23–37][21,74,77]	130 [61–200]	43 [37–65][46,53,73,75,77]	130 [61–200]
Fresh water (lakes and rivers)		40 [8–73][31,32]		40 [8–73][31,32]		40 [8–73][31,32]
Wild animals		15 [15–15][16]		15 [15–15][16]		15 [15–15][16]
Wildfires		3 [1–3][16,47,55,88,89]		3 [1–5][16,47,55,88,89]		3 [1–5][16,47,55,88,89]
Termites		11 [2–11][16,48,55,91]		11 [2–22][16,37,87,91]		11 [2–22][16,37,87,91]
Geological (incl. oceans)		54 [33–75][35,55,90]		54 [33–75][35,55,90]		54 [33–75][35,55,90]
Hydrates		6 [2–9][16,36,87]		6 [2–9][16,36,87]		6 [2–9][16,36,87]
Permafrost (excl. lakes and wetland)		1 [0–1][55]		1 [0–1][55]		1 [0–1][55]
Anthropogenic sources	348 [305–383]	308 [292–323]	372 [290–453]	313 [281–347]	335 [273–409]	331 [304–368]
Agriculture and waste	208 [187–220][19,21,76]	185 [172–197][56]	239 [180–301][21,74,77]	188 [177–196][55,56,81]	209 [180–241][46,53,73,75,77]	200 [187–224][55,56,81]
Biomass burning (incl. biofuels)	46 [43–55][19,21,76]	34 [31–37][78,80]	38 [26–45][21,74,77]	42 [38–45][78,80]	30 [24–45][47,53,72,73,75,77]	35 [32–39][47,78,80,89]
Fossil fuels	94 [75–108][19,21,76]	89 [89–89][56]	95 [84–107][21,74,77]	84 [66–96][55,56,81]	96 [77–123][46,53,73,75,77]	96 [85–105][55,56,81]
Sinks						
Soils	21 [10–27][19,21,76]	28 [9–47][27,42]	27 [27–27][21]	28 [9–47][27,42,89]	32 [26–42][46,53,73,75,86]	28 [9–47][27,42,89]
Total chemical loss	490 [450–533][19,21,76]	539 [411–671][21,29,38,83]	525 [491–554][21,83]	571 [521–621][21,29,38,83]	518 [510–538][46,53,73,75,77]	604 [483–738][21,29,38,83]
Tropospheric OH		468 [382–567][30,38]		479 [457–501][30,38]		528 [454–617][30,38]
Stratospheric loss		46 [16–67][22,38,83]		67 [51–83][21,38,83]		51 [16–84][21,38,83]
Tropospheric Cl		25 [13–37][29]		25 [13–37][29]		25 [13–37][29]
TOTALS						
Sum of sources	551 [500–592]	663 [536–789]	554 [529–596]	649 [511–812]	548 [526–569]	678 [542–852]
Sum of sinks	511 [460–559]	539 [420–718]	542 [518–579]	596 [530–668]	540 [514–560]	632 [592–785]
Imbalance (sources−sinks)	30 [16–40]		12 [7–17]		8 [−4–19]	
Atmospheric growth rate	34		17		6	

Top-down and bottom-up estimates are listed separately for the different categories in Fig. 1. For top-down inversions, the 1980s decade starts in 1984. Numbers in square brackets represent minimum and maximum values. A balance with the atmospheric annual increase and the sum of the sources has been assumed for inversions not reporting their global sink. Stratospheric loss for bottom-up is the sum of the loss by radicals, a 10 Tg yr^{-1} loss due to $O(^1D)$ radicals[22] and a 20–35% contribution due to Cl radicals[29]. Ranges of total chemical loss are about half the reported ranges (for example, [509-619] for the 2000s) when removing one outlier.

estimates for all source categories during the 2000s are more robust, especially for inversions (Fig. 2). Agreement among studies is high (difference is less than 33%) for agriculture and waste (top-down and bottom-up), biomass burning and fossil fuels (bottom-up) and OH loss (top-down), whereas agreement is only medium (33–66% difference) for natural wetlands (top-down and bottom-up), fossil fuel emissions (top-down) and OH sink (bottom-up) estimates. Low agreement (> 66% difference) is found for biomass burning (top-down) and other natural sources (bottom-up). Increasing the number of studies does not necessarily lead to enhanced agreement. This can be seen for the fossil fuel and other sources categories, partly because of poorly constrained models, and partly because the results from a single new study can produce a large increase in the spread of emission estimates when very few studies are available.

No source or sink category reaches the highest level of confidence (highest agreement and highest robustness), emphasizing the large uncertainties that remain in our understanding of CH_4 emissions. Overall, higher confidence in global emissions is found for agriculture and waste (top-down) than for fossil fuels, the OH sink, natural wetlands and other natural sources.

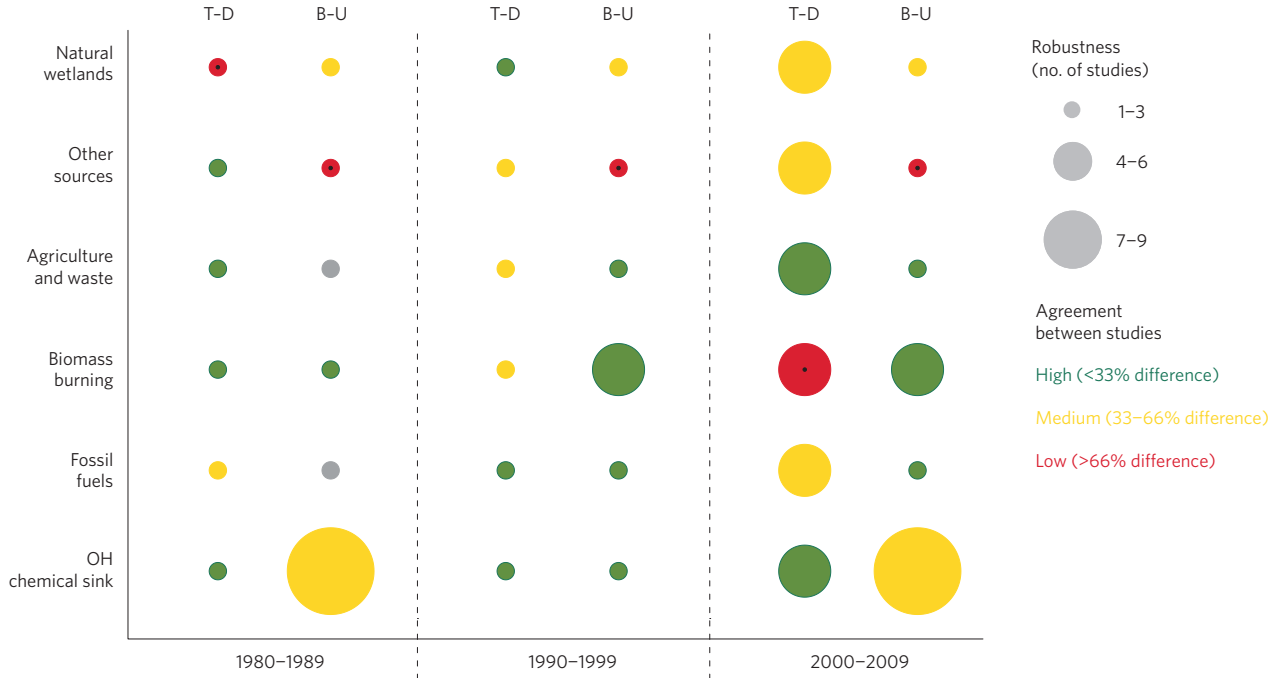

Figure 2 | Evolution of uncertainty on estimates of methane emissions and sinks presented in Table 1. Circle size depicts the robustness of the estimate (number of studies). Circle colour illustrates the level of agreement among studies (min–max ranges): green, high confidence; yellow, medium confidence; red (with black dot), low confidence. Circles are grey when only one study has been used. A large green circle, for example, indicates a very good level of confidence[44].

Regional decadal budget

The geographical breakdown of emissions per category and per region reveals major CH_4 emission zones worldwide and the level of consistency between top-down and bottom-up approaches (Fig. 3 and Supplementary Section ST2 and Tables S2 and S3). Anthropogenic emissions dominate in Europe, North America, China, and the fossil-fuel-producing countries of eastern Europe and central Asia, with good agreement between top-down and bottom-up approaches (Fig. 3). Emission ranges are given in Table S2. Densely populated regions usually emit fossil, agricultural and waste CH_4, making these sources difficult to separate in top-down inversions. Noteworthy is the large range of estimates for anthropogenic fossil CH_4 emissions from China in the top-down approach, possibly due to the low density of atmospheric CH_4 measurements in this region, and to biases in inventories[45]. The large range of anthropogenic CH_4 emission estimates in Europe and North America possibly reflects uncertainties in emission factors, and in the partition between waste and fossil CH_4 sources. In emerging economies, agriculture and waste emissions are highest in China (top-down, 29 Tg CH_4 yr^{-1}; bottom-up, 28 Tg CH_4 yr^{-1}) and India (top-down, 27 Tg CH_4 yr^{-1}; bottom-up, 22 Tg CH_4 yr^{-1}), but are also important in southeast Asia and temperate South America due to extensive rice agriculture and livestock industries (Supplementary Table S2). In India and China, agriculture and waste constitutes the single largest regional source of CH_4. However, per capita CH_4 emissions in India and China are still 35% and 85%, respectively, of the mean for OECD countries.

When aggregated over large regions, wetlands dominate emissions in tropical South America (top-down, 28 Tg CH_4 yr^{-1}; bottom-up, 58 Tg CH_4 yr^{-1}) and Africa (top-down, 36 Tg CH_4 yr^{-1}; bottom-up, 24 Tg CH_4 yr^{-1}), with significant emissions in southeast Asia, temperate South America, boreal North America and boreal Eurasia (Supplementary Table S2). Tropical South America shows the largest regional discrepancy between top-down (17–48 Tg CH_4 yr^{-1}) and bottom-up (39–92 Tg CH_4 yr^{-1}) wetland emissions (Supplementary Tables S2 and S3). The seven inversions using only surface measurements give the lowest estimates for the 2000s decadal mean wetland emission (17–30 Tg CH_4 yr^{-1}), and the two inversions using SCIAMACHY column satellite data combined with surface measurements[46] (27 and 48 Tg CH_4 yr^{-1}) agree better with bottom-up estimates (39–92 Tg CH_4 yr^{-1}). Only short time series of CH_4 *in situ* measurements are available for inland South America, which makes it one of the least constrained regions for inversions using surface measurements. The wetland models used in this study simulate large emissions in the Amazon region, equatorial tropical Africa, tropical Asia (for example, Bangladesh, India, China and Indonesia), Canada and boreal Eurasia. Simulated emission areas are consistent between models for 66 ± 9% of global wetland emissions over the period 1990–2006 (Supplementary Fig. S0).

When aggregated over large regions, emissions from biomass burning are the largest in Africa (top-down, 9 Tg CH_4 yr^{-1}; bottom-up, 8 Tg CH_4 yr^{-1}) and in tropical South America (top-down, 5 Tg CH_4 yr^{-1}; bottom-up, 4 Tg CH_4 yr^{-1}), but play only a minor role in temperate and boreal regional budgets. The bottom-up estimates are likely to be conservative compared to top-down estimates, as small fires are often undetected by satellite retrieval algorithms[47]. For biomass burning, simulated emission areas are consistent between models for 38 ± 9% of global emissions over the period 1997–2000, revealing robust large emission zones around the thermal equator in Africa (for example, Central African Republic, Democratic Republic of the Congo, Republic of the Congo, Angola, Zambia and Cameroon), central South America (Brazil and Bolivia), Indonesia, and to a lesser extent in eastern Russia, Laos, and Mexico (Supplementary Fig. S0). Emission zones in northern Australia and in boreal regions (Canada and Siberia) can also be clearly identified.

Other natural sources, including termites, lakes and other fresh waters, and onshore geological emissions show maximum values in Africa and tropical South America, due to the relatively strong contribution of emissions by termites[48]. A new empirical model of termite CH_4 emissions developed in this study indicates that Africa and tropical South America are major contributors to the global

termite source, contributing 30% and 36%, respectively, of the total (Supplementary Section ST7). Finally, CH_4 loss due to OH radicals is largest in the tropical atmosphere, both over land and oceans, as the tropics are the major region of OH production[49].

Attribution of temporal changes

Year-to-year variations of CH_4 fluxes have been intensively studied[4,14,21,47,50]. The present study confirms the findings from previous ones showing that, over the last three decades, variations in wetland emissions have dominated the year-to-year variability in surface emissions (Supplementary Fig. S5). Interannual variability in wetland emissions surpasses that of biomass burning emissions, except during intensive fire periods[21,50]. Analyses of anomalies in CH_4 fluxes following the Mount Pinatubo[21,51] eruption in 1991 and the record-high El Niño[47,52] in 1997–1998 are summarized in Supplementary Sections ST4 and ST5. Both models and observations compiled in the present study consistently describe small interannual variability in the OH sink in the 2000s compared with the previous two decades (<3%, 1σ of annual means; Supplementary Section ST6), in line with previously reported estimates (<5%)[34,53].

The observed decadal changes remain much more enigmatic than yearly anomalies (Supplementary Fig. S5). We use a scenario approach, built from our synthesis and from recent publications, to investigate these changes, and the contribution of the different CH_4 sources to them (see Methods). We assume that decadal changes in global mean CH_4 emissions since 1985 are well represented by the mean of those five atmospheric inversions covering the past three decades[53], averaged on a five-year basis (Fig. 4 and Methods). A global mass balance model[54] based on the atmospheric observations of the four surface networks and on possible changes in CH_4 lifetime is used to provide uncertainties on the mean inversion (blue shaded area at the top of Fig. 4). These observation-driven global CH_4 emissions show three distinct regimes: an increase before 1990, an oscillation around a constant mean value during 1990–2005, and an increase after 2006[4,14,53]. A storyline (S_0) is constructed by adding wetland emissions from top-down inversions (average of five inversions) to other estimates (EPA (ref. 55) and EDGARv4.2 (ref. 56) inventories).

1985–2005. The S_0 storyline clearly overestimates global emissions after 1990, which calls for corrections to the magnitude of one or several sources in the S_0 scenario (Fig. 4). Using ethane firn air and atmospheric measurements, two recent studies indicated that CH_4 emissions from the fossil fuel sector decreased between 1985 and 2000 at a rate of −0.4 to −0.8 Tg CH_4 yr^{-1} , and attributed such a decline to decreasing fugitive emissions (leaks during extraction, treatment and use of fossil fuels) from oil and gas industries[15,57]. One of these studies further extended the ethane record up to 2010[15], with either a slower decline or a stabilization of fossil fuel emissions

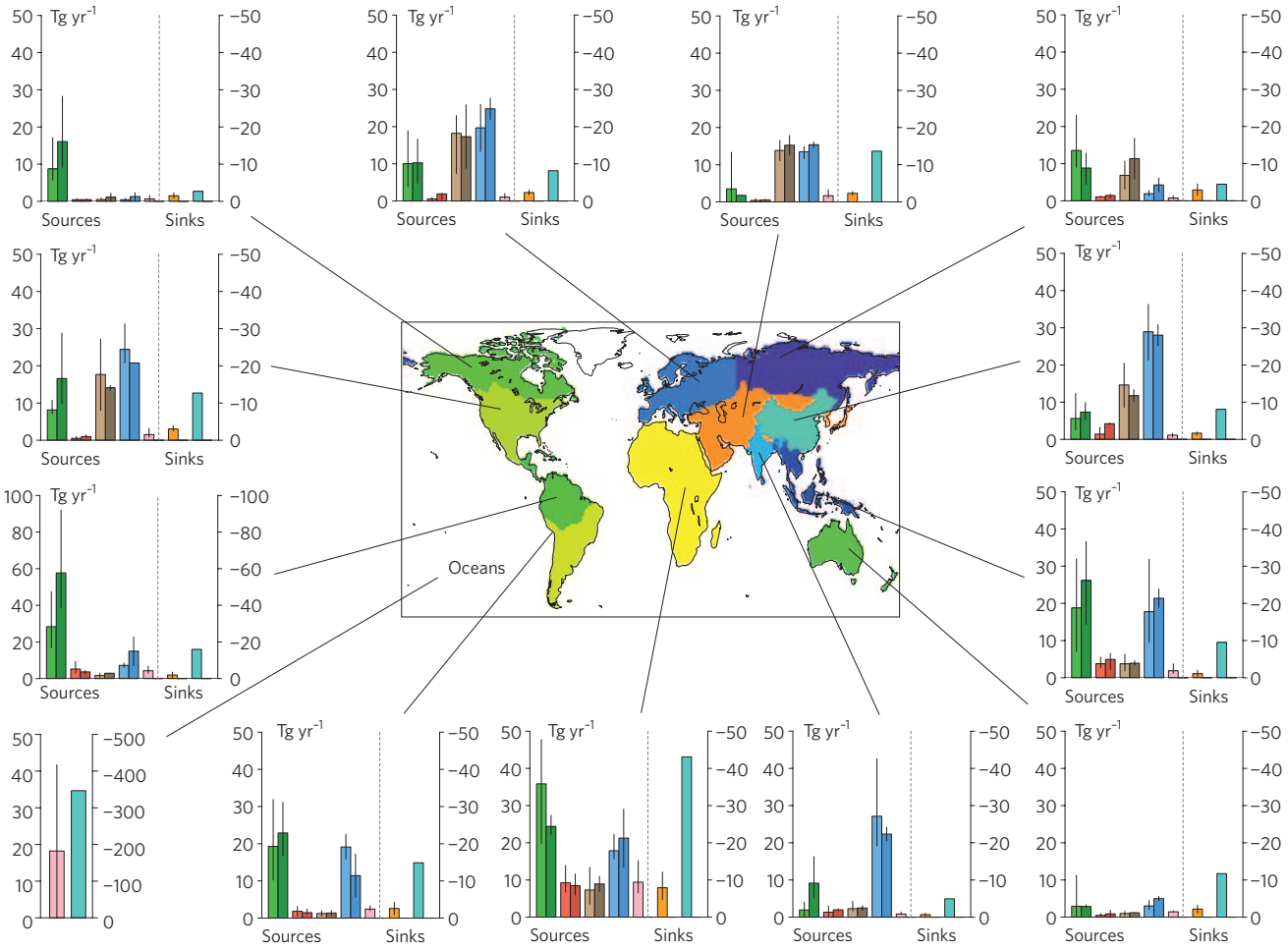

Figure 3 | Regional budgets for 2000–2009 over 13 regions. The considered regions are nine TransCom regions[84], plus separate regions for India, China and southeast Asia, and one region for oceans. Source and sink categories are the same as in Fig. 1. Both top-down (T-D, light-coloured bars) and bottom-up (B-U, dark-coloured bars) approaches are shown. Oceans are considered as one large region (bar chart at the bottom left), with ocean emissions (pink) and chemical loss over the ocean (turquoise). Error bars indicate the spread between the minimum and the maximum values.

after 2000 (see Fig. 4 of ref. 15 and Methods). Indeed, an intensified coal exploitation[45,56] after 2000 may have offset a decline in fugitive emissions. In parallel, rice paddy emissions have decreased (~−0.4 to −0.8 Tg CH_4 yr^{-1}) according to the EDGAR4.2 inventory[56] during the 1980-2000 period, and remained stable between 2000 and 2005. Assuming that CH_4 fossil fuel fugitive emissions decreased between 1985 and 2000[53] and were stable from 2000 to 2005[15], and keeping the other sources as in S_0, leads to a first plausible scenario that is consistent with the observation-driven global emissions (S_1 in Fig. 4). An alternative scenario (S'_1), using bottom-up ecosystem model results for wetland emissions as a storyline instead of top-down inversions, is also consistent with the observation-driven global emissions.

Two different analyses of $\delta^{13}C$-CH_4 isotopic composition trends[58,59] for 1990–2005 reached contradictory conclusions. In one, constant fossil fuel emissions but decreasing microbial emissions in the Northern Hemisphere were inferred[58], the latter mainly attributed to decreasing rice emissions. In the other[59], fossil fuel and microbial emissions remained constant. Assuming constant fossil fuel emissions during 1985–2005 and decreasing microbial emissions[58] produces a second scenario that is mostly consistent with observation-driven global emissions when using wetland fluxes from top-down inversions (S_2 in Fig. 4), but not when using wetland fluxes from bottom-up ecosystem models (S'_2). Assuming decreasing fossil fuel emissions before 1990 (as in S_1), but constant fossil fuel and microbial emissions between 1990 and 2005[59], produces a third scenario that is consistent with observation-driven global emissions, with either top-down or bottom-up wetland emission estimates (S_3 and S'_3 in Fig. 4).

Overall, the three plausible scenarios, among many other possible source compositions matching global decadal changes, suggest that a decrease in fossil fuel CH_4 emissions is a more likely explanation for the stability of global CH_4 emissions between 1990 and 2005 than a reduction in microbial CH_4 emissions. An actual decrease in rice paddy emissions may have been surpassed by an increase in other microbial emissions (natural wetlands, animals, landfills and waste) as found by ecosystem models combined with the EDGAR4.2 inventory. Considering the significant uncertainties reported in a recent isotope study[59] for the 1990–2005 period, decreasing-to-stable fossil fuel emissions, combined with stable-to-increasing total microbial emissions, would reconcile the atmospheric ethane trends with the ^{13}C-CH_4 trends, at least for one ^{13}C-CH_4 data set[59]. Finally, trends in the magnitude of the OH CH_4 sink, which remain uncertain over decadal timescales, can still modulate these incomplete conclusions[34].

The increase resumes from 2006 onwards. Atmospheric CH_4 levels resumed growth after 2006[14], with inferred global emissions being 17–22 Tg CH_4 yr^{-1} greater around 2010 than around 2005 (five-year basis averages; top of Fig. 4). Several studies concluded that a recent surge in natural wetland emissions is one main cause of increasing CH_4 levels, in response to abnormally high temperatures in northern high latitudes in 2007, and increased rainfall over tropical wetlands during 2008–2009 and 2010–2011[13,53,60], two La Niña periods[4]. Furthermore, fossil fuel CH_4 emissions probably increased again after 2005, mostly due to the intensification of shale gas and oil extraction in the United States and coal exploitation by the Chinese and Indian economies[45].

After 2005, the three scenarios use fossil fuel emission changes from the EPA inventory, and the average of EPA and EDGAR4.2 inventories for all other sources barring natural wetlands. Microbial and fossil fuel sources for all scenarios show positive trends after 2005, resulting in an increase of global emissions of 23–33 Tg CH_4 yr^{-1} around 2010 as compared to around 2005 (five-year basis averages). This is a 30% overestimation compared with the mean increase derived from the observations

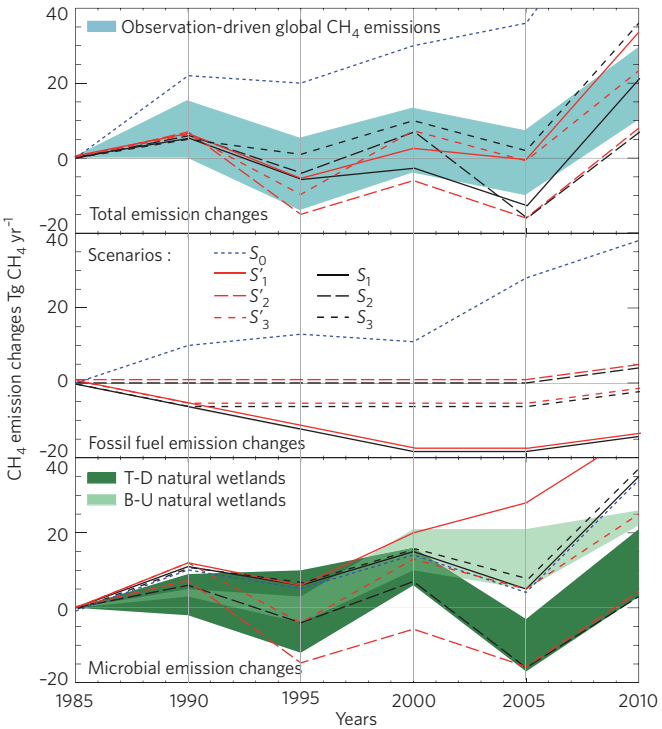

Figure 4 | Plausible scenarios explaining changes in methane emissions over the past three decades. Different lines depict different scenarios of five-year-averaged emission changes since 1985 (see Methods): S_0 (dotted blue lines), S_1 and S'_1 (solid black and red lines), S_2 and S'_2 (long-dashed black and red lines), S_3 and S'_3 (short-dashed black and red lines) Top: range of global CH_4 emission changes (blue shaded area) around a mean inversion (Methods and Supplementary Section ST5). Middle: emission changes from fossil fuels (coal, gas and oil industries). Bottom: emission changes from microbial sources (natural wetlands, rice, animals and waste). The dark and light green shaded areas represent the range of top-down (T-D) and bottom-up (B-U) model results, respectively, for natural wetland emissions.

(17–22 Tg CH_4 yr^{-1}, see above). Thus, either the increase in fossil fuel emissions is overestimated by inventories, or the sensitivity of wetland emissions to precipitation and temperature is too large in some wetland emission models[39]. The contribution of microbial versus fossil emissions to this increase remains largely uncertain; respective contributions vary from 20 to 80%, if accounting for all additional top-down inversions available for the 2000s (Supplementary Fig. S5 and Table 1).

Shortcomings and uncertainty reductions

Our analyses suggest four main shortcomings in the assessment of regional to global CH_4 budgets. First, decadal means and interannual changes in CH_4 emissions from natural wetlands and freshwater systems are too uncertain. It is critically important to improve wetland mapping, both by refining land surface models (for example, through improving estimates of tropical flood plains in hydrological models, specific model developments for peatlands, and the integration of freshwater systems) and by further developing remotely sensed inundation data sets[61] (for instance for dense tropical forests). The scarcity of wetland CH_4 flux measurements and data sets limits the ability to validate large-scale modelled CH_4 emissions for natural wetlands and fresh waters[43]. The extension of the CO_2 FLUXNET measurements and database[62] to CH_4 fluxes is probably achievable at a reasonable cost, and would provide useful constraints for land surface models. For interannual variations in wetland emissions, the sensitivity of emission rates to warming at

high northern latitudes and to rainfall changes in the tropics needs to be more consistently quantified in wetland models. The Amazon drought in 2010[63] should have resulted in a drop in wetland CH_4 emissions, and ongoing analyses may allow researchers to test the hypothesis that tropical wetland CH_4 emissions respond strongly to rainfall anomalies and trends.

Second, the partitioning of CH_4 emissions by region and process is not sufficiently constrained by atmospheric observations in top-down models. Regional partitioning of total emissions would benefit from denser and more evenly distributed CH_4 concentration data. This can be achieved by further developing synergies between high precision monitoring of the surface and the lower atmosphere, including poorly sampled key areas such as the Amazon Basin, Siberia and tropical Africa on one hand, and retrievals of global-scale CH_4 columns by satellites and by high precision remote sensing from the ground on the other. Including continuous measurements of the $\delta^{13}C$ stable isotope ($^{13}CH_4$) at surface stations would help separate biogenic emissions from other sources. Measurements of the δD stable isotope (CH_3D) would provide constraints on the uncertain OH CH_4 sink, which can also be constrained by new proxy tracers[33,34]. Radiocarbon CH_4 data ($^{14}CH_4$) would help constrain the uncertain fossil part of CH_4 emissions, if $^{14}CH_4$ emissions from nuclear installations can be accurately estimated[37]. Estimating long-term trends of fluxes and concentrations requires equally long-term observations, which in turn require stable and coordinated networks[64].

Third, decadal trends in natural and anthropogenic emissions are still very uncertain and limit our ability to definitively attribute changes in emissions from specific sources to observed atmospheric changes since the 1990s. In addition to the (already noted) improvements in land surface models required, inventories for anthropogenic emissions should systematically include an uncertainty assessment, and should improve their representation of emission trends (for instance by more frequently updating the time-dependent factors used in their calculations).

Fourth, uncertainties in the modelling of atmospheric transport and chemistry limit the optimal assimilation of atmospheric observations by increasing uncertainties in top-down inversions. Such uncertainties are also only partly estimated in current inversions. We therefore recommend the continuation of ongoing international model inter-comparisons, which can provide a quantification of transport and chemistry errors to be included in top-down inversions[65,66].

From challenge to opportunity

Our decadal CH_4 budgets reveal that bottom-up models may overestimate total natural CH_4 emissions. The various emission scenarios tested — designed to explain the temporal changes in atmospheric CH_4 levels observed in this and previous studies — suggest that the stabilization of atmospheric CH_4 in the early 2000s is likely to be due to a reduction in or stabilization of fossil fuel emissions, combined with a stabilization of or increase in microbial emissions. After 2006, the renewed global increase in atmospheric CH_4 is consistent with higher emissions from wetlands and fossil fuel burning, but the relative contributions remain uncertain.

In the context of climate change mitigation, atmospheric CH_4 poses both an opportunity and a challenge. The challenge lies in more accurately quantifying the CH_4 budget and its variations. Our synthesis suggests that improvements in models of natural wetland and freshwater emissions, the integration of surface networks monitoring CH_4 concentrations and fluxes (including isotopic composition) and new satellite missions (including active space-borne observations[67]), improvements in anthropogenic emission trends in inventories, and uncertainty reductions in models of atmospheric transport and chemistry, could all help. The opportunity lies in the possibility of developing short-term climate change mitigation policies that take advantage of the relatively short atmospheric lifetime of CH_4 of about 10 years, and the known technological and agronomical options available for reducing emissions[68].

The potential intensive exploitation of natural gas from shale formations around the world may lead to significant additional CH_4 release into the atmosphere[69], although the potential magnitude of these emissions is still debated[70]. Such additional emissions, and combustion of this 'new' fossil fuel source, may offset mitigation efforts and accelerate climate change. In the longer term, the thawing of permafrost or hydrates could increase CH_4 emissions significantly, and introduce large positive feedbacks to long-term climate change[71]. A better quantification of the global CH_4 budget, with regular updates as done for carbon dioxide[72], will be key to both embracing the opportunities and meeting the challenge.

Methods

Data analysis. Top-down and bottom-up studies addressing the evolution of the CH_4 cycle after 1980 and covering at least five years of a decade were gathered. Therefore, the number and the nature of studies used in this work vary from one decade to another. Top-down inversions include atmospheric chemistry transport models and assimilation systems[19,46,53,73–77]. Bottom-up approaches comprise modelling studies for wetland[40–42] and biomass-burning emissions[47,78–80], emission inventories for anthropogenic[55,56,81] and natural sources[82], and a suite of atmospheric chemistry models within the ACCMIP intercomparison project providing CH_4 chemical loss[30,39,83].

The monthly fluxes (emissions and sinks) provided by the different groups were post-processed similarly. They were re-gridded on a common grid (1°× 1) and converted into the same units (Tg CH_4 per grid cell); then monthly, annual and decadal means were computed for 12 regions based on the TransCom[84] intercomparison map, with subdivisions in high-emission regions. Regional and global means were used to construct Figs 1, 2 and 3, Supplementary Figs S2 and S3, Table 1 and Supplementary Tables S2 and S3.

The reported ranges and error bars represent the minimum and maximum values obtained among the different studies (Figs 1, 3 and 4 and Table 1). The small number of studies for some categories makes it difficult to properly apply a standard deviation.

Interannual variability (IAV) was computed as the difference between the 12-month running mean and the long-term mean. However a consistent period for estimating the long-term mean was not compatible with all data sources (Supplementary Fig. S5).

Observation-driven global CH_4 emissions. For 'attribution of temporal changes', we used the only top-down study that estimates CH_4 emissions over the past 30 years[53] with five different set-ups. The mean of these five inversions was assumed to represent average global emissions. However these five inversions only partially represented the full range of global CH_4 emissions, due to differences in prior emission scenarios and errors, observations and their errors, OH fields and atmospheric transport representation. To estimate the full range of global CH_4 emissions we complemented the mean inversion with a sensitivity analysis based on a one-box model for the whole atmosphere[54]. The change in the global burden of CH_4 is given by:

$$\frac{d[CH_4]}{dt} = E - \frac{[CH_4]}{\tau} \quad (1)$$

where $[CH_4]$ is the global CH_4 burden, E is the sum of all emissions, and τ is the total atmospheric CH_4 lifetime. Equation (1) can be rearranged to calculate the annual CH_4 source strength E as follows:

$$E = \frac{d[CH_4]}{dt} + \frac{[CH_4]}{\tau} \quad (2)$$

In this equation, the annual increase $d[CH_4]/dt$ and the burden $[CH_4]$ were given by the yearly–averaged growth rates and mole fractions of Fig. 1. Global CH_4 emissions were generated by computing emissions with equation (2) for each of the four networks and for a lifetime τ varying from 8 to 10 years to include uncertainties in OH changes[34,85]. Minimum and maximum values of E were extracted for five-year periods to produce the range of emissions plotted around the mean of atmospheric inversions (blue shaded area in Fig. 4, top panel).

Emission scenarios. The emission scenarios are based on five-year average CH_4 fluxes around the years 1985, 1990, 1995, 2000, and 2005. For 2010 we used available years between 2008 and 2012, mainly before 2010. Flux changes from 2005 to 2010 might be slightly biased by missing years after 2010. For example, fossil and microbial emissions both increase between 2005 and 2009; if after 2010 these emissions were further increasing (or decreasing), then the 2005-2010 changes will be underestimated (or overestimated). We assume that such a potential bias does not modify the (mostly) qualitative message of our scenario analysis. The five-year

changes from biomass burning remain small (<2 Tg CH_4 per five-year period) and were not considered here.

The scenarios presented in Fig. 4 use either natural wetland emissions from top-down inversions (S_x) or bottom-up models (S'_x). Other data are taken from recent publications and EDGAR4.2 and EPA inventories.

S_0 and S'_0 are built by summing the mean wetland emissions from inversions and the mean of EPA (ref. 55) and EDGAR4.2 (ref. 56) 'other' emissions. Scenarios S_1 and S'_1 sum the mean wetland emissions with decreasing (1985–2000), constant (2000–2005), and increasing (2005–2010) fossil fuel emissions to be compatible with a recent analysis[15]. Scenarios S_2 and S'_2 sum the mean wetland emissions with constant (1985–2005) and increasing (2005–2010) fossil fuel emissions. Other microbial emissions (mean of EPA and EDGAR) are scaled to a recent study[58]. Scenarios S_3 and S'_3 sum the mean wetland emissions with decreasing (1985–1990), constant (1990–2005), and increasing (2005–2010) fossil fuel emissions. Other microbial emissions (mean of EPA and EDGAR) are scaled to remain constant during 1990–2005 according to another recent study[59]. After 2005, all scenarios include fossil fuel emission changes from the EPA inventory, wetland emission changes from inversions or bottom-up studies and other emission changes from the mean of EPA and EDGAR4.2.

Received 17 April 2012; accepted 22 August 2013; published online 22 September 2013

References

1. Etheridge, D. M., Pearman, G. I. & Fraser, P. J. Changes in tropospheric methane between 1841 and 1978 from a high accumulation-rate Antarctic ice core. *Tellus* **44B**, 282–294 (1992).
2. Blake, D. R. *et al.* Global increase in atmospheric methane concentrations between 1978 and 1980. *Geophys. Res. Lett.* **9,** 477–480 (1982).
3. Cunnold, D. M. *et al. In situ* measurements of atmospheric methane at GAGE/AGAGE sites during 1985–2000 and resulting source inferences. *J. Geophys. Res.: Atmos.* http://dx.doi.org/10.1029/2001jd001226 (2002).
4. Dlugokencky, E. J. *et al.* Observational constraints on recent increases in the atmospheric CH burden. *Geophys. Res. Lett.,* **36**, L18803 (2009).
5. Francey, R. J., Steele, L. P., Langenfelds, R. L. & Pak, B. C. High precision long-term monitoring of radiatively active and related trace gases at surface sites and from aircraft in the southern hemisphere atmosphere. *J. Atmos. Sci.* **56,** 279–285 (1999).
6. World Data Centre for Greenhouse Gases (WMO/WDCGG) (2012); http://ds.data.jma.go.jp/gmd/wdcgg/introduction.html.
7. Brenninkmeijer, C. A. M. *et al.* Civil Aircraft for the regular investigation of the atmosphere based on an instrumented container: The new CARIBIC system. *Atmos. Chem. Phys.* **7,** 4953–4976 (2007).
8. Wecht, K. J. *et al.* Validation of TES methane with HIPPO aircraft observations: implications for inverse modeling of methane sources. *Atmos. Chem. Phys.* **12,** 1823–1832 (2012).
9. Schuck, T. J. *et al.* Distribution of methane in the tropical upper troposphere measured by CARIBIC and CONTRAIL aircraft. *J. Geophys. Res.: Atmos.* **117,** D19304 (2012).
10. Crevoisier, C. *et al.* Tropospheric methane in the tropics — first year from IASI hyperspectral infrared observations. *Atmos. Chem. Phys.* **9,** 6337–6350 (2009).
11. Frankenberg, C. *et al.* Global column-averaged methane mixing ratios from 2003 to 2009 as derived from SCIAMACHY: Trends and variability. *J. Geophys. Res.: Atmos.* **116,** D04302 (2011).
12. Morino, I. *et al.* Preliminary validation of column-averaged volume mixing ratios of carbon dioxide and methane retrieved from GOSAT short-wavelength infrared spectra. *Atmos. Meas. Tech.* **4,** 1061–1076 (2011).
13. Dlugokencky, E. J., Nisbet, E. G., Fisher, R. & Lowry, D. Global atmospheric methane: budget, changes and dangers. *Phil. Trans. R. Soc. A* **369,** 2058–2072 (2011).
14. Rigby, M. *et al.* Renewed growth of atmospheric methane. *Geophys. Res. Lett.* **35,** L22805 (2008).
15. Simpson, I. J. *et al.* Long-term decline of global atmospheric ethane concentrations and implications for methane. *Nature* **488,** 490–494 (2012).
16. Denman, K. L. *et al.* in *IPCC Climate Change 2007: Couplings Between Changes in the Climate System and Biogeochemistry* (eds Solomon, S. *et al.*) (Cambridge Univ. Press; 2007).
17. Cicerone, R. J. & Oremland, R. S. Biogeochemical aspects of atmospheric methane. *Glob. Biogeochem. Cycles* **2,** 299–327 (1988).
18. Ehhalt, D. H. The atmospheric cycle of methane. *Tellus* **26,** 58–70 (1974).
19. Fung, I. *et al.* Three-dimensional model synthesis of global methane cycle. *J. Geophys. Res.* **96,** 13033–13065 (1991).
20. Monteil, G. *et al.* Interpreting methane variations in the past two decades using measurements of CH_4 mixing ratio and isotopic composition. *Atmos. Chem. Phys.* **11,** 9141–9153 (2011).
21. Bousquet, P. *et al.* Contribution of anthropogenic and natural sources to atmospheric methane variability. *Nature* **443,** 439–443 (2006).
22. Neef, L., van Weele, M. & van Velthoven, P. Optimal estimation of the present-day global methane budget. *Glob. Biogeochem. Cycles* **24,** GB4024 (2010).
23. Wahlen, M., Tanaka, N., Henry, R. & Yoshinari, T. ^{13}C, D and ^{14}C in methane. *Eos* **68,** 1220 (1987).
24. Fisher, R. E. *et al.* Arctic methane sources: Isotopic evidence for atmospheric inputs. *Geophys. Res. Lett.* **38,** L21803 (2011).
25. Keppler, F., Hamilton, J. T. G., Brass, M. & Rockmann, T. Methane emissions from terrestrial plants under aerobic conditions. *Nature* **439,** 187–191 (2006).
26. Nisbet, R. E. R. *et al.* Emission of methane from plants. *Proc. R. Soc. B-Biol. Sci.* **276,** 1347–1354 (2009).
27. Curry, C. L. Modeling the soil consumption of atmospheric methane at the global scale. *Glob. Biogeochem. Cycles* **21,** GB4012 (2007).
28. Zhuang, Q. *et al.* Methane fluxes between terrestrial ecosystems and the atmosphere at northern high latitudes during the past century: A retrospective analysis with a process-based biogeochemistry model. *Glob. Biogeochem. Cycles* **18,** GB3010 (2004).
29. Allan, W., Struthers, H. & Lowe, D. C. Methane carbon isotope effects caused by atomic chlorine in the marine boundary layer: Global model results compared with Southern Hemisphere measurements. *J. Geophys. Res.: Atmos.* **112,** D04306 (2007).
30. Naik, V. *et al.* Preindustrial to present day changes in tropospheric hydroxyl radical and methane lifetime from the Atmospheric Chemistry and Climate Model Intercomparison Project (ACCMIP). *Atmos. Chem. Phys.* **13,** 5277–5298 (2013).
31. Bastviken, D., Tranvik, L. J., Downing, J. A., Crill, P. M. & Enrich-Prast, A. Freshwater methane emissions offset the continental carbon sink. *Science* **331,** 50 (2011).
32. Walter, K. M., Smith, L. C. & Stuart Chapin, F. Methane bubbling from northern lakes: present and future contributions to the global methane budget. *Phil. Trans. R. Soc. A* **365,** 1657–1676 (2007).
33. Huang, J. & Prinn, R. G. Critical evaluation of emissions of potential new gases for OH estimation. *J. Geophys. Res.* **107,** 4784 (2002).
34. Montzka, S. A. *et al.* Small interannual variability of global atmospheric hydroxyl. *Science* **331,** 67–69 (2011).
35. Etiope, G., Lassey, K. R., Klusman, R. W. & Boschi, E. Reappraisal of the fossil methane budget and related emission from geologic sources. *Geophys. Res. Lett.* **35,** L09307 (2008).
36. Shakhova, N. *et al.* Extensive methane venting to the atmosphere from sediments of the East Siberian Arctic Shelf. *Science* **327,** 1246 (2010).
37. Lassey, K. R., Lowe, D. C. & Smith, A. M. The atmospheric cycling of radiomethane and the "fossil fraction" of the methane source. *Atmos. Chem. Phys.* **7,** 2141–2149 (2007).
38. Voulgarakis, A. *et al.* Analysis of present day and future OH and methane lifetime in the ACCMIP simulations. *Atmos. Chem. Phys.* **13,** 2563–2587 (2013).
39. Melton, J. R. *et al.* Present state of global wetland extent and wetland methane modelling: conclusions from a model intercomparison project (WETCHIMP). *Biogeosciences* **10,** 753–788 (2013).
40. Hodson, E. L., Poulter, B., Zimmermann, N. E., Prigent, C. & Kaplan, J. O. The El Niño Southern Oscillation and wetland methane interannual variability. *Geophys. Res. Lett.* **38,** L08810 (2011).
41. Ringeval, B. *et al.* Climate-CH_4 feedback from wetlands and its interaction with the climate-CO_2 feedback. *Biogeosciences* **8,** 2137–2157 (2011).
42. Spahni, R. *et al.* Constraining global methane emissions and uptake by ecosystems. *Biogeosciences* **8,** 1643–1665 (2011).
43. Riley, W. J. *et al.* Barriers to predicting changes in global terrestrial methane fluxes: analyses using CLM4Me, a methane biogeochemistry model integrated in CESM. *Biogeosciences* **8,** 1925–1953 (2011).
44. Mastrandrea, M. D. *et al. Guidance Note for Lead Authors of the IPCC Fifth Assessment Report on Consistent Treatment of Uncertainties* (IPCC, 2010); http://www.ipcc.ch.
45. Ohara, T. *et al.* An Asian emission inventory of anthropogenic emission sources for the period 1980–2020 *Atmos Chem Phys* **7,** 4419–4444 (2007).
46. Bergamaschi, P. *et al.* Inverse modeling of global and regional CH4 emissions using SCIAMACHY satellite retrievals. *J. Geophys. Res.* http://dx.doi.org/10.1029/2009JD012287 (2009).
47. Van der Werf, G. R. *et al.* Global fire emissions and the contribution of deforestation, savanna, forest, agricultural, and peat fires (1997–2009). *Atmos. Chem. Phys.* **10,** 11707–11735 (2010).
48. Sanderson, M. G. Biomass of termites and their emissions of methane and carbon dioxide: A global database. *Glob. Biogeochem. Cycles* **10,** 543–557 (1996).
49. Bousquet, P., Hauglustaine, D. A., Peylin, P., Carouge, C. & Ciais, P. Two decades of OH variability as inferred by an inversion of atmospheric transport and chemistry of methyl chloroform. *Atmos. Chem. Phys.* **5,** 2635–2656 (2005).

50. Simpson, I. J., Rowland, F. S., Meinardi, S. & Blake, D. R. Influence of biomass burning during recent fluctuations in the slow growth of global tropospheric methane. *Geophys. Res. Lett.* **33,** L22808 (2006).
51. Dlugokencky, E. J. *et al.* Changes in CH_4 and CO growth rates after the eruption of Mt Pinatubo and their link with changes in tropical tropospheric UV flux. *Geophys. Res. Lett.* **23,** 2761–2764 (1996).
52. Langenfelds, R. L. *et al.* Interannual growth rate variations of atmospheric CO_2 and its delta ^{13}C, H_2, CH_4, and CO between 1992 and 1999 linked to biomass burning. *Glob. Biogeochem. Cycles* **16,** 1048 (2002).
53. Bousquet, P. *et al.* Source attribution of the changes in atmospheric methane for 2006–2008 *Atmos. Chem. Phys.* **11,** 3689–3700 (2011).
54. Dlugokencky, E. J., Masarie, K. A., Lang, P. M. & Tans, P. P. Continuing decline in the growth rate of the atmospheric methane burden. *Nature* **393,** 447–450 (1998).
55. Environmental Protection Agency. Global Anthropogenic Non-CO_2 Greenhouse Gas Emissions: 1990–2030. (US Environmental Protection Agency, 2011).
56. European Commission, Joint Research Centre/Netherlands Environmental Assessment Agency. Emission Database for Global Atmospheric Research (EDGAR) (version 4.2) (2011); http://edgar.jrc.ec.europa.eu.
57. Aydin, M. *et al.* Recent decreases in fossil-fuel emissions of ethane and methane derived from firn air. *Nature* **476,** 198–201 (2011).
58. Kai, F. M., Tyler, S. C., Randerson, J. T. & Blake, D. R. Reduced methane growth rate explained by decreased Northern Hemisphere microbial sources. *Nature* **476,** 194–197 (2011).
59. Levin, I. *et al.* No inter-hemispheric $\delta^{13}CH_4$ trend observed. *Nature* **486,** E3–E4 (2012).
60. Bloom, A. A., Palmer, P. I., Fraser, A., Reay, D. S. & Frankenberg, C. Large-scale controls of methanogenesis inferred from methane and gravity spaceborne data. *Science* **327,** 322–325 (2010).
61. Prigent, C., Papa, F., Aires, F., Rossow, W. B. & Matthews, E. Global inundation dynamics inferred from multiple satellite observations, 1993–2000. *J. Geophys. Res.* **112,** D12107 (2007).
62. FLUXNET database; http://fluxnet.ornl.gov.
63. Lewis, S. L., Brando, P. M., Phillips, O. L., van der Heijden, G. M. F. & Nepstad, D. The 2010 Amazon drought. *Science* **331,** 554–554 (2011).
64. Houweling, S. *et al.* Iconic CO2 Time Series at Risk. *Science* **337,** 1038–1040 (2012).
65. Lamarque, J. F. *et al.* The Atmospheric Chemistry and Climate Model Intercomparison Project (ACCMIP): overview and description of models, simulations and climate diagnostics. *Geosci. Model Dev.* **6,** 179–206 (2013).
66. Patra, P. K. *et al.* TransCom model simulations of CH_4 and related species: linking transport, surface flux and chemical loss with CH_4 variability in the troposphere and lower stratosphere. *Atmos. Chem. Phys.* **11,** 12813–12837 (2011).
67. Kiemle, C. *et al.* Sensitivity studies for a space-based methane lidar mission. *Atmos. Meas. Tech.* **4,** 2195–2211 (2011).
68. Shindell, D. *et al.* Simultaneously mitigating near-term climate change and improving human health and food security. *Science* **335**, 183–189 (2012).
69. Howarth, R., Santoro, R. & Ingraffea, A. Methane and the greenhouse-gas footprint of natural gas from shale formations. *Climatic Change* **106,** 679–690 (2011).
70. Cathles, L., Brown, L., Taam, M. & Hunter, A. A commentary on "The greenhouse-gas footprint of natural gas in shale formations" by R. W. Howarth, R. Santoro, and Anthony Ingraffea. *Climatic Change* **113,** 525–535 (2012).
71. Koven, C. D. *et al.* Permafrost carbon-climate feedbacks accelerate global warming. *Proc. Natl Acad. Sci. USA* **108,** 14769–14774 (2011).
72. Global Carbon Project (2013); http://www.globalcarbonproject.org/index.htm.
73. Bruhwiler, L., Dlugokencky, E. J. & Masarie, K. *AGU Fall Meeting* abstr. B11G-01 (2011).
74. Chen, Y. H. & Prinn, R. G. Estimation of atmospheric methane emissions between 1996 and 2001 using a three-dimensional global chemical transport model. *J. Geophys. Res.* **111,** D10307 (2006).
75. Fraser, A. *et al.* Estimating regional methane surface fluxes: the relative importance of surface and GOSAT mole fraction measurements. *Atmos. Chem. Phys.* **13,** 5697–5713 (2013).
76. Hein, R., Crutzen, P. J. & Heimann, M. An inverse modeling approach to investigate the global atmospheric methane cycle. *Glob. Biogeochem. Cycles* **11,** 43–76 (1997).
77. Pison, I., Bousquet, P., Chevallier, F., Szopa, S. & Hauglustaine, D. Multi-species inversion of CH4, CO and H-2 emissions from surface measurements. *Atmos. Chem. Phys.* **9,** 5281–5297 (2009).
78. Mieville, A. *et al.* Emissions of gases and particles from biomass burning during the 20th century using satellite data and an historical reconstruction. *Atmos. Environ.* **44,** 1469–1477 (2010).
79. Van het Bolscher, M. *et al.* Emission data sets and methodologies for estimating emissions (eds Schultz, M. G. & Rast, S.) (2007).
80. Wiedinmyer, C. *et al.* The Fire INventory from NCAR (FINN): a high resolution global model to estimate the emissions from open burning. *Geosci. Model Dev.* **4,** 625–641 (2011).
81. Dentener, F. *et al.* The impact of air pollutant and methane emission controls on tropospheric ozone and radiative forcing: CTM calculations for the period 1990–2030 *Atmos. Chem. Phys.* **5,** 1731–1755 (2005).
82. Environmental Protection Agency. Methane and Nitrous Oxide Emissions From Natural Sources. (US Environmental Protection Agency, 2010).
83. Williams, J. E., Strunk, A., Huijnen, V. & van Weele, M. The application of the Modified Band Approach for the calculation of on-line photodissociation rate constants in TM5: implications for oxidative capacity. *Geosci. Model Dev.* **5,** 15–35 (2012).
84. Gurney, K. R. *et al.* Transcom 3 inversion intercomparison: Model mean results for the estimation of seasonal carbon sources and sinks. *Glob. Biogeochem. Cycles* **18**, GB2010 (2004).
85. Prinn, R. G. *et al.* Evidence for substantial variations of atmospheric hydroxyl radicals in the past two decades. *Science* **292,** 1882–1888 (2001).
86. Beck, V. *et al.* Methane airborne measurements and comparison to global models during BARCA. *Journal of Geophysical Research: Atmospheres* **117**, D15310 (2012).
87. Dickens, G. R. Methane hydrates in quaternary climate change — The clathrate gun hypothesis. *Science* **299,** 1017–1017 (2003).
88. Hoelzemann, J. J., Schultz, M. G., Brasseur, G. P., Granier, C. & Simon, M. Global Wildland Fire Emission Model (GWEM): Evaluating the use of global area burnt satellite data. *J. Geophys. Res.* **109,** D14S04 (2004).
89. Ito, A. & Penner, J. E. Global estimates of biomass burning emissions based on satellite imagery for the year 2000. *J. Geophys. Res.* **109**, D14S05 (2004).
90. Rhee, T. S., Kettle, A. J. & Andreae, M. O. Methane and nitrous oxide emissions from the ocean: A reassessment using basin-wise observations in the Atlantic. *J. Geophys. Res.* **114,** D12304 (2009).
91. Sugimoto, A., Inoue, T., Kirtibutr, N. & Abe, T. Methane oxidation by termite mounds estimated by the carbon isotopic composition of methane. *Glob. Biogeochem. Cycles* **12,** 595–605 (1998).
92. Kasibhatla, K. *et al. Inverse Methods in Global Biogeochemical Cycles, Volume 114* (AGU, 2000).
93. Rodgers, C. D. *Inverse Methods for Atmospheric Sounding: Theory and Practice* (World Scientific, 2000).
94. Krol, M. & Lelieveld, J. Can the variability in tropospheric OH be deduced from measurements of 1,1,1-trichloroethane (methyl chloroform)? *J. Geophys. Res.* **108,** 4125 (2003).

Acknowledgements

This paper is the result of an international collaboration of scientists organized by the Global Carbon Project, a joint project of the Earth System Science Partnership. This work was supported by: the UK NERC National Centre for Earth Observation; the European Commission's 7th Framework Programme (FP7/2007-2013) projects MACC (grant agreement no. 218793) and GEOCARBON (grant agreement no. 283080); contract DE-AC52-07NA27344 with different parts supported by the US DOE IMPACTS and SciDAC Climate Consortium projects; computing resources of NERSC, which is supported by the US DOE under contract DE-AC02-05CH11231; NOAA flask data for CH_3CCl_3 (made available by S. Montzka); the Australian Climate Change Science Program, and ERC grant 247349. Simulations from LSCE were performed using HPC resources from DSM-CCRT and CCRT/CINES/IDRIS under the allocation 2012-t2012012201 made by GENCI (Grand Equipement National de Calcul Intensif). We thank the EDGAR group at JRC (Italy) and US-EPA for providing estimates of anthropogenic emissions.

Author contributions

S.K., P. Bousquet, P.C., J.G.C. and C.L.Q. designed the study and provided conceptual advice. S.K., P. Bousquet and M. Saunois processed data sets, developed figures and wrote the manuscript. E.J.D., M. Schmidt, P.J.F., P.B.K., L.P.S., R.L.L., R.G.P., M.R., R.F.W., D.R.B. and I.J.S. provided atmospheric *in situ* data. P.Bousquet, P.Bergamaschi, L.B., F.C., L.F., A.F., S.H., P.I.P. and I.P. provided top-down inversion results (all five emission categories). S.C., E.L.H., B.P., B.R., M.Santini, R.S. and G.R.v.d.W provided bottom-up modelling and inventory data sets for wetland, biomass burning and termite emissions. D.B., P.C.-S., B.J., J.-F.L., V.N., D.P., D.T.S., S.A.S., K.S., S.S., A.V., M.v.W., J.E.W. and G.Z. provided bottom-up estimates of CH_4 loss due to OH. All authors contributed extensively to the work presented in this paper, and to revisions of the manuscript.

Additional information

Reprints and permissions information is available online at www.nature.com/reprints. Correspondence should be addressed to philippe.bousquet@lsce.ipsl.fr.

Competing financial interests

The authors declare no competing financial interests.

Stefanie Kirschke[1], Philippe Bousquet[1]*, Philippe Ciais[1], Marielle Saunois[1], Josep G. Canadell[2], Edward J. Dlugokencky[3], Peter Bergamaschi[4], Daniel Bergmann[5], Donald R. Blake[6], Lori Bruhwiler[3], Philip Cameron-Smith[5], Simona Castaldi[7,8], Frédéric Chevallier[1], Liang Feng[9], Annemarie Fraser[9], Martin Heimann[10], Elke L. Hodson[11], Sander Houweling[12,13], Béatrice Josse[14], Paul J. Fraser[15], Paul B. Krummel[15], Jean-François Lamarque[16], Ray L. Langenfelds[15], Corinne Le Quéré[17], Vaishali Naik[18], Simon O'Doherty[19], Paul I. Palmer[9], Isabelle Pison[1], David Plummer[20], Benjamin Poulter[1], Ronald G. Prinn[21], Matt Rigby[22], Bruno Ringeval[13,23,24], Monia Santini[8], Martina Schmidt[1], Drew T. Shindell[25], Isobel J. Simpson[6], Renato Spahni[26], L. Paul Steele[15], Sarah A. Strode[27,28], Kengo Sudo[29], Sophie Szopa[1], Guido R. van der Werf[30], Apostolos Voulgarakis[25,31], Michiel van Weele[32], Ray F. Weiss[33], Jason E. Williams[32] and Guang Zeng[34]

[1]LSCE-CEA-UVSQ-CNRS, Orme des Merisiers, 91190 Gif-sur-Yvette, France, [2]Global Carbon Project, CSIRO Marine and Atmospheric Research, GPO Box 3023, Canberra, ACT 2601, Australia, [3]NOAA ESRL, 325 Broadway, Boulder, Colorado 80305, USA, [4]Institute for Environment and Sustainability, Joint Research Centre, TP290, I-21027 Ispra (Va), Italy, [5]Lawrence Livermore National Laboratory, PO Box 808, Livermore, California 94551-0808, USA, [6]University of California Irvine, 570 Rowland Hall, Irvine, California 92697, USA, [7]Department of Environmental Sciences, Second University of Naples, via Vivaldi 43, 81100 Caserta, Italy, [8]Centro Euro-Mediterraneo sui Cambiamenti Climatici (CMCC), via Augusto Imperatore 16, 73100 Lecce, Italy, [9]School of Geosciences, University of Edinburgh, Crew Building, West Mains Road, Edinburgh, EH9 3JN, UK, [10]Max Planck Institute for Biogeochemistry, PF 100164, D-07701 Jena, Germany, [11]Swiss Federal Research Institute WSL, Zuercherstrasse 111, 8903 Mensdorf, Switzerland, [12]SRON, Netherlands Institute for Space Research, Sorbonnelaan 2, 3584 CA Utrecht, The Netherlands, [13]Institue for Marine and Atmospheric Research Utrecht, Sorbonnelaan 2, 3584 CA Utrecht, The Netherlands, [14]Météo France, CNRM/GMGEC/CARMA, 42 av G. Coriolis, 31057 Toulouse, France, [15]Centre for Australian Weather and Climate Research/CSIRO Marine and Atmospheric Research, Aspendale, Victoria 3195, Australia, [16]NCAR, PO Box 3000, Boulder, Colorado 80307-3000, USA, [17]Tyndall Centre for Climate Change Research, University of East Anglia, Norwich Research Park, Norwich, NR4 7TJ, UK, [18]UCAR/NOAA Geophysical Fluid Dynamics Laboratory, 201 Forrestal Road, Princeton, New Jersey 08540, USA, [19]University of Bristol, Office Old Park Hill, Cantock's Close, Clifton, Bristol BS8 1TS, UK, [20]Canadian Centre for Climate Modelling and Analysis, Environment Canada, 550 Sherbrooke Street West, West Tower, Montréal, Quebec, H3A 1B9, Canada, [21]Massachusetts Institute of Technology, Building 54-1312, Cambridge, Massachusetts 02139-2307, USA, [22]School of Chemistry, University of Bristol, Cantocks Close, Bristol BS8 1TS, UK, [23]IMAU, Utrecht University, Princetonplein 5, 3584 CC Utrecht, The Netherlands, [24]Department of Systems Ecology, VU University Amsterdam, De Boelelaan 1085, 1081 HV Amsterdam, The Netherlands, [25]NASA Goddard Institute for Space Studies, 2880 Broadway, New York, New York 10025, USA, [26]University of Bern, Physics Institute, Climate and Environmental Physics, Sidlerstrasse 5, CH-3012 Bern, Switzerland, [27]NASA Goddard Space Flight Centre, Greenbelt, Maryland 20771, USA, [28]Universities Space Research Association, NASA Goddard Space Flight Centre, Greenbelt, Maryland 20771, USA, [29]Graduate School of Environmental Studies, Nagoya University Furo-cho, Chikusa-ku, Nagoya 464-8601, Japan, [30]VU University, Faculty of Earth and Life Sciences, De Boelelaan 1085, 1081 HV Amsterdam, The Netherlands, [31]Department of Physics, Imperial College London, London SW7 2AZ, UK, [32]Royal Netherlands Meteorological Institute (KNMI), PO Box 201, 3730 AE De Bilt, The Netherlands, [33]Scripps Institution of Oceanography, UCSD, La Jolla, California 92093-0244, USA, [34]National Institute of Water and Atmospheric Research, Private Bag 50061, Omakau, Central Otago 9352, New Zealand. *e-mail: Philippe.Bousquet@lsce.ipsl.fr

nature geoscience
SUPPLEMENTARY INFORMATION
DOI: 10.1038/NGEO1955

Three decades of global methane sources and sinks

Stefanie Kirschke[1], Philippe Bousquet[1], Philippe Ciais[1], Marielle Saunois[1], Josep G. Canadell[2], Edward J. Dlugokencky[3], Peter Bergamaschi[4], Daniel Bergmann[5], Donald R. Blake[6], Lori Bruhwiler[3], Philip Cameron-Smith[5], Simona Castaldi[7,8], Frédéric Chevallier[1], Liang Feng[9], Annemarie Fraser[9], Paul J. Fraser[15], Martin Heimann[10], Elke L. Hodson[11], Sander Houweling[12,13], Béatrice Josse[14], Paul B. Krummel[15], Jean-François Lamarque[16], Ray L. Langenfelds[15], Corinne Le Quéré[17], Vaishali Naik[18], Simon O'Doherty[19], Paul I. Palmer[9], Isabelle Pison[1], David Plummer[20], Benjamin Poulter[1], Ronald G. Prinn[21], Matt Rigby[22], Bruno Ringeval[13,23,24], Monia Santini[8], Martina Schmidt[1], Drew T. Shindell[25], Isobel J. Simpson[6], Renato Spahni[26], L. Paul Steele[15], Sarah A. Strode[27,28], Kengo Sudo[29], Sophie Szopa[1], Guido R. van der Werf[30], Apostolos Voulgarakis[25,31], Michiel van Weele[32], Ray F. Weiss[33], Jason E. Williams[32], Guang Zeng[34]

[1]LSCE-CEA-UVSQ-CNRS France, [2]Global Carbon Project, CSIRO Marine and Atmospheric Research, Australia, [3]NOAA ESRL, USA [3]Institute for Environment and Sustainability, [4]Joint Research Centre, Italy, [5]Lawrence Livermore National Laboratory, USA, [6]University of California Irvine, USA, [7]Department of Environmental Sciences, Second University of Naples, Italy, [8]Centro euro-Mediterraneo per i Cambiamenti Climatici CMCC, Lecce, Italy, [9]School of Geosciences, University of Edinburgh, UK, [10]MPI Biogeochemistry, Germany, [11]Swiss Federal Research Institute WSL, Switzerland, [12]SRON, Netherlands institute for space research, The Netherlands, [13]Institue for Marine and Atmospheric research Utrecht, The Netherlands, [14]Météo France, France, [15]Centre for Australian Weather and Climate Research/CSIRO Marine and Atmospheric Research, Aspendale, Victoria, Australia, [16]NCAR, USA, [17]Tyndall Centre for Climate Change Research, UK, [18]UCAR/GFDL, USA, [19]University of Bristol, UK, [20]CCCma, Environment Canada, [21]Massachusetts Institute of Technology, USA, [22]School of Chemistry, University of Bristol, Bristol, UK, [23]IMAU,

Utrecht University, The Netherlands, [24]Department of Systems Ecology, VU University Amsterdam, The Netherlands, [25]NASA GISS, USA, [26]University of Bern, Switzerland, [27]NASA GSFC, USA, [28]Universities Space Research Association, USA, [29]Graduate School of Environmental Studies, Nagoya University Furo-cho, Japan, [30]VU University, The Netherlands, [31]Department of Physics, Imperial College, London, UK, [32]Royal Netherlands Meteorological Institute (KNMI), The Netherlands, [33]Scripps Institution of Oceanography, USA [34]National Institute of Water and Atmospheric Research, New Zealand.

Corresponding author: Philippe Bousquet, philippe.bousquet@lsce.ipsl.fr

I Supporting text, figures, and tables

I.1 Supporting text

ST1 - Atmospheric CH_4 observations and growth rates for the different atmospheric networks (Figure 1).

Several types of measurements exist for atmospheric methane. High precision measurements (±3 ppb), traceable to the World Meteorological Organisation (WMO) mole fraction international calibration scale, are available from 160 fixed surface stations[1-4] and more than 30 mobile stations (ships and aircraft)[5,6,7]. Atmospheric observations consist of both flask samples (grab samples, weekly or bi-weekly) and continuous data (hourly or better resolution). Precise measurements of total column CH_4 mixing ratio (XCH_4) are provided from the Total Column Carbon Observing Network (TCCON) of 25 ground based remote-sensing stations which are only indirectly linked to the WMO scale[8,9]. Isotopic measurements (^{13}C-CH_4 and deuterium-methane, CH_3D) are performed at a subset of surface stations and help separate biogenic from other CH_4 sources[10-15]. Measurements of ^{14}C-CH_4 at one station help quantify the contribution of fossil CH_4 to the total source mix[16]. Finally, space-borne XCH_4 retrievals (over the last decade only) predominantly originate from three satellites[17-21] providing global coverage albeit with much lower precision (e.g. random error of ~30 ppb for SCIAMACHY[22] and latitudinal biases of up to 40 ppb[23]).

Figure 1 of the paper plots the atmospheric globally averaged CH_4 mole fractions and the associated growth rates for the four global trace gas atmospheric monitoring networks with a global coverage NOAA/ESRL[24], AGAGE[25], CSIRO[26] and UCI[27]. For NOAA/ESRL, AGAGE AND CSIRO. The growth rates have been calculated as the derivative of a trend curve computed according to Thoning et al., (1989)[28]. The growth rate calculations for the UCI network are described further below. Decadal global means of CH_4 mole fractions for the 1990s (1746 ppb) and the 2000s (1776 ppb) are remarkably consistent between the four networks, with respective ranges of [1743-1747 ppb] and [1775-1779 ppb]. Differences on the decadal means are mostly due to representativeness and sampling

differences between networks, and to a lesser extent to instrumental errors. Indeed, regular inter-comparison between networks at various sites shows differences smaller than ±2 ppb. The decadal mean for the 1980s is more uncertain [1663-1690 ppb], possibly because of a more limited spatial and temporal coverage of some of the networks at that time. Growth rates are also very similar in the 1980s [11.3-12.3 ppb.yr^{-1}], the 1990s [4.9-6.5 ppb.yr^{-1}] and the 2000s [2.3-3.6 ppb.yr^{-1}] with mean values of 12±6 ppb.yr^{-1}, 6±8 ppb.yr^{-1}, 2±3 ppb.yr^{-1}, respectively. The associated uncertainty represents the 1-sigma variation from one year to another (inter-annual variability). The difference in the decadal growth rates between the four networks is less than 1 ppb.yr^{-1}.

ST2 - Regional and latitudinal distributions of wetland and biomass burning emissions (Figure S0 and S1)

Using the different top-down and bottom-up models and inventories gathered in this work, we computed averaged maps (Fig. S0) and zonally averaged emission fluxes of CH_4 from natural wetlands (Fig. S0 & S1, top), and biomass-burning (Fig. S0 & S1, bottom). To calculate the mean emissions we used the following time periods: 1990-2006 for wetland emissions and 1980-2006 for biomass burning emissions. As a result, the FINN inventory is not included in Fig S0 and S1. Averaged spatial pattern present common zones of emissions (stippled points on the right panels of Fig. S0): 66±9% for wetland emissions and 38±9% for biomass burning emissions. In Fig. S1, the bottom-up zonal means are presented as coloured solid lines whereas for top-down, only the range (min-max) is shown with the coloured areas. Wetland emissions are mainly located in the Tropics and in the high latitudes. ORCHIDEE's estimates are higher and with more spatial variations than those of LPJ except below 30°S. In the Tropics, LPJ's estimates by 1° band of latitude are around 10-20 Tg/yr, generally below ORCHIDEE's estimates. In the mid and high latitudes, the B-U models show a larger spread. In particular, the ORCHIDEE-P07 estimate is much higher than any other estimate (including ORCHIDEE-TOP) around 45°N and north of 60°N. LPJ-wsl follows ORCHIDEE-P07, but only up to 57°N. This shows that the wetland emission estimate is highly sensitive to the wetland extent, which remains a challenge for modellers. The top-down estimates are generally in the lower range of the

bottom-up values, except around 30°S. Regarding the top-down range, the minimum is mainly due to the estimates from GEOS-Chem while the Carbon-Tracker-CH_4 model retrieves the highest estimates, except north of 60°N where LMDZt-SACS is the highest. The biomass burning emissions, including biofuel, occur essentially in the Tropics where the highest fluxes are found along with a great spread between the models. Note the different scale compared to the wetland emissions. For biomass burning emissions, the ranges of estimates from top-down are similar to the bottom-up estimates. The model LMDZ-MIOP produces the maximum observed in the Tropics. The lowest estimates come from the GEOS-Chem model. The other top-down models lie in-between. In the mid latitudes, CH_4 emissions from biomass burning and biofuel essentially originate from biofuel burning.

ST3 - Time series of CH_4 emissions from natural wetlands and biomass-burning for northern regions and tropical regions (Figures S2 and S3)

Deseasonalized time series (12 month running means) for CH_4 emissions from natural wetlands (top, in green) and biomass burning (bottom in red) are plotted in Fig. S2, for both the Tropics (<30°N, left) and the northern high latitudes (50-90° N, right). Lines represent the different bottom-up models. Coloured ranges represent the top-down inversions. Fig. S3 is the same as Fig. S2 for natural wetlands, but plots the anomaly computed as the deseasonalized time series minus the long-term mean of each time series. Fig. S2 illustrates the large uncertainties remaining in the estimation of the long-term mean emissions from natural wetlands and biomass burning in the Tropics. It also shows that a large climate event, such as the 1997-98 El Niño, can have a very different impact on biomass burning among models. Fig. S3 shows that the IAV of CH_4 emissions from natural wetlands is more robustly estimated than the long-term mean. There is a better agreement on the phasing of year-to-year changes among studies than on their magnitude. Most approaches show an increasing long-term trend for CH_4 emissions from natural wetlands since the mid 1990s.

ST4 - Latitudinal distribution of the IAV of emissions and sinks (Figure S4)

Figure S4 shows the latitudinal distribution of the inter-annual variability of emissions and sinks. For both the emissions and the sinks, we calculated the 12-month running means of monthly zonal mean for band of 1 degree of latitude. For the emissions, in order to avoid interpreting long-term changes and focus on year-to-year changes, we subtracted a linear trend from the deseasonalized zonal means. The inter-annual variability was then defined as the standard deviation of the de-trended time series of the deseasonalized zonal means over the period 1995-2005. This calculation was possible for all approaches except those providing only yearly data.

For the CH_4 loss, we applied a slightly different calculation in order to allow comparison to the IAV estimates performed in Montzka et al. (2011)[29]. Instead of expressing the anomaly as the standard deviation of the deseasonalized zonal mean, we defined the IAV as the difference between monthly deseasonalized zonal mean and long-term mean. This calculation enhances the estimated IAV by 0.1-0.4%.

Over the three decades, natural wetland variability dominates the year-to-year changes in emissions with a tropical maximum spread between 30°S and 30°N, and a secondary maximum at northern latitudes around 50°N (Fig. S4-a). The magnitude of the year-to-year variability of other emissions is 4-8 times smaller than for natural wetlands (Fig. S4-b-d), except for biomass burning due to the 1997-98 El Niño (Fig. S4-b). Fossil fuel IAV dominates at mid latitudes of the northern hemisphere (fig. S4 c) and produces a secondary peak in the zonal average of CH_4 emission IAV at 30°S. Both regions are home to most of the developed countries (northern hemisphere, mid-latitudes) and some rapidly developing tropical countries in Southeast Asia, South America, Central Africa, and Oceania. The bottom-up inventories produce a third intriguing peak of fossil CH_4 emission IAV in the high northern latitudes, not consistent with the observation-driven top-down inversions. IAV of agriculture/waste emissions (Fig. S4-d) from top-down is largest between 10°N and 40°N where most of the rice agriculture and waste production from animal husbandry in China, India and South-East Asia are

located. OH IAV is largest in the Tropics (Fig. S4-e,f) where most of the OH is produced. Top-down inversions are more in agreement in the 2000s than in the 1990s with bottom-up models as explained in the main text.

ST5 - Year-to-year variations of emissions (Figure S5)

Figure S5 represents the evolution of the anomalies of each emission category over the last three decades. The emission anomalies were calculated as the difference between deseasonalized emissions (12-month running mean), and the long-term mean of the emissions. A consistent period for estimating the long-term mean is not suitable to all the data sources. As a result, the long-term mean was calculated as the mean emission over the stable period 1999-2006, except for wetland (1985-2006) and for fossil fuel and agriculture/waste inventory estimates (1990-2006). For studies covering shorter time periods (mainly in the 2000s), the long-term mean was calculated over the period 2000-2006. For studies starting after the year 2000, the time period used for calculating the long-term mean was reduced accordingly (e.g. TM5-4DVAR: 2003-2009). The ranges of the anomalies given in the main text are consistent with those presented in Figure S5.

The IAV of CH_4 emissions and sinks is defined by year-to-year fluctuations, superimposed on decadal trends (see main text for the decadal trend analysis). Over the three decades, natural wetlands dominate the year-to-year emission variability (Fig. S4). Bottom-up and top-down generally agree on this result, although different models compute different IAV magnitudes (Fig. S5). Bottom-up models for wetland emissions, for instance, may differ in their estimation of year-to-year changes, mainly because of different: 1) spatial distribution of emissions (Fig. S0), 2) structure and parameter values of wetland extent and CH_4 production, oxidation and transport processes, and 3) modelled sensitivity of enzyme kinetic and microbial processes to temperature and precipitation. For instance, the IAV of wetland extent is not fully represented in all wetland-emission models.

Two large events are driving the observed year-to-year changes in the atmosphere during the 1990s (Fig. S5): The Mount Pinatubo volcanic eruption in the Philippines (June 1991) and the large El Niño

Southern Oscillation event of 1997-98. The Pinatubo volcanic eruption induced a large seesaw in the CH_4 growth rate. The initial increase in the growth rate in 1991 was likely caused by the negative impact of volcanic SO_2 and aerosols on OH production, which may have decreased by 3-5%[10,30]. The subsequent cooling of the northern hemisphere (NH) following the eruption reduced CH_4 emissions from wetlands from 1991-93 by 13[3-21] Tg of CH_4 for top-down and 15[9-23] Tg of CH_4 for bottom-up models, with 67-75% of the emission perturbation located in the Tropics. This consequently decreased the atmospheric growth rate in 1992-93. The economic collapse of the former USSR also impacted the growth rate in 1991 and during the following years[31,32,66] with stagnant anthropogenic emissions at global scale estimated by both top-down and bottom-up.

The large El Niño Southern Oscillation event of 1997-98 also affected the CH_4 IAV. At that time, widespread dry spells caused increased fire activity in the tropics and in boreal regions of Eurasia[33,34] and reductions in natural wetland emissions. Above-average biomass-burning emissions of up to 21[8-32] Tg of CH_4 for bottom-up and 10[5-25] Tg of CH_4 for top-down are estimated for 1997-1998, mostly (85-90%) in tropical regions (Fig. S1 and S2). The 1997-98 large positive anomaly in biomass-burning emissions is on average two times more prominent in the bottom-up approach than in top-down inversions, possibly due to the lack of atmospheric measurements near the Indonesian peat fires attributing the CH_4 anomaly to other regions or sources, or due to dilution by fast vertical mixing. Natural wetland emissions from bottom-up and top-down consistently show a northern hemisphere-driven reduction in 1997 of 9[4-12] and 6[1-19] Tg of CH_4 respectively, followed by a tropical-driven increase in 1998 of 16[9-23] and 17[12-20] Tg of CH_4, respectively (Fig. S5 and S2).

ST6 – IAV variations of sinks

As with the Pinatubo eruption, climate variability can impact the IAV of the chemical destruction of CH_4 by OH radicals. Fluctuations in OH concentration could explain a large part of the observed variability of atmospheric CH_4. Typically, a 1% change in global OH concentration impacts the global CH_4 budget by up to 5 Tg of CH_4. The analysis of top-down inversions and bottom-up CCM results reveals a much better agreement for the IAV of CH_4 loss by OH in the 2000s compared to the 1990s

(Fig. S4-e, f): a maximum of IAV is found in the tropics (Fig. S4), and the global IAV of CH_4 loss by OH is 0.9 and 0.4% for two of the top-down inversions, and 0.9, 0.5 and 0.4% for the three CCMs providing a full IAV analysis. Indeed, the mean IAV of the CH_4 chemical loss computed from ACCMIP models is 0.4±0.2%. This value is to be considered as a lower limit because time-slices only account for internal variability of the models as emissions and sea surface temperatures are constant within each time-slice. GISS and LMDzORINCA provided transient runs so the calculated inter-annual variability is somewhat more complete, although annual emissions are interpolated between varying emissions between decades. The TM5 model provided results with full representation of IAV. For these three models, IAV is estimated at 0.5% and 0.4% and 0.9% respectively as mentioned above. These values are the largest of the CCM models used in this work. Without these two models, the IAV decreases to 0.3±0.2%, suggesting that at least half of the IAV of the CH_4 chemical loss is due to IAV in trace gas and aerosol emissions.

This small IAV during the 2000s, with top-down inversion IAV still twice that of the CCMs, is consistent with recent estimates of OH concentration IAV since 1998 reported to be less than 5% when using a box model and less than 3% when using a three dimensional top-down inversion with an estimate of 1.8±1.2%[29]. The large IAV of CH_4 loss by OH before 1998 is now analysed as an artefact of the overly large sensitivity of OH concentration inferred from methyl chloroform measurements to uncertainties in its emissions[29]. An alternative scenario invokes the occurrence of several large El Nino events[35] before 1998. Finally since 2007, as for the CH_4 sink, year-to-year changes in OH concentrations are found to be small[29,36](< 1% per year), and possibly partially offset by the increase of atmospheric CH_4[37].

In addition, even if ACCMIP models simulate IAV, we cannot discuss specific climate events using the ACCMIP CH_4 chemical loss because the climate models used for the simulations are not nudged to meteorological reanalyses. Meteorology depends on the climate that is being simulated in the climate portion of the models, which will show year-to-year variations, but not necessarily in phase with

observed climate events such as El Niño. Finally, only two top-down inversions provided OH fields to calculate IAV, which explains why only two estimates are shown.

ST7 - A simple model for CH_4 emissions from termites (Figure S6)

Several up-scaling approaches have been carried out to quantify the global contribution of termites to CH_4 emissions[38-40]. However, although the number of available information is increasing, estimates still show large uncertainties, related to: 1) the effect of soil and mound environments on net CH_4 emissions, 2) the quantification of termite biomass for each ecosystem type, and 3) the impact of land use change on termite biomass.

We have computed CH_4 emission from termites at global scale as the product of termite biomass (derived by gross primary production, as proxy of net primary production for tropical ecosystems), a termite emission factor (fix), and a crop reduction effect (fix). Using as input global GPP products (GPP_{MET}[41,42]) and crop distribution maps[43] (new version of Ramankutty and Foley, 1999; http://www.geog.mcgill.ca/~nramankutty/Datasets/Datasets.html) from 1982 to 2007, the equation in Fig. S6 was applied in a GIS environment to obtain yearly CH_4 emission estimates. First, the GPP of the "Other-Than-Crop" (OTC) land covers was extracted from $GPP_{MET,}$ and termite biomass (g m^{-2}) was calculated. Termite biomass in the crop area was estimated to be 40% of the original pristine ecosystem, whereas no consistent effect from conversion into pastries and secondary forests was found [44-47]. Total biomass (Tg of CH_4 per year) per pixel was then aggregated on the basis of natural vegetation classification[43] for land regions between 35°S and 35°N. To calculate CH_4 emissions outside ± 35°, i.e. temperate forests, temperate grasslands, and Mediterranean shrublands, the total suitable land surface (10^6 km^2) was multiplied with a termite biomass value of 3.0 g m^{-2} for temperate ecosystems[38], and 4.0 g m^{-2} for Mediterranean areas (average value derived from GPP of Australian mallee areas and data reported for a similar Australian ecosystem[48]).

Based on a literature analysis[38,49-51], we used a CH_4 emission factor of 2.8 ± 1.0 mg CH_4 (g^{-1} termite) for tropical and Mediterranean ecosystems. For temperate forests and grasslands we use the value of

1.7 mg CH_4 g^{-1} termite[52]. No significant conversion of natural ecosystems into crops was assumed in these areas during the period 1980-2009.

Yearly CH_4 emissions (g m^{-2} y^{-1}) were finally computed and averaged over three periods 1982-1989, 1990-1999 and 2000-2007 representative of the 1980s', 1990s' and 2000s', respectively. We find 8.7±3.1 Tg of CH_4 per year for the 1980s, 8.7±3.1 Tg of CH_4 per year for the 1990s, and 8.8±3.2 Tg of CH_4 per year for the 2000s. The uncertainty of the total estimate was calculated 1) by applying error propagation of products to calculations, which included main variables (termite biomass, CH_4 emission factor, and land use effect), and 2) by means of error propagation of the sum when global estimates of CH_4 were computed. These estimates are in the lower bound of current estimates and show only little inter-annual variability. Regionally, tropical South America and Africa are the main sources (36 and 30% of the global total emission, respectively) due to the extent of their natural forests and savanna ecosystems.

ST8 - The "plant" source

After the 4th IPCC Assessment Report one study concluded that plants were able to emit CH_4 under aerobic conditions contributing a moderate-to-large global source of 62-236 Tg of CH_4 per year to the global CH_4 budget[53]. This finding was consistent with the first maps of column CH_4 retrieved from the SCIAMACHY space-borne instrument that revealed a large excess of CH_4 above tropical forests[54], although not in agreement on the magnitude of potential plant emissions. However, this correlation appeared to be fortuitous. Indeed, later improvements to the spectroscopy led to large reductions of the satellite-observed atmospheric CH_4 excess in the tropics[55]. Although plants may emit CH_4 under aerobic conditions, additional measurements on plant emissions[56-59] and atmospheric analyses[60] have not supported that plants, under aerobic conditions, are a significant player in the global CH_4 budget.

I.2 Supporting figures

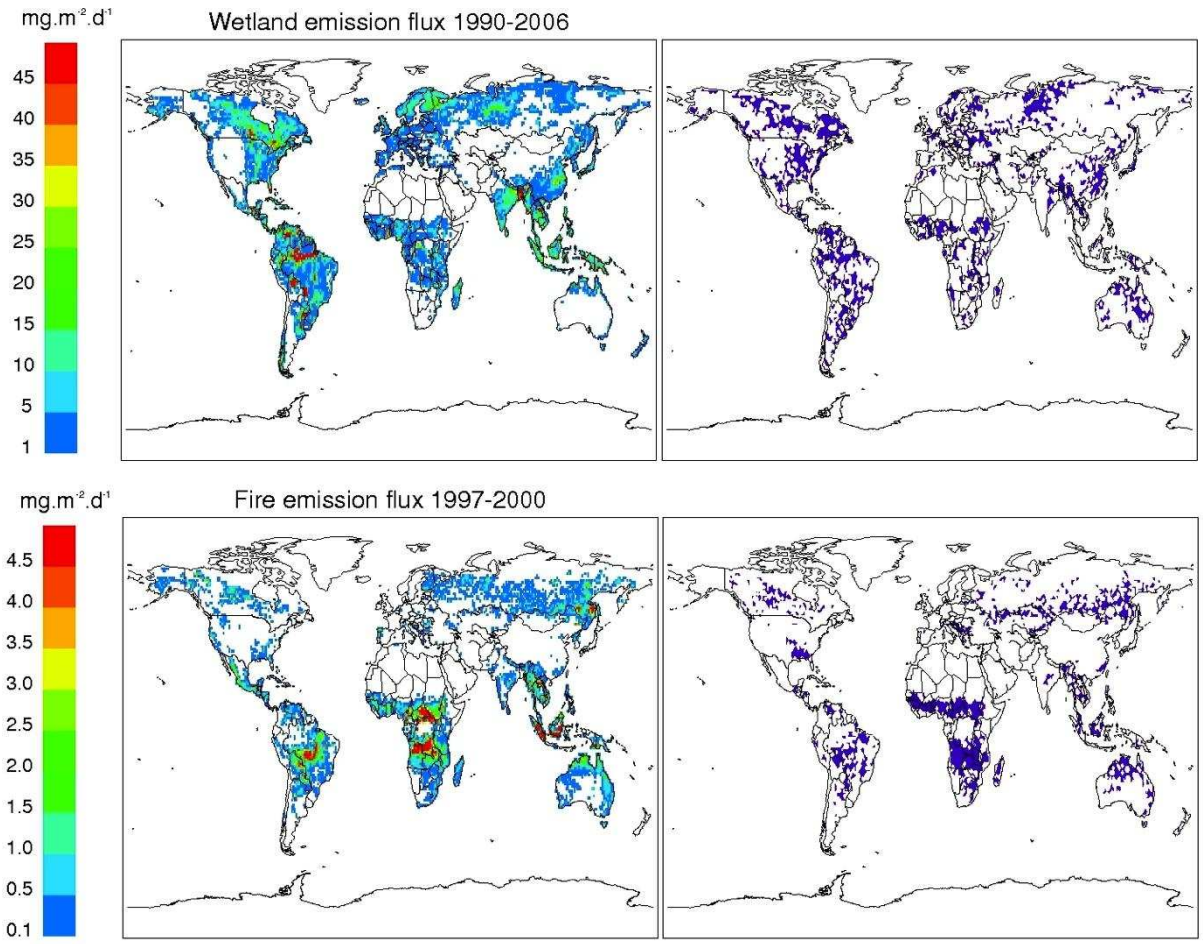

Figure S0: (Left) Distribution of methane emissions from natural wetlands (top) and fires (bottom) at 1x1° resolution in $mgCH_4/m^2/day$. Note the different color scales. Emissions lower than 1 $mgCH_4/m^2/day$ (0.1 for fires) are not shown. Each map is an average over the maximum common period of time of the different models aggregated in this study. On the right, purple areas indicate grid cells where the mean emission is larger than the standard deviation between the B-U studies aggregated to build the map.

s

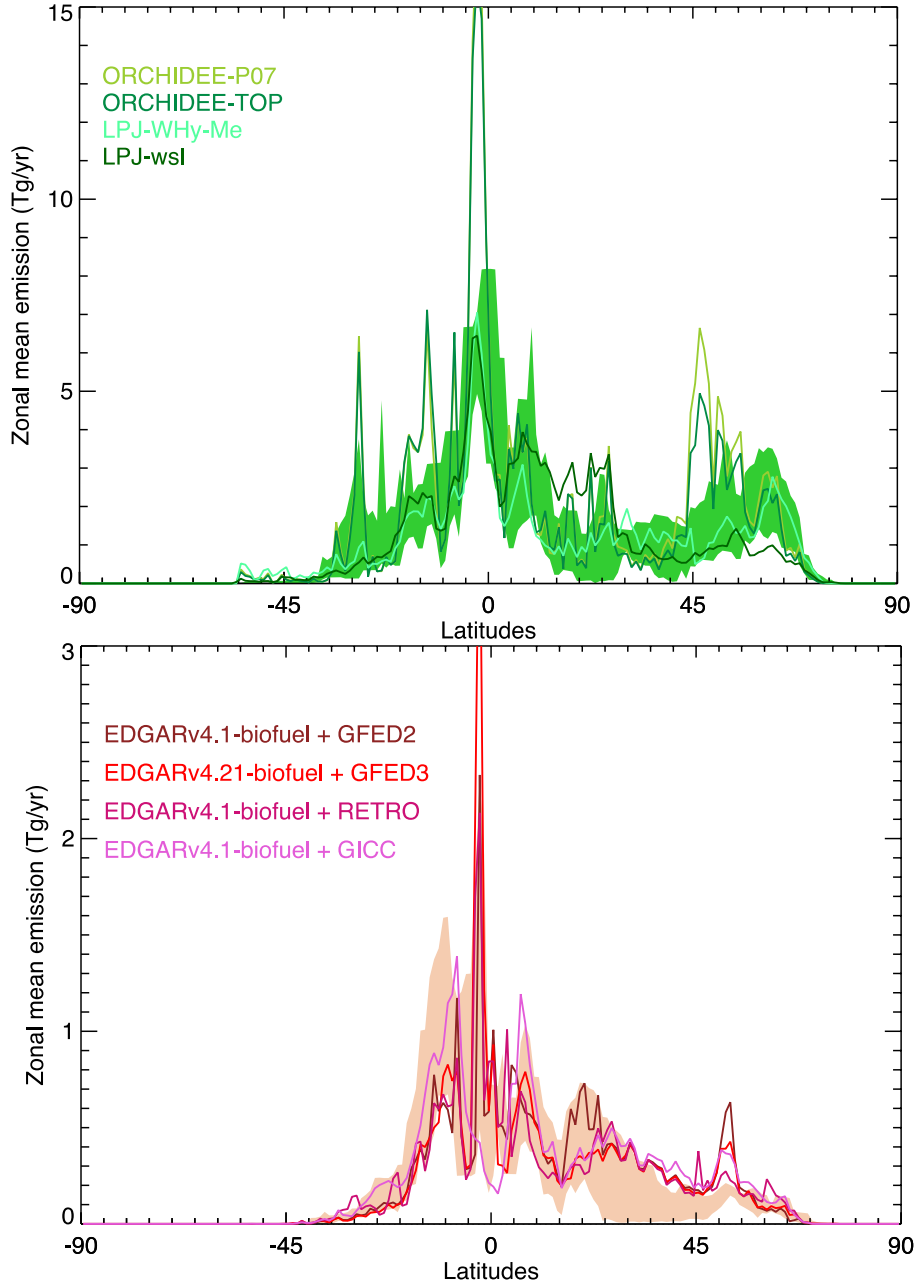

Figure S1: Zonal mean fluxes of CH_4 from natural wetlands (top), biomass burning (including biofuel, middle), and OH loss (bottom). The zonal mean has been computed over the period 1990-2006 for wetland emissions and 1980-2005 for biomass burning emissions. The coloured lines correspond to B-U models or inventories as specified in the legend (the same as those used to compute the gridded maps in Fig. S0). Coloured ranges indicate the minimum and maximum of the zonal mean fluxes derived from T-D inversions. Zonal mean of methane loss through OH oxidation is computed by the ACCMIP models and the T-D inversions (PYVAR and LMDZ-MIOP), temporal average being calculated over the 2000s. Note that vertical scales are different for the three plots.

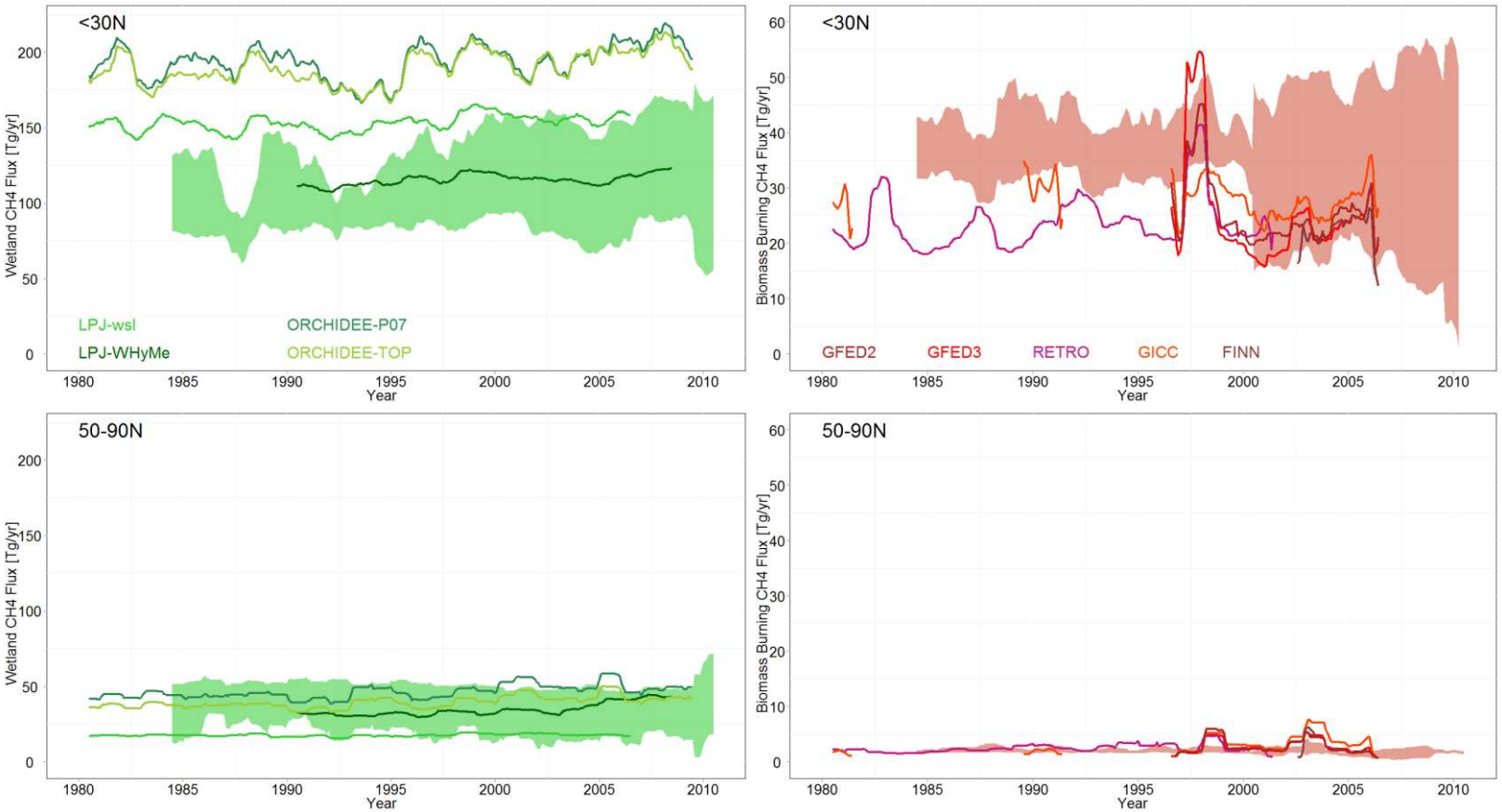

Figure S2: Deseasonalized CH_4 emissions from natural wetland emissions (top, in green) and fires (bottom, in red) for two latitudinal bands (Left: Tropics <30°N, Right: Northern latitudes, 50-90°N). Lines represent B-U models and inventories. Colored ranges are for T-D inversions. Wetland emissions are from ORCHIDEE[61], LPJ-WHyMe[62] and LPJ-WSL[63], and inversions[36,64-66]; biomass-burning emissions are from RETRO[67], GFEDv2 [68], GFEDv3[34], GICC[69] and FINN [70], and inversions (same as for wetlands). Note that y-axis scales are different for wetland and biomass-burning emissions.

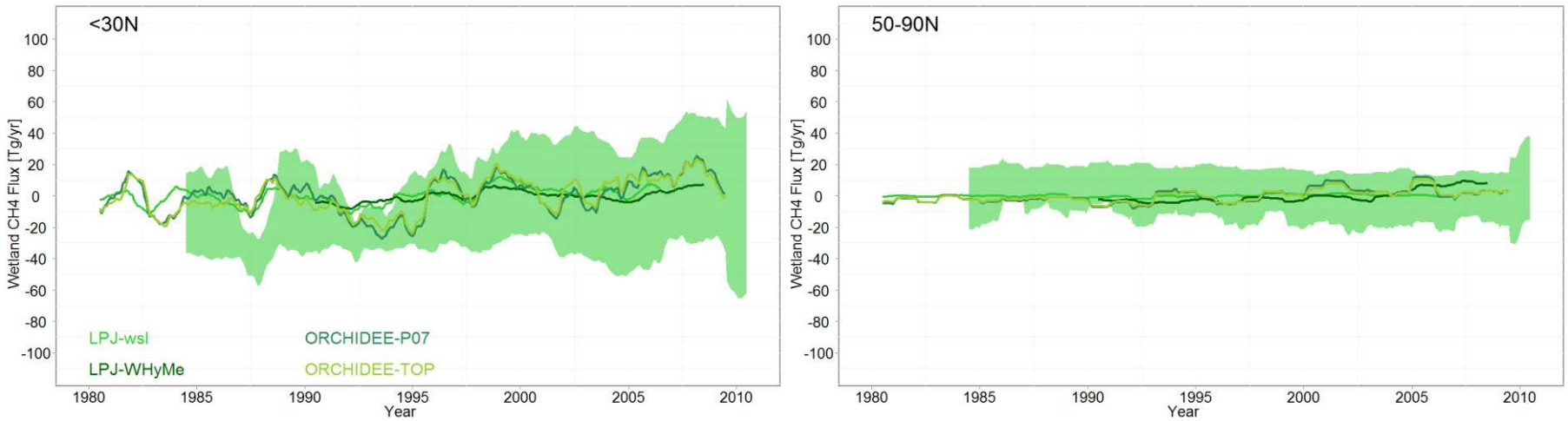

Figure S3: Same as figure S2 but for the anomaly (de-seasonalized time series minus their long-term mean) of CH_4 emissions from natural wetlands (in $TgCH_4.yr^{-1}$) for two latitudinal bands (Left: Tropics <30°N, Right: Northern latitudes, 50-90°N). Lines represent B-U models and inventories. Colored ranges are for T-D inversions.

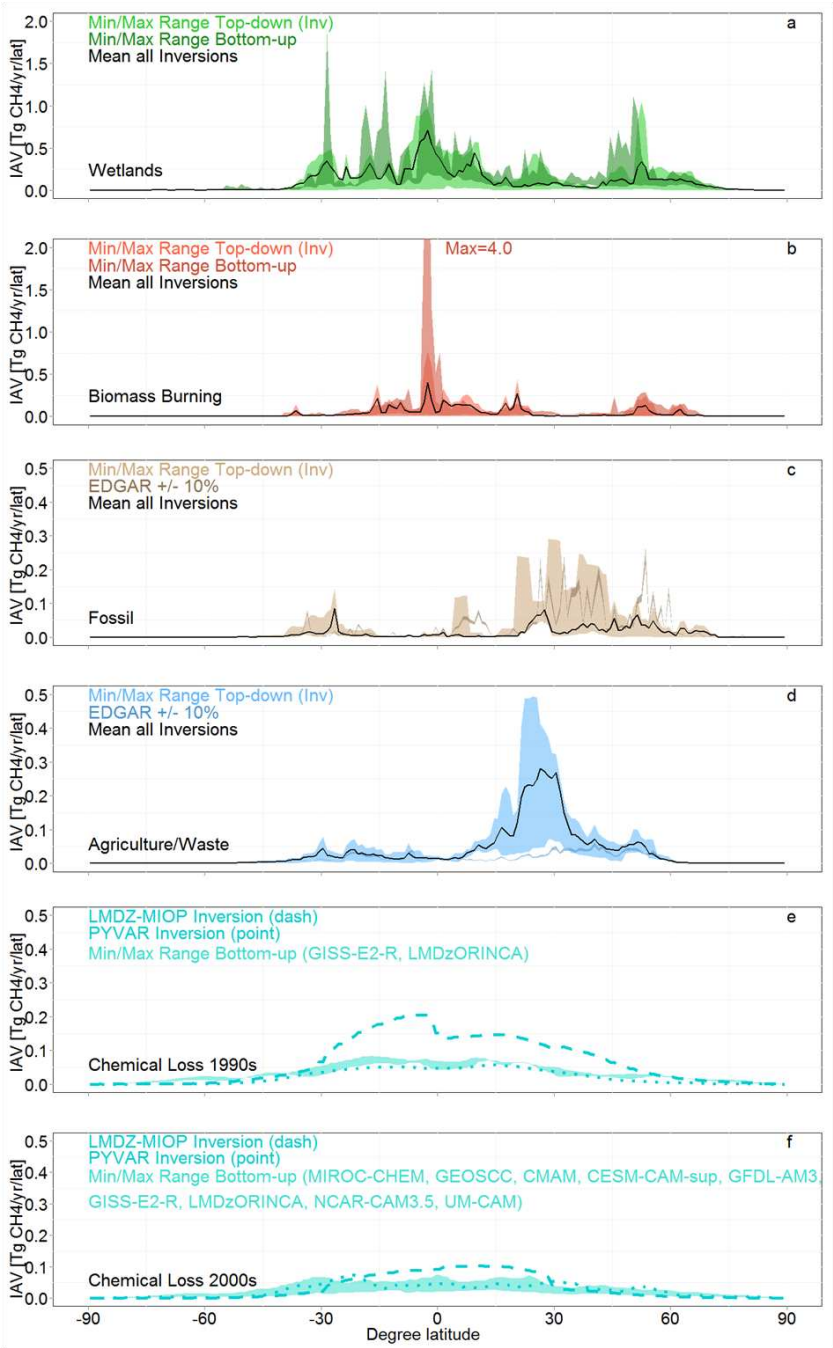

Figure S4: Inter-annual variability (IAV) of T-D and B-U emissions and sinks as a function of latitude. IAV is calculated as the de-trended standard deviation of the zonal emissions and sinks at 1° resolution. Range of all T-D inversions is shown as light coloured shaded area (except for chemical loss). Range of all B-U approaches is shown as dark-coloured shaded area (wetland models, fire models and inventories). From top to bottom: natural wetlands (green), fires (red), fossil fuels (brown), agriculture/waste (blue), and chemical loss (turquoise) for the 1990s and the 2000s. For chemical loss, T-D inversions are shown as lines. Note that y-axis scales are extended for wetland and biomass-burning emission IAV.

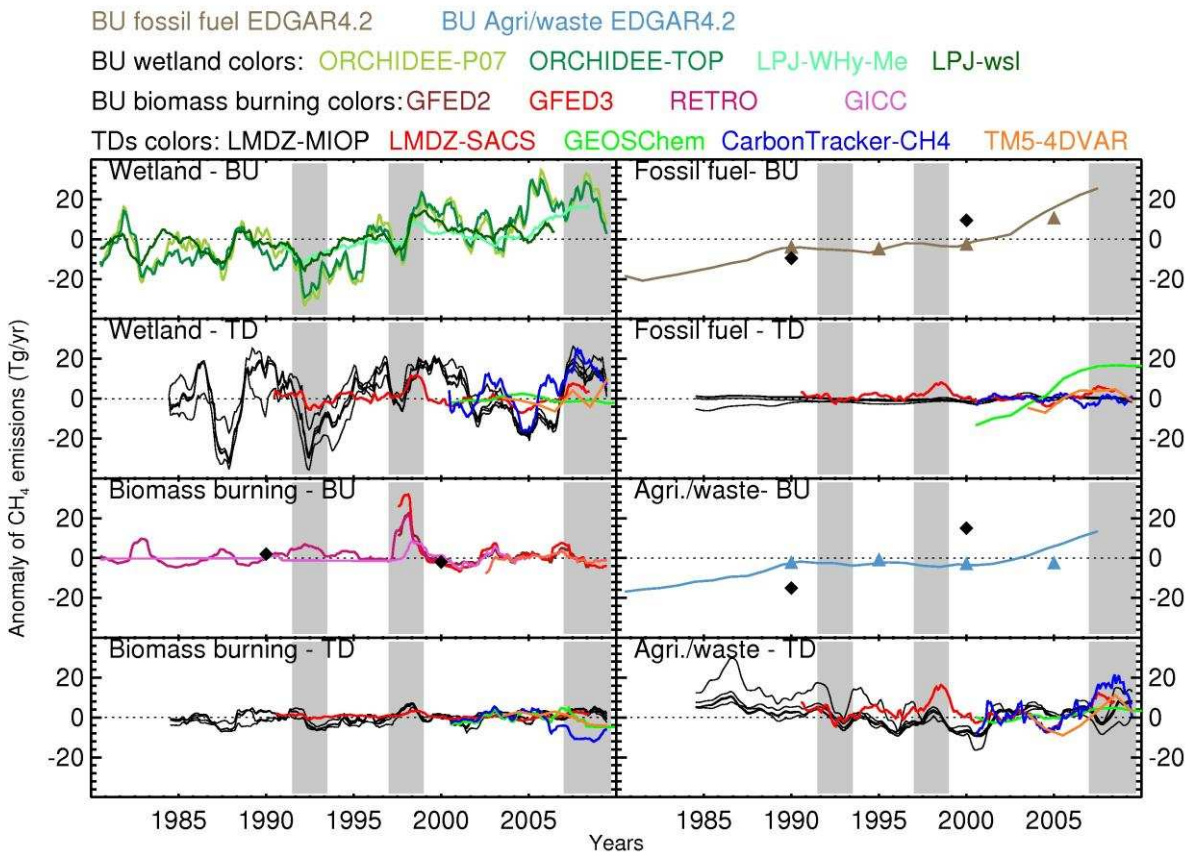

Figure S5: Inter-annual variability (IAV) of T-D and B-U emissions over the last three decades. Anomalies are calculated as the difference between deseasonalized emissions (12-month running mean), and a long-term mean of the same emission. Long-term mean is calculated as the mean emission over the stable period 1999-2006, except for wetland (both T-D and B-U, 1985-2006) and for fossil fuel and agriculture/waste inventories (1990-2006). For studies covering shorter periods the long term mean is based on a subset of the 1999-2006 period (except for TM5-4DVARbn 2003-2009). The decadal IIASA and EPA inventory values are represented as black diamonds and coloured triangles, respectively. The shaded grey areas highlight the three time periods discussed in the text (post-Pinatubo period, 1997-98 El-Nino, and the recent years).

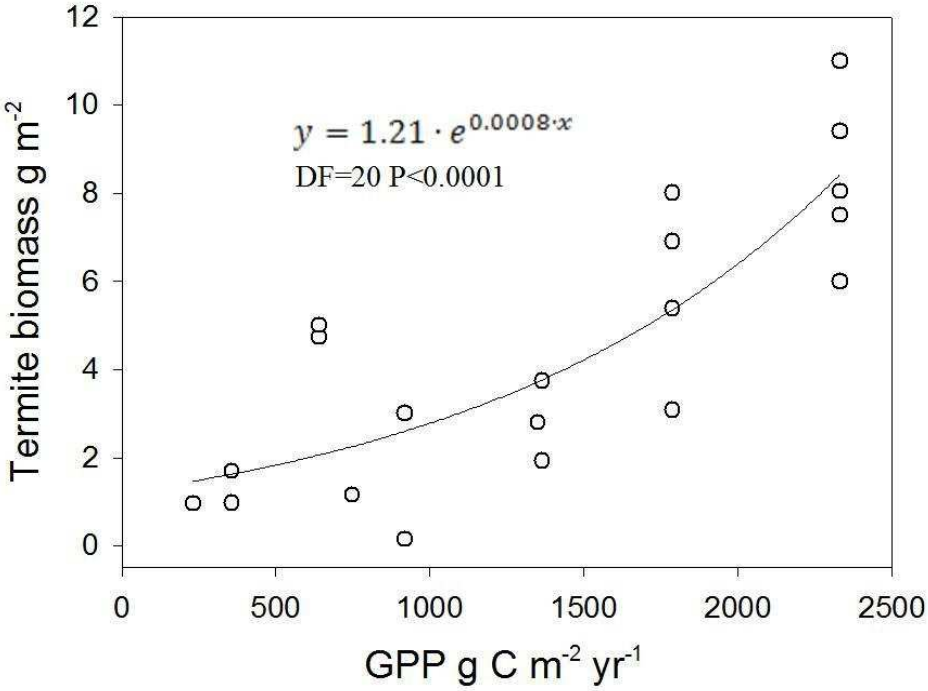

Figure S6: Termite biomass vs. mean annual GPP derived from different sources [71,72]for tropical areas. Termites biomass data are extracted from the main published studies[48,49,73-82].

I.3 Supporting tables

Table S1: T-D Model main characteristics

	TM5-4DVAR (Bergamaschi et al., 2009)	**LMDZ-MIOP (Bousquet et al., 2011)**	**CarbonTracker-CH4 (Bruhwiler et al., 2011)**	**GEOS-Chem (Fraser et al., 2011)**	**TM5-4DVAR (Houweling et al., 2012)**	**LMDZt-SACS (Pison et al., 2009, Bousquet et al., 2011)**	**GCM used by Fung et al., 1991**	**TM2 (Hein et al., 1997)**	**MATCH (Chen & Prinn, 2006)**
Data sets (indicate network/instrument)									
Satellite	IMAPv5.5 retrievals (Frankenberg et al., 2011)[1]	/		/	SCIAMACHY IMAPv5.5	/		/	/
Ground based	NOAA / ESRL (only marine and continental background sites)	MCF=AGAGE CH4=CSIRO, NOAA, LSCE	NOAA-ESRL and Environment Canada sites (88 sites)	48 ESRL sites	NOAA-ESRL	MCF=NOAA, AGAGE, CH4=CSIRO, EC, NOAA, RAMCES, NIWA, AGAGE (continuous), SAWS, INMA, ENEA, JMA, UBAG	NOAA/CMDL (19 sites), CSIRO (2 sites), 2 additional sites (Cape Point, South Africa; Tsukuba, Japan)	NOAA (30 stations for CH4) 13CH4 observations (6 stations from UCI, and 1 from NIWA)	NOAA (54 flask sites) AGAGE (5 high frequency sites)
Satellite + Ground based	bias correction of satellite data (2nd order polynomial as function of latitude and month) (Bergamaschi et al., JGR, 2009)	/		/	SCIAMACHY inversions are always carried out in combination with surface data	/		/	/

Prior scenarios									
Emissions	anthropogenic emissions (except biomass burning): EDGARv4.1, biomass burning: GFEDv3.1, wetlands: inventory from Jed Kaplan (Bergamaschi et al., JGR, 2007), further minor natural sources as described in (Bergamaschi et al., 2009)	MCF=Montzka et al., 2000 + Bousquet et al., 2006, CH4= EDGAR 3.2, GFED-v2 (van der Werf et al., 2006), Matthews et Fung (1987)	EDGARV3.2, GFED3, Bergamaschi et al. 2007 wetlands	ruminant animals, coal mining, oil production, landfills: EDGAR 3.2 FT (Olivier et al., 2005); biomass burning: GFEDv2 (van der Werf et al., 2006); oceans: Houweling et al., 1999; wetlands and rice: Bloom et al., 2010; termites, hydrates: Fung et al., 1991	EDGARv4.1 (Anthropogenic), GFED3 (BMB), LPJ-WhyMe (Wetlands) + minor processes	MCF=Montzka et al., 2000 + Bousquet et al., 2006, CH4= EDGAR 3, GFED-v2 (van der Werf et al., 2006), Fung et al. (1991), constant over the oceans	Wetlands: Matthews and Fung, 1987; rice: Matthews et al., 1991; animals: based on Crutzen et al., 1986 and Lerner et al., 1988; natural gas: U.S. Department of Energy, 1986, U.N. Department of International Economic and Social Affairs, 1986; coal: Espenshade, 1978, Central Intelligence Agency, 1978 and 1986, Seydliyz Weltatlas 1984, U.N. Department of International Economic and Social Affairs, 1986; biomass burning: Houghton et al., 1987; termites: based on Matthews, 1983, Zimmermann et al., 1982 and 1983, Fraser et al., 1986; hydrates: based on Kvenvolden, 1988	Based on Fung et al., 991	Adapted from Fung et al., 1991 For wetland and rice EDGAR3.0 for anthropognic Hao and Liu [1994] for biomass burning

Sinks	troposphere: TM5-OH (Bergamaschi et al., 2009), stratosphere: OH, O(1D) and Cl from 2D MPI model (Brühl and Crutzen, 1993), soil sink: (Ridgwell et al., 1999)	Prior OH Field from MOZART model (Hauglustaine 2004)	troposphere: TM5-OH (Bergamaschi et al., 2007), stratosphere: OH, O(1D) and Cl from 2D MPI model (Brühl and Crutzen, 1993), soil sink: (Ridgwell et al., 1999)	OH: 3D monthly fields from a full-chemistry Ox-NOx-VOC run of the GEOS-Chem model (Fiore et al., 2003); soil sink: Fung et al. 1991; stratospheric loss: adapted from a 2-D stratospheric model (Wang et al., 2004)	Climatological OH based on Montzka, Science, 2011	Prior OH fields by INCA	OH: Spivakovsky et al., 1990a,b; soils: based on Born et al., 1990 and Matthews, 1983	OH Computed with the chemistry-transport model of the paper	OH output of a T62 run of the MATCH model,
Meteorological forcing	ECMWF Era-Interim	LMDZ on-line nudged on ERA40	ECMWF Forecast	GEOS5	ECMWF ERA-interim	LMDZ on-line nudged on ERA40	Hansen et al., 1983	ECMWF analysis	NCEP reanalysis
Model characteristics									
Resolution (lonxlatxlev)	6x4 degrees; 25 vertical layers	3.75degreesx2.5degreesx19 sigma-pressure levels	6x4 degrees, 25-34 levels	5x4x47	6x4x25 (degree lon, degree lat, # layers)	3.75degreesx2.5degreesx19 sigma-pressure levels	4x5 (degree lat, degree lon), 9 vertical layers	7.5x7.5 (degree lat, degree lon), 14 vertical layers	1.8x1.8 lat, degree lon), 28 vertical layers
PBL scheme	Holtslag and Moeng, 1991]	Local closure	Holtslag and Moeng, 1991	VDIFF (Lin & McElroy, 2010)	Holtslag & Moeng (J. Atmos. Sci., 1991)	Local closure		Local closure based on Louis, 1979	
Convection scheme	Tiedke, 1989	Tiedtke et al., 1989	Tiedke, 1989	Relaxed Arakawa-Schubert scheme (Moorthi and Suarez, 1992)	Tiedtke (Mon. Wea. Rev., 1989)	Tiedtke et al., 1989	Arakawa scheme B	Tiedtke et al., 1989	
Inversion									
Time resolution (flux domain)	monthly	one month	Weekly aggregated to monthly	8 day	monthly	one week		monthly	Monthly

Spatial resolution	grid cell (6x4 degrees)	10 land regions + 1 ocean region	120 land regions based on source process and Transcom region, 1 ocean	Based on Transcom (Gurney et al., 2002): 99 land regions + 11 ocean regions + 1 ice region	6x4 degree	grid cell (3.75 °x2.5°)		Global per process	Large regions and processes
Correlation length (flux domain)	500 km	/		/	1000 km	500 km on land, 1000 km on ocean		/	
Minimizer	m1qn3	Analytical solution	Ensemble Kalman smoother	ensemble Kalman filter	Variational approach	m1qn3	/	/	Kalman filter
Time window	2003-2010	1983-2010	2000-2011	2000-2010	2003-2010	1990-2008	1980-1989	1983-1989	1996-2001

Table S2: Estimated CH_4 fluxes corresponding to the regional bar plots in Fig. 3. Values are given in Tg yr^{-1} (**mean** [min-max]) for the 2000s.

Region		Wetlands	Biomass-burning	Fossil Fuels	Agriculture/ Waste	Other Sources	Soil Sink	OH Chemical Sink
Africa	T-D	**36** [20-48]	**9** [7-14]	**7** [3-13]	**18** [16-22]	**9** [7-15]	**8** [5-12]	**43** [NA]
	B-U	**24** [22-27]	**8** [6-12]	**9** [7-11]	**21** [13-29]	NA	NA	NA
Australia	T-D	**4** [0-11]	**0** [0-1]	**1** [0-2]	**3** [2-5]	**1** [1-2]	**2** [1-3]	**12** [NA]
	B-U	**3** [2-3]	**1** [0-2]	**1** [1-2]	**5** [4-6]	NA	NA	NA
China	T-D	**6** [2-12]	**1** [0-3]	**15** [9-21]	**29** [21-36]	**1** [1-2]	**2** [1-2]	**8** [NA]
	B-U	**7** [5-10]	**4** [4-5]	**12** [10-13]	**28** [25-31]	NA	NA	NA
Eurasia, boreal	T-D	**14** [9-23]	**1** [1-2]	**7** [3-11]	**2** [1-3]	**1** [0-1]	**3** [1-5]	**4** [NA]
	B-U	**9** [4-13]	**1** [1-2]	**11** [6-17]	**4** [2-6]	NA	NA	NA
Eurasia, temperate	T-D	**4** [0-13]	**0** [0-1]	**14** [9-17]	**13** [12-15]	**2** [1-3]	**2** [2-3]	**14** [NA]
	B-U	**2** [2-2]	**1** [0-1]	**15** [13-18]	**15** [15-16]	NA	NA	NA
Europe	T-D	**10** [4-19]	**0** [0-1]	**18** [7-23]	**20** [13-26]	**1** [1-2]	**2** [2-3]	**8** [NA]
	B-U	**10** [5-17]	**2** [0-2]	**17** [9-26]	**25** [22-28]	NA	NA	NA
India	T-D	**2** [0-4]	**1** [0-3]	**2** [2-4]	**27** [19-43]	**1** [1-1]	**1** [0-1]	**5** [NA]
	B-U	**9** [5-16]	**2** [2-2]	**2** [2-3]	**22** [20-24]	NA	NA	NA
North America, boreal	T-D	**9** [6-17]	**0** [0-1]	**0** [0-1]	**0** [0-1]	**1** [0-2]	**2** [1-2]	**3** [NA]
	B-U	**16** [9-28]	**0** [0-1]	**1** [0-2]	**1** [0-2]	NA	NA	NA
North America, temperate	T-D	**8** [6-11]	**0** [0-1]	**18** [8-27]	**24** [21-31]	**2** [1-3]	**3** [2-4]	**13** [NA]
	B-U	**17** [10-29]	**1** [0-1]	**14** [13-15]	**21** [21-21]	NA	NA	NA
South America, temperate	T-D	**19** [10-32]	**2** [0-3]	**1** [0-2]	**19** [16-23]	**2** [2-3]	**3** [1-4]	**15** [NA]
	B-U	**23** [17-31]	**1** [1-2]	**1** [1-2]	**11** [6-17]	NA	NA	NA
South America, tropical	T-D	**28** [17-48]	**5** [3-9]	**2** [1-3]	**7** [6-9]	**4** [3-7]	**2** [0-4]	**16** [NA]
	B-U	**58** [39-92]	**4** [2-4]	**3** [3-3]	**15** [7-23]	NA	NA	NA
South East Asia	T-D	**19** [7-32]	**4** [3-6]	**4** [2-6]	**18** [10-32]	**2** [1-4]	**1** [0-2]	**10** [NA]
	B-U	**26** [14-37]	**5** [2-7]	**4** [3-5]	**21** [19-24]	NA	NA	NA

Table S3: Estimated regional CH_4 fluxes for each model corresponding to bar plots in Fig. 3. Values are given in Tg yr^{-1} for the 2000s.

	LMDZ-MIOP (Bousquet et al., 2011)	TM5-4DVAR (Houweling et al., 2012)	CarbonTracker-CH_4 (Bruhwiler et al., 2011)	TM5-4DVAR (Bergamaschi et al., 2009)	GEOS-Chem (Fraser et al., 2011)	LMDZt-SACS (Pison et al., 2009; Bousquet et al., 2011)	LPJ-wsl (Hodson et al., 2011)	LPJ-WhyMe (Spahni et al., 2011)	ORCHIDEE (Ringeval et al., 2011)	GFEDv3 (Van der Werf et al., 2010)	RETRO (Schultz et al., 2007)	GICC (Mieville et al., 2010)	FINNv1 (Wiedinmeyer et al., 2011)	GFEDv2 (Van der Werf et al., 2004)	EDGARv4.1 (EDGAR4.1, 2009)	EPA, 2011
North America, boreal																
Wetland	9.0	5.9	6.6	8.1	5.7	17.0	10.8	9.2	28.3							
Biomass Burning	0.5	0.7	0.3	0.6	0.3	0.3				0.5	0.6	0.7	0.2	0.3		
Fossil	1.0	0.4	0.2	0.2	0.3	0.9									0.1	2.2
Agriwaste	0.8	0.6	0.2	0.4	0.3	0.4									0.2	2.3
Other	0.3	1.6	0.4	0.9	0.6	0.2										
Soil	-1.8	/	-0.8	-1.1	-2.3	/										
North America, temperate																
Wetland	7.6	7.1	8.9	7.2	10.8	7.4	9.8	11.2	28.8							
Biomass Burning	0.9	0.2	0.2	0.5	0.2	1.0				0.6	1.2	1.5	0.9	0.8		
Fossil	27.2	15.9	8.0	14.1	15.0	25.8									13.4	14.8
Agriwaste	20.8	23.4	31.3	21.8	23.8	25.5									20.7	20.9
Other	1.1	3.2	0.8	1.3	1.4	1.2										
Soil	-2.8	/	-2.8	-3.9	-2.5	/										

South America, tropical

Wetland	20.4	26.6	28.8	47.5	29.8	16.8	38.6	42.4	92.1							
Biomass Burning	9.4	4.2	3.1	3.1	2.9	8.4				2.5	3.4	3.8	4.5	4.1		
Fossil	1.1	2.4	0.7	2.8	1.2	1.8									2.8	3.0
Agriwaste	6.8	6.1	8.6	7.9	6.3	7.6									7.1	22.8
Other	3.2	6.8	4.9	4.9	2.9	2.6										
Soil	-0.9	/	-3.0	-3.6	-0.4	/										

South America, temperate

Wetland	20.3	10.2	31.9	16.7	15.0	21.4	16.7	20.9	31.1							
Biomass Burning	3.0	1.7	0.5	1.5	1.2	3.0				1.0	2.0	2.4	1.0	1.0		
Fossil	1.0	2.0	0.5	1.9	1.2	0.9									2.1	0.7
Agriwaste	16.8	20.8	22.6	20.3	15.9	18.3									17.2	5.6
Other	2.0	3.3	2.2	2.8	2.1	2.1										
Soil	-1.6	/	-3.6	-4.3	-0.9	/										

Europe

Wetland	10.4	5.0	6.8	3.8	15.4	18.8	4.8	16.7	9.4							
Biomass Burning	1.1	0.2	0.2	1.0	0.2	0.7				1.8	1.9	0.4	2.1	1.8		
Fossil	23.0	21.1	19.0	18.3	7.4	20.3									25.9	8.8
Agriwaste	22.3	14.9	26.0	13.3	18.6	22.8									27.6	22.0
Other	0.8	2.0	0.9	0.8	1.2	0.6										
Soil	-2.2	/	-2.3	-1.7	-2.9	/										

Africa

Wetland	36.2	20.4	46.2	44.7	47.8	19.7	22.1	23.7	27.4							

Biomass Burning	13.9	7.6	6.7	8.3	7.3	11.6				8.6	7.7	11.6	5.9	8.4		
Fossil	3.8	13.4	8.9	8.9	5.4	3.5									6.8	11.0
Agriwaste	16.0	20.4	16.8	22.3	16.1	15.6									13.4	29.1
Other	6.9	15.2	9.0	12.0	6.5	6.7										
Soil	-5.6	/	-9.2	-12.1	-4.7	/										

Eurasia, temperate

Wetland	3.5	-1.3	1.8	0.9	13.3	2.9	1.7	1.7	1.8							
Biomass Burning	0.9	0.1	0.1	0.5	0.0	0.9				0.5	0.3	0.7	0.6	0.5		
Fossil	14.6	14.1	11.1	16.5	14.5	12.1									12.6	17.9
Agriwaste	12.3	13.3	14.8	13.9	11.6	14.8									14.6	16.1
Other	1.2	3.3	1.2	1.5	1.6	1.2										
Soil	-2.0	/	-2.8	-2.7	-1.7	/										

Eurasia, boreal

Wetland	12.5	9.1	12.2	10.6	13.9	22.9	4.4	12.8	9.3							
Biomass Burning	1.3	0.9	0.9	1.0	1.3	1.0				1.5	0.7	1.8	1.5	1.7		
Fossil	10.7	4.6	9.3	3.2	3.6	9.7									5.9	16.8
Agriwaste	2.8	1.6	1.9	1.3	1.4	2.5									2.4	6.1
Other	0.7	1.4	0.6	0.8	0.7	0.5										
Soil	-3.9	/	-1.8	-1.4	-4.5	/										

China

Wetland	4.8	5.0	4.2	2.5	12.4	4.9	6.8	9.9	5.3							
Biomass Burning	3.0	0.1	0.1	1.8	0.2	3.2				4.1	4.2	4.2	4.4	4.1		
Fossil	13.7	17.9	8.6	11.1	20.5	16.0									13.4	10.1
Agriwaste	27.4	28.0	36.3	26.5	21.3	33.7									30.9	25.2
Other	1.2	1.5	0.9	0.6	1.2	1.3										

Soil	-2.0	/	-2.0	-1.2	-1.5	/										
India																
Wetland	1.4	4.0	0.2	4.0	1.9	0.2	16.3	5.2	6.0							
Biomass Burning	2.8	0.3	0.1	1.6	0.1	3.0				1.8	1.7	2.3	2.2	1.8		
Fossil	1.8	4.3	1.6	2.1	1.8	2.0									1.9	3.1
Agriwaste	26.0	22.2	42.6	19.1	22.7	30.0									20.5	24.2
Other	0.8	1.3	0.8	0.7	0.7	0.8										
Soil	-0.6	/	-1.1	-0.8	-0.3	/										
Australia																
Wetland	1.1	-0.4	11.2	1.2	0.5	4.0	3.3	2.7	2.6							
Biomass Burning	0.5	0.1	0.6	0.3	0.5	1.0				0.7	0.9	1.9	0.2	0.8		
Fossil	0.4	0.6	1.6	0.5	1.5	1.4									1.1	1.2
Agriwaste	2.9	2.3	3.1	2.0	3.3	4.5									4.4	5.6
Other	1.3	1.5	1.3	1.4	1.7	1.4										
Soil	-1.7	/	-3.2	-2.7	-1.1	/										
South East Asia																
Wetland	21.9	7.1	32.0	21.9	13.3	16.4	36.6	14.4	27.5							
Biomass Burning	4.9	3.3	3.1	3.1	2.6	5.6				6.3	4.8	2.1	4.8	6.6		
Fossil	3.3	6.4	4.5	2.9	1.8	3.5									3.2	4.6
Agriwaste	14.5	19.9	31.9	15.6	9.5	15.0									18.9	23.8
Other	1.3	3.8	1.8	1.8	1.5	1.2										
Soil	-0.6	/	-2.1	-1.4	-0.3	/										

II Observations and model descriptions

II.1 Description of atmospheric CH_4 datasets

NOAA/ESRL (Dlugokencky et al., 2011)

NOAA air samples are collected in pairs, approximately weekly, in 2.5 L borosilicate-glass flasks with Teflon O-ring sealed stopcocks from sites in NOAA's global cooperative air sampling network[83]. Flasks are flushed and pressurized to ~1.2 atm with a portable sampler. Methane is measured by gas chromatography with flame ionization detection against the NOAA 2004 CH_4 standard scale (it is also the WMO Global Atmosphere Watch CH_4 mole fraction scale)[84] and reported in dry air mole fractions (nmol mol^{-1}, abbreviated ppb). Repeatability of the measurements averages 1.5 ppb (1 s.d.). For this study, measurements from 46 globally-distributed remote boundary layer sites were fitted with curves to smooth variability with periods less than ~40 days[83]. Synchronized points were extracted from these curves at approximately weekly intervals and smoothed as a function of latitude to define an evenly spaced matrix of surface CH_4 mole fractions as a function of time and latitude (data path: ftp://ftp.cmdl.noaa.gov/ccg/ch4/flask/). This matrix was used to calculate global CH_4 averages.

AGAGE (Rigby et al., 2008)

Global-average GAGE/AGAGE CH_4 mole fractions

GAGE CH_4 measurements began between 1985 and 1987 at Adrigole, Ireland, Cape Grim, Tasmania, Cape Mears, Oregon and Cape Matatula, Samoa[2]. These observations have been ongoing throughout the GAGE and subsequent AGAGE project, but with a relocation of the Adrigole (Ireland) and Cape Matatula (California) sites to Mace Head (Ireland) and Trinidad Head (California) respectively, and the addition of CH_4 measurements to the ALE/GAGE/AGAGE site at Ragged Point (Barbados) in 1996. These locations were chosen to sample the remote atmosphere in four "semi-hemispheres". Measurements are made using automated gas chromatograph/flame ionization detectors (GC/FID) at approximately hourly frequency. "Background" concentrations were extracted from the high-

frequency measurement time series at each site using a statistical filter[85]. In order to account for data gaps, global average CH_4 mole fractions were calculated using a 2D model of the atmosphere [86,87,88], into which AGAGE observations had been assimilated. CH_4 emissions were estimated in the model in each semi-hemisphere during each month between 1986 and 2011, using AGAGE observations[37]. The global averages were then calculated based on the optimized semi-hemispheric model mole fractions.

CSIRO (Francey et al., 1999)

Sampling:

The CSIRO data used in this manuscript have been obtained from flask air samples returned to GASLAB for analysis. The flasks are of 6 types, 4 of which are the property of CSIRO (items a-d below) and 2 of which are the property of Environment Canada for air sampling at the Canadian sites, Alert and Estevan Point (items e and f): (a) glass 0.5 litre, sealed with two stopcocks fitted with PTFE, PFA or Viton O-rings (flask identifier prefix "G050"), (b) glass 5.0 litre, sealed with two stopcocks fitted with PTFE O-rings ("G500"), (c) glass 0.8 litre, sealed with two stopcocks fitted with PTFE or PFA O-rings ("G080"), (d) electropolished stainless steel 1.6 litre "Sirocans" fitted with two stainless steel valves manufactured by either Nupro or Hoke ("S160"), (e) glass 2.0 litre sealed with a single stopcock fitted with a Viton O-ring ("F", "FF", "FA", "FE", "EP", "ALT") or (f) glass 2.0 litre sealed with two stopcocks fitted with Viton O-rings ("M1", "S", "P2", "TEMP"). Experiments carried out to test for any change in sample CH_4 mixing ratio during storage have shown no drift to within detection limits over test periods of several months to years[89]. Typical sample storage times range from days to weeks for some sites (e.g. Cape Grim, Aircraft) to as much as 1 year for Macquarie Island and the Antarctic sites.

The CSIRO sampling sites used in this study are: South Pole, Antarctica (89° 59'S, 24° 48'W, 2810 metres altitude); Mawson, Australian Antarctic Territory (67° 37'S, 62° 52'E, 32 m); Macquarie Island, Australia (54° 29'S, 158° 58'E, 12 m); Cape Grim, Australia (40° 41'S, 144° 41'E, 94 m);

Cape Ferguson, Australia (19° 17'S, 147° 03'E, 2 m); Mauna Loa, Hawaii, USA (19° 32'N, 155° 35'W, 3397 m); Estevan Point, Canada (49° 23'N, 126° 32'W, 39 m); Shetland, Scotland (60° 10'N, 01° 10'W, 30 m); and Alert, Canada (82° 27'N, 62° 31'W, 6 m).

Analysis:

Samples were analysed by gas chromatography with flame ionisation detection (FID). Three individual but similarly configured Carle gas chromatographs were used over the length of the record. Further details are provided elsewhere of CSIRO's global sampling network, sampling and analytical techniques[26] and measurement uncertainty[90].

Calibration:

Data are reported in the NOAA04 CH_4scale[84]. The link to this scale was established with 8 high pressure cylinders containing dry, natural air with a CH_4 mole fraction range of 690 - 1870 ppb. These standards were calibrated by NOAA on one or more occasions between 1987 and 2001. Stability of the CSIRO scale is monitored with ~25 assorted long-lived standards. Instrument response has been further evaluated with a suite of six Nippon Sanso CH_4-in-air standards (volumetrically prepared, calibrated against a gravimetric scale at Tohoku University) spanning the range 310-1845 ppb. Details of calibration and measurement uncertainty are given by ref([90]).

Data Processing:

Flask data are assigned flags to indicate whether they are classified as retained or rejected. Cause of rejection falls into three broad categories: (i) the sample is considered to be not representative of the atmosphere at the time and place of sampling due to identified or inferred sampling or analytical problems (eg. sample contamination, poor analysis), (ii) the sample is considered to be "non-baseline" as indicated by the meteorological conditions at the time of sampling and (iii) any remaining outliers are flagged on the basis of a 3 sigma filter. Only data marked as retained have been used in this manuscript.

UCI (Simpson et al., 2012)

The University of California, Irvine (UCI) has monitored global CH_4 mixing ratios since 1978[1,27,91,92]. Each season (March, June, September, December) more than 80 whole air samples are collected over a 3-week period in a latitudinal transect of the Pacific Basin from 71°N (Barrow, AK) to 47°S (Slope Point, New Zealand), with occasional sampling at more northerly and southerly latitudes. Individual air samples are collected at sites that our experience has shown to give remote concentrations, usually along the coast when the wind is arriving from the ocean. A map of the sampling locations for the UCI network is given in ref([27]). Each air sample is collected into a conditioned, evacuated 2 L stainless steel canister equipped with a bellows valve, over a period of about one minute. The air samples are returned to our UCI laboratory and analyzed for CH_4 using gas chromatography (HP-5890A) with flame ionization detection. Other light hydrocarbons and halocarbons are measured from the same air samples using multi-column gas chromatography. Primary CH_4 calibration standards dating back to late 1977 ensure that our measurements are internally consistent. The CH_4 mixing ratios are reported for dry air and are relative to a primary standard purchased from the Matheson Gas Company in 1977, and to a National Bureau of Standards standard that was purchased in 1982 and has an uncertainty of ±1% (comparison with a NIST standard), which is our measurement accuracy. Systematic offsets between networks are regularly quantified and can be corrected when using several international networks in a modelling work. Our analytical precision, which is determined by alternating measurements of secondary standards with aliquots from an individual air sample, is currently about 1 ppbv.

Each data point is individually inspected, and those that do not represent remote values are removed from the data set (typically 2−5 samples per season). The remaining samples are used to calculate a global trace gas mixing ratio for each season of measurements as follows. The earth is divided into 16 latitudinal bands, each with an equal volume of air. The mixing ratios measured in each latitudinal band are averaged, and the global CH_4 mixing ratio for each season is the mean of the 16 band averages. Its uncertainty is the sum of standard errors for each band, added in quadrature, divided by

16. Because we do not routinely collect air samples in the southernmost two latitudinal bands, their CH_4 concentrations are inferred from concentrations measured in neighbouring bands in the southern hemisphere, where CH_4 is well-mixed. The annual global CH_4 mixing ratio is the average of 4 consecutive seasonal means, and its uncertainty is the sum of the standard errors of the seasonal means, added in quadrature, divided by 4. The annual global growth rate is the difference between two consecutive annual global CH_4 mixing ratios. Its uncertainty is the sum of the standard errors of the two annual means from which it was calculated, added in quadrature.

II.2 Description of top-down inversions (T-D)

Model main characteristics are summarized in table S1.

TM5-4DVAR (Bergamaschi et al., 2009)

Model simulations are based on the TM5-4DVAR inverse modelling system described in detail by Meirink[93], including subsequent further developments described by Bergamaschi et al. (2009; 2010)[23,94]. TM5 is an offline transport model[95] , driven by the meteorological fields from the ERA-INTERIM reanalysis. We employ the standard TM5 version (TM5 cycle 1), with 25 vertical layers, and apply a horizontal resolution of $6^{o}x4^{o}$. The 4-dimensional variational (4DVAR) optimization technique minimizes iteratively a cost function taking into account an a priori estimate of the emissions, based on the emission inventories used by Bergamaschi et al. (2010)[94]. Column-averaged CH_4 mixing ratios from the Scanning Imaging Absorption Spectrometer for Atmospheric Cartography (SCIAMACHY) instrument[18] onboard ENVISAT are assimilated together with surface observations from the NOAA Earth System Research Laboratory (ESRL) global cooperative air sampling[3], which serve as 'anchor-points' to correct for biases in the satellite retrievals[23] . The CH_4 inversions used in this paper are from the CH_4 re-analysis over the period 2003-2010 in the framework of the Monitoring Atmospheric Composition and Climate (MACC) project http://www.gmes-atmosphere.eu/.

LMDZ-MIOP (Bousquet et al., 2011)

The LMDZ-MIOP inversion model is an analytical inversion that has been used to infer the sources and sinks of carbon dioxide[96,97], methyl-chloroform[98] CH_3CCl_3, and recently di-hydrogen[99] H_2. Briefly, it solves for monthly surface CH_4 emissions for the different categories of sources and sinks and for 11 large regions (10 land regions + 1 ocean), as described in the TRANSCOM experiment[100]. It uses monthly mean observations at up to 68 surface stations from the NOAA/ESRL, CSIRO and IPSL/LSCE surface monitoring networks. The offline version LMDZt version 3 of the LMDZ-GCM, nudged to analysed winds[101], is used to model atmospheric transport[102,103]. Prior emissions are taken from inventories[104-106]. The OH 3-dimensional fields are pre-optimized by an inversion of CH_3CCl_3 (MCF) observations as described by Bousquet et al. (2005)[98]. Monthly uncertainties are prescribed for prior CH_4 emissions of ±150% for each region each month, and for CH_4 observations (from ±5 ppb to ±50ppb, with a median of ±10 ppb), with no error correlations. A simple filter is also added in the time domain: changes of the inferred fluxes from one month to the next are limited to ±250% (sources with a seasonal cycle in the prior data) or to ±50% (sources with no seasonal cycle in the prior data) of the prior month-to-month differences, according to previous studies[107,108]. This noise filter avoids the creation of unrealistic large month-to-month flux differences. A more complete description of the method can be found in Bousquet et al. (2005)[98]. We define a reference inversion scenario based on these assumptions, complemented by four additional scenarios varying the number of atmospheric stations (only NOAA/ESRL stations), the OH IAV (OH is maintained constant), the wetland scenario[109], and the noise filter (no noise filter used).

CarbonTracker-CH_4 (Bruhwiler et al., 2012)

The global CH_4 assimilation, CarbonTracker-CH_4, estimates anthropogenic and natural emissions from 2000 through to the end of 2010. Anthropogenic prior emissions are from the EDGAR 3.2FT2000 dataset and were kept constant over the period of the simulation in order to see whether trends in emissions would be captured by the assimilation. Prior wetland emissions were taken from Bergamaschi et al. (2007)[110] and were based on the work by Mathews and Fung (1987)[104]. Natural

prior CH_4 sources also included emissions from wildfires using the GFED product[106], as well as the global soil uptake[111]. Smaller prior emissions from the oceans, termites and wild animals were also included. A diagonal prior covariance matrix was assumed with the uncertainty of individual processes taken to be 75% of the magnitude of each source. To produce flux estimates, CarbonTracker-CH_4 uses the ensemble Kalman smoother described by Peters et al. (2005)[112], and the TM5 transport model with driving meteorology from ECMWF. The estimated parameters are multipliers of the prior flux estimates at weekly intervals, aggregated to monthly values. Air samples from 88 sites distributed globally are used to constrain the flux estimates. Most of the sites were located at the surface; however, at a few sites samples were collected from towers. Aircraft observations were not used, but instead retained for evaluation. The model-data mismatch errors are difficult to quantify for each site; however, sites located in the marine boundary layer and deep Southern Hemisphere were given more weight in the assimilation than continental sites that are more difficult to model due to proximity to local sources. More details on CarbonTracker-CH_4 are given by Bruhwiler et al. (2011)[64].

GEOS-Chem (Fraser et al., 2013)

GEOS-Chem is a global 3-D chemical transport model (v8-01-01) driven by v5 of the analyzed meteorological fields from the NASA Global Modeling and Assimilation Office. A comprehensive description and evaluation of the CH_4 simulation is given by ref([65,113]). Here, the model was run at 4x5 resolution with 47 vertical levels. We use prior year-specific emission inventories for anthropogenic activity (EDGAR 3.2 FT[114]), biomass-burning (GFEDv2[106]), and wetlands and rice[115]; and climatological seasonal emissions for the ocean[116] and all other natural emissions and the soil sink (Fung et al, 1991). We use monthly-mean 3-D fields for the tropospheric OH sink generated from the Ox-NOx-VOC chemistry version of GEOS-Chem[117]. Stratospheric loss rates are adapted from a 2D stratospheric model[118]. We use an ensemble Kalman filter[119] to estimate surface CH_4 fluxes by fitting surface measurements (2000-2010) at 48 sites[108] with measurement errors described by Wang et al. (2004)[118]. We estimate fluxes on an 8-day time step, using a 3.5 month lag window, over 110 regions defined by subdividing each of the 23 continental TransCom regions into 9 regions[100]. For regions

with significant contribution from both seasonal and constant sources (temperate North America, North Africa, temperate Eurasia, Europe) we estimate seasonal and constant emissions separately, assigning a prior uncertainty of 50% for land-regions with seasonal emissions and 25% for constant emissions. For all other regions we estimate all emissions together, with a prior uncertainty of 50%. We report monthly mean fluxes on the original 23 TransCom regions.

TM5-4DVAR (Beck et al., 2012)

The TM5-4DVAR inversions make use of the global atmospheric transport model TM5[95]. The off-line TM5 model is driven by meteorological fields from the ERA-interim reanalysis from ECMWF at a resolution 6x4 degree (lat x long) and 25 hybrid sigma pressure levels. The optimization algorithm is based on the variational approach, and uses the conjugate gradients technique for cost function minimization[93]. The inversion solves for net monthly CH_4 fluxes at the resolution of the transport model for the period 2003-2010. A priori emissions are taken from the EDGAR4.1 emission inventory (http://edgar.jrc.ec.europa.eu) for anthropogenic fluxes, LPJ-WhyMe[62] for natural wetlands, and GFED3[34] for biomass-burning, complemented by minor sources[13]. The photochemical removal of CH_4 is calculated using an MCF calibrated OH climatology[29] and accounts for oxidation by Cl and O^{1D} radicals in the stratosphere[120]. TM5-4DVAR optimizes CH_4 surface fluxes to minimize the misfit with measurements of the CH_4 dry air mole fraction from 46 sites of the NOAA-ESRL cooperative flask sampling network[3] and retrievals of vertical column averaged CH_4 from the SCIAMACHY satellite instrument[18] for the period 2003-2010. Posterior flux estimates per source category are derived from the optimized grid box totals using the a priori assumed partitioning between the processes per grid box.

LMDZt-SACS (Pison et al., 2009; Bousquet et al., 2011)

We use the variational scheme[121] including the off-line version of the LMDZt (Laboratoire de Météorologie Dynamique – Zoom) transport model version 4 coupled with the atmospheric chemistry module SACS (Simplified Atmospheric Chemistry System)[122]. LMDz's grid is 3.75 degrees x 2.5

degrees (longitude-latitude) on 19 sigma-pressure levels. The air mass fluxes are pre-computed by the on-line LMDz version nudged to ECMWF analysis for horizontal winds. SACS represents a simplified CH_4 oxidation chain that links CH_4 and CO through reactions with hydroxyl radicals (OH) and formaldehyde (HCHO)[122]; the reaction between OH and methyl-chloroform (MCF, CH_3CCl_3) is also represented as a constraint on OH concentrations. Methane prior inventories are combined from the Emission Database for Global Atmospheric Research (EDGAR~3) inventory for the year 1995[105] for anthropogenic emissions, the Global Fire and Emission database (GFED-v2)[106] for monthly biomass-burning emissions, the study by Fung et al. (1991)[123] for emissions due to wetlands and termites, and a constant source (total 15 Tg/year) for oceans. MCF emissions are based on the inventory of Montzka et al. (2000)[124], rescaled according to an update of the study by Bousquet et al. (2006)[10]. The prior variances in each grid cell are set at ±100% of the monthly maximum flux over the eight neighbouring grid cells and the current grid cell[122]). The error correlations of the CH_4 fluxes are optimized using correlation lengths of 500 km on land and 1000 km on oceans, without time correlations[121]. Daily mean CH_4 and MCF observations at continuous measurement stations and individual flask observations at flask stations are assimilated at 66 surface stations from the NOAA/ESRL, CSIRO and IPSL/LSCE surface monitoring networks. The inversion is run from January 1990 to March 2009. The relevant cost function and the norm of its gradient (computed by the adjoint) are minimized with the algorithm M1QN3[125]. The inversion results consist of eight-day maps (7081 cells) of net CH_4 emission fluxes and four correction coefficients for OH columns (one per latitudinal band 90S-30S; 30S-0, 0-30N, 30N-90N). To compare our results with the other inventories, the total net fluxes are broken into categories. The global monthly analysis-to-prior ratio is computed and then applied to each source category used in the prior in each grid cell over the month.

MATCH model (Chen & Prinn, 2006)

See Table S1

TM2 model (Hein et al., 1997)

See Table S1

GISS model (Fung et al. 1991)

See Table S1

II.3 Description of bottom-up studies (B-U)

LPJ-wsl (Hodson et al, 2011)

The LPJ-wsl CH_4 model output used in this analysis is the same as presented by Hodson et al., (2011)[63]. The wetland CH_4 flux E (Tg CH_4 grid cell^{-1} month^{-1}) at each 0.5° grid cell (x) and monthly time step (t) is calculated as a linear function of wetland extent (A) and heterotrophic respiration (R_h) according to the following equation:

$$E(x,t) = R_h(x,t)A(x,t)\beta F(x) \qquad (1)$$

R_h is calculated using the LPJ-wsl dynamic global vegetation model (DGVM), based on the LPJv3.1 DGVM[126,127]. The monthly climatology inputs (precipitation, mean temperature, cloud cover, wet days) and the non-gridded annual CO_2 concentration inputs to LPJ-wsl are described by Hodson et al. (2011). In addition, we prescribed[63] soil texture from the Food and Agriculture Organization[128], using a 2-soil layer hydrological model with a total soil depth of 1.5 metres. A 1000-year spin up was implemented by recycling the first 30 years of climate data (1901-1930) with pre-industrial CO_2 concentrations to equilibrate soil and vegetation carbon pools, followed by a transient simulation running from 1901-2005.

Wetland extent (A) represents natural wetland area and lakes only and is a monthly-varying combined model and satellite product at 0.5° x 0.5° spatial resolution[63].

The scaling ratio βF converts C to CH_4 fluxes and is a combination of two scaling factors, one for tropical (TR) and one for boreal (B) wetland conditions, which allows the model to account for broad ecosystem differences in CH_4 emitting capacity between wetland types (Eqn. 2). The fraction of wetland type found in each grid cell is calculated based on surface temperature (Eqn. 3).

$$\beta F = \sigma F_{TR} + (1- \sigma)F_B \qquad (2)$$

$$\sigma = \exp((T(x) - T_{max})/8) \qquad (3)$$

where T is the mean near-surface temperature between 1960–1990, and T_{max} = 303.35 K. F_{TR} and F_B were fit to match regional estimates of wetland CH_4 fluxes for the Hudson Bay lowlands and the central Amazon Basin as described by Hodson et al. (2011).

ORCHIDEE (Ringeval et al., 2011)

The ORCHIDEE model[129] has been implemented with a wetland CH_4 emissions scheme. Such an ORCHIDEE version has been used for various studies on different time-scales[61,130]. The model explicitly represents both the mechanisms leading to CH_4 flux at the atmosphere/soil interface and the dynamic wetland extent. Basically, the wetland CH_4 emissions $E_{CH4}(g,t)$ are computed in ORCHIDEE-WET for each grid-cell g and for each time-step t through the following equation:

$$E_{CH4}(g,t)=\Sigma_{WTDi}(S_{WTDi}(g,t).D_{WTDi}(g,t))$$

Where S_{WTDi} is the fraction of g covered by a wetland where the water table depth is equal to WTD_i and D_{WTDi} is the CH_4 flux density (i.e. g CH_4 per m^2 per unit time) for a wetland where the water table depth is equal to WTD_i. Here, the WTD_i values for each grid-cell are taken as: 0, -3 and -6cm. S_{WTDi} and D_{WTDi} are respectively computed by (i) the coupling between a TOPMODEL approach and ORCHIDEE[131] and (ii) the coupling between a slight modification of the Walter model [132] and ORCHIDEE[130]. As in a previous version[61], the wetland extent is corrected to subtract the systematic biases of the model using a mean climatology of the remote sensing data of inundation extent[133]. Moreover, in the present study, two ORCHIDEE estimates are given in which the seasonal cycle of the

wetland extent is either prescribed (ORCHIDEE-P07) or computed (ORCHIDEE-TOP). In both estimates, the IAV of the wetland extent is computed.

LPJ-WhyMe (Spahni et al., 2011)

Global CH_4 emissions and sinks have been estimated with the B-U approach using the LPJ-WhyMe dynamic global vegetation model[62]. The model was forced by the CRU-NCEP climate data set[134] and run over the period of 1990-2009. The model runs were performed for four wetland source types of atmospheric CH_4 (northern high latitude peatlands, tropical and subtropical inundated wetlands, global rice paddies and global wet mineral soils) and the global CH_4 soil sink. For peatlands, inundated wetlands and rice paddies the fractional emission area was prescribed according to IGBP-DIS soil carbon map (Global Soil Data Task Group, 2000), inundation map[135], and fractional rice cover map[136], respectively. Areas were treated to be conformal (Spahni et al., 2011) and the non-inundated fractional area of mineral soils could be a CH_4 source or a sink depending on soil moisture content as calculated by the LPJ-WhyMe hydrology[62]. CH_4 emission fluxes per unit area were calculated as being proportional to the model's soil carbon respiration, differentially for each emission and sink type. The global scaling parameters were calibrated by a T-D optimization of the global budget using the TM5 atmospheric chemistry and transport model on the basis of monthly fluxes in 2004[62].

GICC (Mieville et al., 2010)

The Global Inventory for Chemistry-Climate studies (GICC)[69] gridded decadal (for the 1980s and 1990s) and yearly (1997-2005) biomass burning emission fields were downloaded from the ECCAD portal (http://eccad.sedoo.fr, date of access: 14 November, 2011).

RETRO (Schultz et al., 2007)

Yearly gridded emission data sets from the Reanalysis of the TROpospheric chemical composition over the last 40 years project (RETRO)[67] for the period 1980-2000 were downloaded from ftp://ftp.retro.enes.org/pub/emissions/ch4/.

GFEDv2 (Van der Werf et al., 2004)

The Global Fire Emission Database version 2 (GFEDv2)[68] gridded monthly biomass burning emission fields for the period 1997-2008 were downloaded from the ECCAD portal (http://eccad.sedoo.fr, date of access: 30 January, 2012).

GFEDv3 (Van der Werf et al., 2010)

The Global Fire Emission Database version 3 (GFEDv3)[34] gridded monthly biomass burning emission fields for the period 1997-2009 were downloaded from http://www.falw.vu/~gwerf/GFED/GFED3/emissions/ (date of access: 20 July 2011).

FINNv1 (Wiedinmyer et al., 2011)

The Fire Inventory from NCAR (FINNv1)[70] gridded emission fields were gathered by Christine Wiedinmyer and downloaded from the ftp server (date of access: 3 January 2012).

IIASA (Dentener et al., 2005)

IIASA CH_4 data for the 1990's and 2000s and the fossil fuel, agriculture/waste and biomass burning categories[137] were downloaded from http://www.iiasa.ac.at/rains/global_emiss/global_emiss.html (date of access: 7 November 2011).

EPA, 2011

EPA[138,139] CH_4 data for the 1990's and 2000s and the fossil fuel and agriculture/waste categories were downloaded from http://www.epa.gov/climatechange/economics/downloads/Data%20Annexes%20-%202012.zip (date of access: 14 November 2011).

EDGARv4.1 (EDGAR4.1, 2009)

EDGARv4.1[140] gridded emission fields for anthropogenic fluxes were downloaded from the EDGAR website (http://edgar.jrc.ec.europa.eu/datasets_grid_list41.php#, date of access: 26 August, 2011).

EDGARv4.2 (EDGAR4.2, 2011)

EDGARv4.2[140] gridded emission fields for anthropogenic fluxes were downloaded from the EDGAR website (http://edgar.jrc.ec.europa.eu/datasets_list.php?v=42&edgar_compound=CH4, date of access: 20, November 2012).

Description of models contributing to the Atmospheric Chemistry and Climate Model Intercomparison Project (ACCMIP, Lamarque et al., 2013; Voulgarakis et al., 2013; Naik et al., 2013)

The Atmospheric Chemistry and Climate Model Intercomparison Project (ACCMIP)[141,142,152] (http://www.giss.nasa.gov/projects/accmip/) consists of a series of timeslice experiments targeting the long-term changes in atmospheric composition between 1850 and 2100, with the goal of documenting radiative forcing and the associated composition changes. Methane chemical destruction due to OH from 9 of the 12 ACCMIP models is included in this study. All the models are run as coupled chemistry-climate models (CCMs), driven by monthly mean sea-surface temperatures and sea-ice coverage either from observations or from the corresponding coupled ocean-atmosphere model integrations submitted to the Coupled Model Intercomparison Project Phase 5 (CMIP5). All details about model specifications and performed simulations can be found in the related publications[142,143].

In most models, CH_4 concentration was prescribed at the surface using the historical reconstruction but was allowed to undergo chemical processing in the rest of the atmosphere. In LMDzORINCA surface CH_4 emissions were specified following ref([144]), while UM-CAM used a globally constant concentration. In all models, CH_4 varies between different timeslices. Ozone photolysis is the primary source of hydroxyl radicals (OH), the main sink for CH_4, in the troposphere. CESM-CAM-superfast, CMAM, GFDL-AM3[145], LMDzORINCA, MIROC-CHEM, NCAR-CAM3.5, and UM-CAM employed a lookup table approach wherein calculated clear-sky photolysis frequencies are adjusted for modelled clouds, overhead ozone column, and surface albedo. The GEOSCCM, and GISS-E2-R models used versions of the Fast-J scheme[146], which calculates photolysis frequencies online

accounting for modelled clouds, overhead ozone column, surface albedo and aerosols. Overhead stratospheric ozone column determines the level of incoming ultraviolet radiation, important for the formation of tropospheric OH radicals. Six of the nine models simulated full stratospheric chemistry. Stratospheric ozone concentrations in the UM-CAM and LMDzORINCA were prescribed from a database[147] developed in support of CMIP5 and a climatology[148], respectively. In CESM-CAM-superfast, a simplified "linearized ozone chemistry" (LINOZ) scheme was used.

We used data from the 1980 and 2000 timeslices simulated within the ACCMIP intercomparison, representing the CH_4 chemical loss for the years around 1980 and 2000. This provides estimates of CH_4 loss due to OH for the 1980s and the 2000s, two of the decades we are interested in. Only two of the models, LMDzORINCA and GISS-E2-R, provided a full year-to-year dataset from transient simulations for all three decades. Since no model simulated a 1990 timeslice, we only used those two models to estimate CH_4 chemical loss for the 1990s. This explains why we get fewer estimates in the 1990s than in the 1980s and the 2000s (Fig. 2).

TM5 full chemistry model (Williams et al., 2012; Huijnen et al., 2010)

Forward simulations using the TM5 chemistry-transport model in full chemistry mode and relaxation to CH_4 surface concentrations provide information on the global sink term. Information on CH_4 emissions is obtained following a semi-inverse approach[149]. Forward simulations using TM5 and including CH_4 emissions[62] and latest anthropogenic emission inventories[140] provide information on the 3D time evolution of the OH field. The full chemistry simulations are performed on 3x2 degrees (longitude x latitude) grid and 34 sigma-pressure vertical levels. The calculated CH_4 losses for the years 2000-2009 are given for the TM5 model version referenced in refs ([150,151]).

III References

1 Blake, D. R. et al. Global Increase in Atmospheric Methane Concentrations between 1978 and 1980. Geophys. Res. Lett. **9**, 477-480 (1982).

2 Cunnold, D. M. et al. In situ measurements of atmospheric methane at GAGE/AGAGE sites during 1985-2000 and resulting source inferences. J. Geophys. Res.-atmos. **107**, ACH 20-21-ACH 20-18, doi:10.1029/2001jd001226 (2002).

3 Dlugokencky, E. J. et al. Observational constraints on recent increases in the atmospheric CH burden, . Geophys. Res. Lett., **36**, L18803, doi:doi:10.1029/2009GL039780. (2009).

4 Francey, R. J. et al. Atmospheric carbon dioxide and its stable isotope ratios, methane, carbon monoxide, nitrous oxide and hydrogen from Shetland Isles. Atmos. Environ. **32**, 3331-3338 (1998).

5 Brenninkmeijer, C. A. M. et al. Civil Aircraft for the regular investigation of the atmosphere based on an instrumented container: The new CARIBIC system. Atmos. Chem. Phys. **7**, 4953-4976, doi:10.5194/acp-7-4953-2007 (2007).

6 Wecht, K. J. et al. Validation of TES methane with HIPPO aircraft observations: implications for inverse modeling of methane sources. Atmos. Chem. Phys. **12**, 1823-1832, doi:10.5194/acp-12-1823-2012 (2012).

7 WMO. WMO World Data Centre for Greenhouse Gases, <http://ds.data.jma.go.jp/gmd/wdcgg/introduction.html> (2012).

8 Sussmann, R., Forster, F., Rettinger, M. & Bousquet, P. Renewed methane increase for five years (2007,Äì2011) observed by solar FTIR spectrometry. Atmos. Chem. Phys. **12**, 4885-4891, doi:10.5194/acp-12-4885-2012 (2012).

9 Wunch, D. et al. The Total Carbon Column Observing Network, . Phil. Trans. R. Soc. A, **369**, doi: 10.1098/rsta.2010.0240 (2011).

10 Bousquet, P. et al. Contribution of anthropogenic and natural sources to atmospheric methane variability. Nature **443**, 439-443 (2006).

11 Fisher, R. E. et al. Arctic methane sources: Isotopic evidence for atmospheric inputs. Geophys. Res. Lett. **38**, L21803, doi:10.1029/2011gl049319 (2011).

12 Mikaloff Fletcher, S. E. M., Tans, P. P., Bruhwiler, L. M., Miller, J. B. & Heimann, M. CH4 sources estimated from atmospheric observations of CH4 and its C-13/C-12 isotopic ratios: 1. Inverse modeling of source processes. Global. Biogeochem. Cycles **18**, GB4004, doi:4010.1029/2004GB002223 (2004).

13 Monteil, G. et al. Interpreting methane variations in the past two decades using measurements of CH(4) mixing ratio and isotopic composition. Atmos Chem Phys **11**, 9141-9153 (2011).

14 Neef, L., van Weele, M. & van Velthoven, P. Optimal estimation of the present-day global methane budget. Global. Biogeochem. Cycles **24** (2010).

15 Wahlen, M. The Global Methane Cycle. Annual Review of Earth and Planetary Sciences **21**, 407-426, doi:doi:10.1146/annurev.ea.21.050193.002203 (1993).

16 Lassey, K. R., Lowe, D. C. & Smith, A. M. The atmospheric cycling of radiomethane and the "fossil fraction" of the methane source. Atmos Chem Phys **7**, 2141-2149 (2007).

17 Crevoisier, C. et al. First year of upper tropospheric integrated content of CO(2) from IASI hyperspectral infrared observations. Atmos Chem Phys **9**, 4797-4810 (2009).

18 Frankenberg, C. et al. Global column-averaged methane mixing ratios from 2003 to 2009 as derived from SCIAMACHY: Trends and variability. J. Geophys. Res.-atmos. **116**, D04302, doi:10.1029/2010jd014849 (2011).

19 Morino, I. et al. Preliminary validation of column-averaged volume mixing ratios of carbon dioxide and methane retrieved from GOSAT short-wavelength infrared spectra. Atmos Meas Tech **4**, 1061-1076 (2011).

20 Butz, A. et al. Toward accurate CO(2) and CH(4) observations from GOSAT. Geophys. Res. Lett. **38**, L14812, doi:10.1029/2011gl047888 (2011).

21 Parker, R. et al. Methane observations from the Greenhouse Gases Observing SATellite: Comparison to ground-based TCCON data and model calculations. Geophys. Res. Lett. **38**, L15807, doi:10.1029/2011gl047871 (2011).

22 Frankenberg, C. et al. Satellite chartography of atmospheric methane from SCIAMACHY on board ENVISAT: Analysis of the years 2003 and 2004. J. Geophys. Res.-atmos. **111**, D07303, doi:DOI: 10.1029/2005JD006235 (2006).

23 Bergamaschi, P. et al. Inverse modeling of global and regional CH4 emissions using SCIAMACHY satellite retrievals. J. Geophys. Res.-atmos. **114**, doi:10.1029/2009JD012287 (2009).

24 Dlugokencky, E. J., Nisbet, E. G., Fisher, R. & Lowry, D. Global atmospheric methane: budget, changes and dangers. Philos T R Soc A **369**, 2058-2072 (2011).

25 Rigby, M. et al. Renewed growth of atmospheric methane. Geophys. Res. Lett. **35**, - (2008).

26 Francey, R. J., Steele, L. P., Langenfelds, R. L. & Pak, B. C. High precision long-term monitoring of radiatively active and related trace gases at surface sites and from aircraft in the southern hemisphere atmosphere. J Atmos Sci **56**, 279-285 (1999).

27 Simpson, I. J. et al. Long-term decline of global atmospheric ethane concentrations and implications for methane. Nature **488**, 490-494, doi:http://www.nature.com/nature/journal/v488/n7412/abs/nature11342.html (2012).

28 Thoning, K. W., Tans, P. P. & Komhyr, W. D. Atmospheric carbon dioxide at Mauna Loa Observatory. 2. Analysis of the NOAA GMCC data, 1974,1985. J. Geophys. Res. **94**, 8549-8565 (1989).

29 Montzka, S. A. et al. Small Interannual Variability of Global Atmospheric Hydroxyl. Science **331**, 67-69 (2011).

30 Dlugokencky, E. J. et al. Changes in CH4 and CO growth rates after the eruption of Mt Pinatubo and their link with changes in tropical tropospheric UV flux. Geophys. Res. Lett. **23**, 2761-2764 (1996).

31 Chen, Y. H. & Prinn, R. G. Estimation of atmospheric methane emissions between 1996 and 2001 using a three-dimensional global chemical transport model. J. Geophys. Res.-atmos. **111**, doi:10.1029/2005JD006058 (2006).

32 Dlugokencky, E. J. et al. Atmospheric methane levels off: Temporary pause or a new steady-state? Geophys. Res. Lett. **30**, 1992, doi:1910.1029/2003GL018126, doi:ftp://ftp.cmdl.noaa.gov/ccg (2003).

33 Langenfelds, R. L. et al. Interannual growth rate variations of atmospheric CO2 and its delta C-13, H-2, CH4, and CO between 1992 and 1999 linked to biomass burning. Global. Biogeochem. Cycles **16**, 1048, doi: doi:10.1029/2001GB001466 (2002).

34 van der Werf, G. R. et al. Global fire emissions and the contribution of deforestation, savanna, forest, agricultural, and peat fires (1997-2009). Atmos Chem Phys **10**, 11707-11735 (2010).

35 Prinn, R. G. et al. Evidence for variability of atmospheric hydroxyl radicals over the past quarter century. Geophys. Res. Lett. **32**, L07809, doi:07810.01029/02004GL022228 (2005).

36 Bousquet, P. et al. Source attribution of the changes in atmospheric methane for 2006-2008. Atmos Chem Phys **11**, 3689-3700 (2011).

37 Rigby, M. et al. Renewed growth of atmospheric methane. Geophys. Res. Lett. **35**, L22805, doi:10.1029/2008gl036037 (2008).

38 Sanderson, M. G. Biomass of termites and their emissions of methane and carbon dioxide: A global database. Global Biogeochem. Cycles **10**, 543-557, doi:10.1029/96gb01893 (1996).

39 Sugimoto, A., Inoue, T., Kirtibutr, N. & Abe, T. Methane oxidation by termite mounds estimated by the carbon isotopic composition of methane. Global Biogeochem. Cycles **12**, 595-605, doi:10.1029/98gb02266 (1998).

40 Bignell, D. E., Eggleton, P., Nunes, L. & Thomas, K. L. in Forests and Insects (ed N.E. Stork and M.D. Hunter (Editors) A.D. Watt) 109-134 (Chapman and Hall, 1997).

41 Jung, M., Reichstein, M. & Bondeau, A. Towards global empirical upscaling of FLUXNET eddy covariance observations: validation of a model tree ensemble approach using a biosphere model. Biogeosciences **6**, 2001-2013, doi:10.5194/bg-6-2001-2009 (2009).

42 Jung, M. et al. Global patterns of land-atmosphere fluxes of carbon dioxide, latent heat, and sensible heat derived from eddy covariance, satellite, and meteorological observations. J. Geophys. Res. **116**, G00J07, doi:10.1029/2010jg001566 (2011).

43 Ramankutty, N. & Foley, J. A. Estimating historical changes in global land cover: Croplands from 1700 to 1992. Global Biogeochem. Cycles **13**, 997-1027, doi:10.1029/1999gb900046 (1999).

44 Attignon, S. E., Lachat, T., Sinsin, B., Nagel, P. & Peveling, R. Termite assemblages in a West-African semi-deciduous forest and teak plantations Agr. Ecosys. Environ. **110**, 318–326 (2005).

45 Jones, D. T. et al. Termite assemblage collapse along a land-use intensification gradient in lowland central Sumatra, Indonesia, . J. Appl. Ecol. **40**, 380–391 (2003).

46 Kagezi, G. H. et al. Decomposition of tissue baits and termite density along a gradient of human land-use intensification in Western Kenya, Afr. J. Ecol. **49**, 267–276 (2011).

47 Rahman, P. M., Varma, R.V., Sileshi, G.W.: . Abundance and diversity of soil invertebrates in annual crops, agroforestry and forest ecosystems in the Nilgiri biosphere reserve of Western Ghats, India, . Agroforest Syst. , DOI 10.1007/s10457-10011-19386-10453, doi:DOI 10.1007/s10457-011-9386-3 (2011).

48 Abensperg-Traun, M. & de Boer, E. S. Species abundances and habitat differences in biomass of subterranean termites (isoptera) in the wheatbelt of western Australia. Aust. J. Ecol. **15**, 219-226 (1990).

49 Martius, C. et al. Methane emission from wood- feeding termites in Amazonia. Chemosphere **26**, 623-632 (1993).

50 Macdonald, J. A., Eggleton, P., Bignell, D. E., Forzi, F. & Fowler, D. Methane emission by termites and oxidation by soils, across a forest disturbance gradient in the Mbalmayo Forest Reserve, Cameroon. Glob. Change Biol. **4**, 409-418 (1998).

51 Macdonald, J. A. et al. The effect of termite biomass and anthropogenic disturbance on the CH4 budgets of tropical forests in Cameroon and Borneo. Glob. Change Biol. **5**, 869-879. (1999).

52 Fraser, P. J., Rasmussen, R. A., Creffield, J. W., French, J. R. & Khalil, M. A. K. Termites and global methane – another assessment. J. Atmos. Chem., **4**, 295-310 (1986).

53 Keppler, F., Hamilton, J. T. G., Brass, M. & Rockmann, T. Methane emissions from terrestrial plants under aerobic conditions. Nature **439**, 187-191 (2006).

54 Frankenberg, C., Meirink, J. F., van Weele, M., Platt, U. & Wagner, T. Assessing methane emissions from global space-borne observations. Science **308**, 1010-1014 (2005).

55 Frankenberg, C. et al. Tropical methane emissions: A revised view from SCIAMACHY onboard ENVISAT. Geophys. Res. Lett. **35**, L15811, doi:doi:10.1029/2008GL034300 (2008).

56 Dueck, T. A. et al. No evidence for substantial aerobic methane emission by terrestrial plants: a 13C-labelling approach,. New Phytologist **10.1111/j.1469-8137.2007.02103.x.** (2007).

57 Nisbet, R. E. R. et al. Emission of methane from plants. P Roy Soc B-Biol Sci **276**, 1347-1354 (2009).

58 Vigano, I. et al. Effect of UV radiation and temperature on the emission of methane from plant biomass and structural components. Biogeosciences **5**, 937-947 (2008).

59 Bloom, A. A. et al. Global methane emission estimates from ultraviolet irradiation of terrestrial plant foliage. New Phytologist **doi:10.1111/j.1469-8137.2010.03259.x** (2010).

60 Houweling, S., van der Werf, G. R., Goldewijk, K. K., Rockmann, T. & Aben, I. Early anthropogenic CH4 emissions and the variation of CH4 and (CH4)-C-13 over the last millennium. Global. Biogeochem. Cycles **22**, - (2008).

61 Ringeval, B. et al. Climate-CH(4) feedback from wetlands and its interaction with the climate-CO(2) feedback. Biogeosciences **8**, 2137-2157 (2011).

62 Spahni, R. et al. Constraining global methane emissions and uptake by ecosystems. Biogeosciences **8**, 1643-1665, doi:10.5194/bg-8-1643-2011 (2011).

63 Hodson, E. L., Poulter, B., Zimmermann, N. E., Prigent, C. & Kaplan, J. O. The El Niño Southern Oscillation and wetland methane interannual variability. Geophys. Res. Lett. **38**, L08810, doi:10.1029/2011gl046861 (2011).

64 Bruhwiler, L., Dlugokencky, E. J. & Masarie, K. in AGU Fall Meeting Vol. Abstract B11G-01 (San Francisco, Calif., , 2011).

65 Fraser, A. et al. Estimating regional methane surface fluxes: the relative importance of surface and GOSAT mole fraction measurements. Atmos. Chem. Phys. **13**, 5697-5713, doi:10.5194/acp-13-5697-2013 (2013).

66 Beck, V. et al. Methane airborne measurements and comparison to global models during BARCA. Journal of Geophysical Research: Atmospheres **117**, D15310, doi:10.1029/2011jd017345 (2012).

67 Schultz, M. G. et al. Emission data sets and methodologies for estimating emissions., (Hamburg., 2007).

68 van der Werf, G. R. et al. Continental-scale partitioning of fire emissions during the 1997 to 2001 El Nino/La Nina period. Science **303**, 73-76 (2004).

69 Mieville, A. et al. Emissions of gases and particles from biomass burning during the 20th century using satellite data and an historical reconstruction. Atmos. Environ. **44**, 1469-1477, doi:10.1016/j.atmosenv.2010.01.011 (2010).

70 Wiedinmyer, C. et al. The Fire INventory from NCAR (FINN): a high resolution global model to estimate the emissions from open burning. Geosci Model Dev **4**, 625-641 (2011).

71 Beer, C. et al. Terrestrial Gross Carbon Dioxide Uptake: Global Distribution and Covariation with Climate. Science **329**, 834-838, doi:10.1126/science.1184984 (2010).

72 Kanniah, K. D., Beringer, J. & Hutley, L. B. Environmental controls on the spatial variability of savanna productivity in the Northern Territory Australia. Agr. Forest Meteorol. **151**, 1429– 1439 (2011).

73 Maldague, M. E. in Trans. 8th Int. Congr. Soil Sci., . (eds C. Martius, R. Wassmann, & U. Thein) 743-751.

74 Lepage, M. *Les termites d'une savane sahélienne (Ferlo Septentrional, Sénégal): peuplement, populations, consummation, rôle dans l'écosystème*, Univ. of Djion, , (1974).

75 Ohiagu, C. E. Nest and soil populations of Trinervitermes spp. with particular reference to T. geminatus (Wasmann), (Isoptera), in Southern Guinea savanna near Mokwa, Nigeria, . Oecologia **40**, 167-178 (1978).

76 Wood, T. G., Johnson, R. A. & Ohiagu, C. E. Populations of termites (Isoptera) in natural and agriculturalecosystems in Southern Guinea savanna near Mokwa,Nigeria. Geo. Eco. Trop. **1**, 139-148 (1977).

77 Abe, T. & Matsumoto, T. Studies on the distribution and ecological role of termites in a lowland rain forest of west Malaysia, 3, Distribution and abundance of termites in Pasoh forest reserve. Jpn. J. Ecol. **29**, 337-351 (1979).

78 Ferrar, P. Termites of a south African savanna, I, List of species and subhabitat preferences. Oecologia **52**, 125-132 (1982).

79 Ferrar, P. Termites of a south African savanna, IV, Subterranean populations, mass determination and biomass estimations. Oecologia **52**, 147-151 (1982).

80 Wood, T. G., Johnson, R. A., Bacchus, S., Shittu, M. O. & Anderson, J. M. Abundance and distribution of termites (Isoptera) in a riparian forest in the Southern Guinea savanna zone of Nigeria. Biotropica **14**, 25–39 (1982).

81 Holt, J. A. & Easey, J. F. Numbers and biomass of mound-building termites (isopteran) in a semi-arid tropical woodland near Charters Towers, north Queensland, Australia. Sociobiolog **21**, 281-286 (1993).

82 Inoue, T. et al. The abundance and biomass of subterranean termites (Isoptera) in a dry evergreen forest of northeast Thailand. Sociobiology **37**, 41-52 (2000).

83 Dlugokencky, E. J., Steele, L. P., Lang, P. M. & Masarie, K. A. The Growth-Rate and Distribution of Atmospheric Methane. J. Geophys. Res.-atmos. **99**, 17021-17043 (1994).

84 Dlugokencky, E. J. et al. Conversion of NOAA atmospheric dry air CH4 mole fractions to a gravimetrically prepared standard scale. J. Geophys. Res., **110**, doi:10.1029/2005JD006035. (2005).

85 O'doherty, S. et al. In situ chloroform measurements at Advanced Global Atmospheric Gases Experiment atmospheric research stations from 1994 to 1998. J. Geophys. Res.-atmos. **106**, 20429-20444 (2001).

86 Cunnold, D. M. et al. The Atmospheric Lifetime Experiment .3. Lifetime Methodology and Application to 3 Years of Cfcl3 Data. J Geophys Res-Oc Atm **88**, 8379-8400 (1983).

87 Cunnold, D. M. et al. Global Trends and Annual Releases of Ccl3f and Ccl2f2 Estimated from Ale/Gage and Other Measurements from July 1978 to June 1991. J. Geophys. Res.-atmos. **99**, 1107-1126 (1994).

88 Rigby, M. et al. Re-evaluation of the lifetimes of the major CFCs and CH3CCl3 using atmospheric trends. Atmos. Chem. Phys. **13**, 2691-2702, doi:10.5194/acp-13-2691-2013 (2013).

89 Cooper, L. N., Steele, L. P., Langenfelds, R. L., Spencer, D. A. & P., L. M. Atmospheric methane, carbon dioxide, hydrogen, carbon monoxide and nitrous oxide from Cape Grim flask air samples analysed by gas chromatography. . 98pp (Bureau of Meteorology and CSIRO Atmospheric Research, Melbourne, 1999).

90 Francey, R. J. & Steele, L. P. Measuring atmospheric carbon dioxide - the calibration challenge. Accredit Qual Assur **8**, 200-204 (2003).

91 Simpson, I. J., Blake, D. R., Rowland, F. S. & Chen, T. Y. Implications of the recent fluctuations in the growth rate of tropospheric methane. Geophys. Res. Lett. **29** (2002).

92 Simpson, I. J., Rowland, F. S., Meinardi, S. & Blake, D. R. Influence of biomass burning during recent fluctuations in the slow growth of global tropospheric methane. Geophys. Res. Lett. **33** (2006).

93 Meirink, J. F., Bergamaschi, P. & Krol, M. C. Four-dimensional variational data assimilation for inverse modelling of atmospheric methane emissions: method and comparison with synthesis inversion. Atmos Chem Phys **8**, 6341-6353 (2008).

94 Bergamaschi, P. et al. Inverse modeling of European CH(4) emissions 2001-2006. J. Geophys. Res.-atmos. **115** (2010).

95 Krol, M. et al. The two-way nested global chemistry-transport zoom model TM5: algorithm and applications. Atmos Chem Phys **5**, 417-432 (2005).

96 Peylin, P. et al. Multiple constraints on regional CO2 flux variations over land and oceans. Global. Biogeochem. Cycles **19**, - (2005).

97 Bousquet, P. et al. Regional changes in carbon dioxide fluxes of land and oceans since 1980. Science **290**, 1342-1346 (2000).

98 Bousquet, P., Hauglustaine, D. A., Peylin, P., Carouge, C. & Ciais, P. Two decades of OH variability as inferred by an inversion of atmospheric transport and chemistry of methyl chloroform. Atmos Chem Phys **5**, 2635-2656 (2005).

99 Bousquet, P. et al. A three-dimensional synthesis inversion of the molecular hydrogen cycle: Sources and sinks budget and implications for the soil uptake. J. Geophys. Res.-atmos. **116**, - (2011).

100 Gurney, K. R. et al. Transcom 3 inversion intercomparison: Model mean results for the estimation of seasonal carbon sources and sinks. Global. Biogeochem. Cycles **18**, GB2010, doi:10.1029/2003gb002111 (2004).

101 Uppala, S. M. et al. The ERA-40 Reanalysis. J. Roy. Met. Soc. **131**, 2961-3012 (2005).

102 Hourdin, F. & Talagrand, O. Eulerian backtracking of atmospheric tracers. I: Adjoint derivation and parametrization of subgrid-scale transport. Quarterly Journal of the Royal Meteorological Society **132**, 567-583 (2006).

103 Hourdin, F. D., Couvreux, F. & Menut, L. Parameterization of the dry convective boundary layer based on a mass flux representation of thermals. J Atmos Sci **59**, 1105-1123 (2002).

104 Matthews, E. & Fung, I. Methane emissions from natural wetlands, global distribution, area and environmental characteristics of sources. Global. Biogeochem. Cycles **1**, 61-86 (1987).

105 Olivier, J. G. J. & Berdowski, J. J. M. in *The Climate System,* (eds J. Berdowski, R. Guichert, & B. Heij) p. 33–78 (A.A. Balkema Publishers/Swets & Zeitlinger Publishers, 2001).

106 van der Werf, G. R. et al. Interannual variability in global biomass burning emissions from 1997 to 2004. Atmos Chem Phys **6**, 3423-3441 (2006).

107 Peylin, P., Bousquet, P., Ciais, P. & Monfray, P. in Inverse methods in global biogeochemical cycles, Geophysical Monograph 114 (eds P. Kashibata et al.) (American Geophysical Union,, 1999).

108 Peylin, P., Baker, D., Sarmiento, J., Ciais, P. & Bousquet, P. Influence of transport uncertainty on annual mean and seasonal inversions of atmospheric CO2 data. J. Geophys. Res.-atmos. **107**, 4385, doi:4310.1029/2001JD000857 (2002).

109 Kaplan, J. O. Wetlands at the Last Glacial Maximum: Distribution and methane emissions. Geophys. Res. Lett. **29**, 1079, doi:10.1029/2001gl013366 (2002).

110 Bergamaschi, P. et al. Satellite chartography of atmospheric methane from SCIAMACHYon board ENVISAT: 2. Evaluation based on inverse model simulations. J. Geophys. Res.-atmos. **112**, - (2007).

111 Ridgwell, A. J., Marshall, S. J. & Gregson, K. Consumption of atmospheric methane by soils: A process-based model. Global Biogeochem. Cycles **13**, 59-70, doi:10.1029/1998gb900004 (1999).

112 Peters, W. et al. An ensemble data assimilation system to estimate CO2 surface fluxes from atmospheric trace gas observations. J. Geophys. Res.-atmos. **110**, D24304, doi:24310.21029/22005JD006157 (2005).

113 Fraser, A. et al. The Australian methane budget: Interpreting surface and train-borne measurements using a chemistry transport model. Journal of Geophysical Research: Atmospheres **116**, D20306, doi:10.1029/2011jd015964 (2011).

114 Olivier, J. G. J., van Aardenne, J. A., Dentener, F., Ganzeveld, L. & Peters, J. A. H. W. in Non- CO2 Greenhouse Gases (NCGG- 4), . (ed A. van Amstel) pp. 325–330, (Millpress, Rotterdam).

115 Bloom, A. A., Palmer, P. I., Fraser, A., Reay, D. S. & Frankenberg, C. Large-Scale Controls of Methanogenesis Inferred from Methane and Gravity Spaceborne Data. Science **327**, 322-325, doi:10.1126/science.1175176 (2010).

116 Houweling, S., Kaminski, T., Dentener, F., Lelieveld, J. & Heimann, M. Inverse modeling of methane sources and sinks using the adjoint of a global transport model. J. Geophys. Res.-atmos. **104**, 26137-26160 (1999).

117 Fiore, A. et al. Variability in surface ozone background over the United States: Implications for air quality policy. J. Geophys. Res. **108**, 4787, doi:10.1029/2003jd003855 (2003).

118 Wang, J. S. et al. A 3-D model analysis of the slowdown and interannual variability in the methane growth rate from 1988 to 1997. Global. Biogeochem. Cycles **18**, 3011, doi:3010.1029/2003GB002180 (2004).

119 Feng, L. et al. Evaluating a 3-D transport model of atmospheric CO2 using ground-based, aircraft, and space-borne data. Atmos. Chem. Phys. **11**, 2789-2803, doi:10.5194/acp-11-2789-2011 (2011).

120 Law, K. S. & Pyle, J. A. Modeling trace gas budgets in the troposphere: 1. Ozone and odd nitrogen. Journal of Geophysical Research: Atmospheres **98**, 18377-18400, doi:10.1029/93jd01479 (1993).

121 Chevallier, F. et al. Inferring CO2 sources and sinks from satellite observations: Method and application to TOVS data. J. Geophys. Res.-atmos. **110**, doi:D24309 10.1029/2005jd006390 (2005).

122 Pison, I., Bousquet, P., Chevallier, F., Szopa, S. & Hauglustaine, D. Multi-species inversion of CH4, CO and H-2 emissions from surface measurements. Atmos Chem Phys **9**, 5281-5297 (2009).

123 Fung, I. et al. Three-dimensional model synthesis of global methane cycle. J. Geophys. Res. **96**, 13033-13065 (1991).

124 Montzka, S. A. et al. New observational constraints for atmospheric hydroxyl on global and hemispheric scales. Science **288**, 500-503 (2000).

125 Gilbert, J.-C. & Lemaréchal, C. Some numerical experiments with variable-storage quasi-Newton algorithms. Mathematical programming **45**, 407–435. (1989).

126 Sitch, S. et al. Evaluation of ecosystem dynamics, plant geography and terrestrial carbon cycling in the LPJ dynamic global vegetation model. Glob Change Biol **9**, 161-185 (2003).

127 Gerten, D., Schaphoff, S., Haberlandt, U., Lucht, W. & Sitch, S. Terrestrial vegetation and water balance—hydrological evaluation of a dynamic global vegetation model. Journal of Hydrology **286**, 249-270, doi:10.1016/j.jhydrol.2003.09.029 (2004).

128 Zobler, L. A world soil file for global climate modelling. 32 pages. (NASA/GISS, New York USA, 1986).

129 Krinner, G. et al. A dynamic global vegetation model for studies of the coupled atmosphere-biosphere system. Global. Biogeochem. Cycles **19**, - (2005).

130 Ringeval, B. et al. An attempt to quantify the impact of changes in wetland extent on methane emissions on the seasonal and interannual time scales. Global. Biogeochem. Cycles **24**, doi:Gb2003 10.1029/2008gb003354 (2010).

131 Ringeval, B. et al. Modelling sub-grid wetland in the ORCHIDEE global land surface model: evaluation against river discharges and remotely sensed data. Geosci. Model Dev. **5**, 941-962, doi:10.5194/gmd-5-941-2012 (2012).

132 Walter, B. P., Heimann, M. & Matthews, E. Modeling modern methane emissions from natural wetlands 2. Interannual variations 1982-1993. J. Geophys. Res.-atmos. **106**, 34207-34219 (2001).

133 Papa, F. et al. Interannual variability of surface water extent at the global scale, 1993–2004. J. Geophys. Res. **115**, D12111, doi:10.1029/2009jd012674 (2010).

134 Viovy, N. & Ciais, P. Vol. http://dods.extra.cea.fr/data/p529viov/cruncep/readme.htm (2009).

135 Prigent, C., Papa, F., Aires, F., Rossow, W. B. & Matthews, E. Global inundation dynamics inferred from multiple satellite observations, 1993-2000. J. Geophys. Res.-atmos. **112**, -, doi:doi:10.1029/2006JD007847 (2007).

136 Leff, B., Ramankutty, N. & Foley, J. A. Geographic distribution of major crops across the world. Global Biogeochem. Cycles **18**, GB1009, doi:10.1029/2003gb002108 (2004).

137 Dentener, F. et al. The impact of air pollutant and methane emission controls on tropospheric ozone and radiative forcing: CTM calculations for the period 1990-2030. Atmos Chem Phys **5**, 1731-1755 (2005).

138 EPA. Global Anthropogenic Non-CO2 Greenhouse Gas Emissions: 1990 - 2030. (U.S. Environmental Protection Agency, Washington, DC 20460, 2011).

139 Environmental Protection Aagency report: Methane and Nitrous Oxide Emissions From Natural Sources. http://www.epa.gov/methane/pdfs/Methane-and-Nitrous-Oxide-Emissions-From-Natural-Sources.pdf, U.S. Environmental Protection Agency, Washington, DC 20460 (2010).

140 European Commission, Joint Research Centre (JRC)/Netherlands Environmental Assessment Agency (PBL). Emission Database for Global Atmospheric Research (EDGAR), release version 4.2. http://edgar.jrc.ec.europa.eu, 2011.

141 Lamarque, J. F. et al. The Atmospheric Chemistry and Climate Model Intercomparison Project (ACCMIP): overview and description of models, simulations and climate diagnostics. Geosci. Model Dev. **6**, 179-206, doi:10.5194/gmd-6-179-2013 (2013).

142 Voulgarakis, A. et al. Analysis of present day and future OH and methane lifetime in the ACCMIP simulations. Atmos. Chem. Phys. **13**, 2563-2587, doi:10.5194/acp-13-2563-2013 (2013).

143 Lamarque, J. F. et al. The Atmospheric Chemistry and Climate Model Intercomparison Project (ACCMIP): overview and description of models, simulations and climate diagnostics. Geosci. Model Dev. **6**, 179-206, doi:10.5194/gmd-6-179-2013 (2013).

144 Lamarque, J. F. et al. Historical (1850–2000) gridded anthropogenic and biomass burning emissions of reactive gases and aerosols: methodology and application. Atmos. Chem. Phys. **10**, 7017-7039, doi:10.5194/acp-10-7017-2010 (2010).

145 Donner, L. J. & al., e. The Dynamical Core, Physical Parameterizations, and Basic Simulation Characteristics of the Atmospheric Component AM3 of the GFDL Global Coupled Model CM3. . J. Climate **24**, 3484–3519, doi:doi: http://dx.doi.org/10.1175/2011JCLI3955.1 (2011).

146 Wild, O., Zhu, X. & Prather, M. J. Fast-J: Accurate simulation of in- and below-cloud photolysis in tropospheric chemical models. J. Atmos. Chem., **37**, 245-282 (2000).

147 Cionni, I. et al. Ozone database in support of CMIP5 simulations: results and corresponding radiative forcing. Atmos. Chem. Phys. **11**, 11267-11292, doi:10.5194/acp-11-11267-2011 (2011).

148 Li, D. & Shine, K. P. A 4-Dimensional Ozone Climatology for UGAMP Models, . (1995).

149 Dentener, F., van Weele, M., Krol, M., Houweling, S. & van Velthoven, P. Trends and inter-annual variability of methane emissions derived from 1979-1993 global CTM simulations. Atmos Chem Phys **3**, 73-88 (2003).

150 Huijnen, V. et al. The global chemistry transport model TM5: description and evaluation of the tropospheric chemistry version 3.0. Geosci. Model Dev. **3**, 445-473, doi:10.5194/gmd-3-445-2010 (2010).

151 Williams, J. E., Strunk, A., Huijnen, V. & van Weele, M. The application of the Modified Band Approach for the calculation of on-line photodissociation rate constants in TM5: implications for oxidative capacity. Geosci. Model Dev. **5**, 15-35, doi:10.5194/gmd-5-15-2012 (2012).

152 Naik, V. et al. Preindustrial to present-day changes in tropospheric hydroxyl radical and methane lifetime from the Atmospheric Chemistry and Climate Model Intercomparison Project (ACCMIP). Atmos. Chem. Phys. **13**, 5277-5298, doi:10.5194/acp-13-5277-2013 (2013).